THE UNIVERSITY OF MICHIGAN

INDUSTRY PROGRAM OF THE COLLEGE OF ENGINEERING

AN ANALYTICAL AND EXPERIMENTAL INVESTIGATION IN SIMILAR SOLUTIONS OF THREE DIMENSIONAL LAMINAR INCOMPRESSIBLE BOUNDARY LAYERS

Ward Otis Winer

A dissertation submitted in partial fulfillment
of the requirements for the degree of
Doctor of Philosophy in The
University of Michigan
Department of Mechanical Engineering
1961

September, 1961

IP-530

Doctoral Committee:

Associate Professor Arthur G. Hansen, Chairman
Associate Professor Vedat S. Arpaci
Professor Nathanial Coburn
Professor Arnold M. Kuethe
Professor Gordon J. Van Wylen
Professor Chia-Shun Yih

ACKNOWLEDGMENTS

It has been the author's privilege to have had the following gentlemen on his doctoral committee:

Associate Professor Arthur G. Hansen, Chairman
Associate Professor Vedat S. Arpaci
Professor Nathaniel Coburn
Professor Arnold M. Kuethe
Professor Gordon J. Van Wylen
Professor Chia-Shun Yih

The author is particularly indebted to his chairman, Professor A. G. Hansen, for his understanding, encouragement and assistance throughout the period of this research. Gratitude is also extended to Professors Van Wylen, Yih, Kuethe, Coburn and Arpaci for their assistance, interest, and co-operation.

The assistance of the Mechanical Engineering Department in the purchasing of the experimental equipment, and the use of the Aeronautical and Astronautical Engineering Department's wind-tunnel plenum are gratefully acknowledged.

Fellowship support from the Institute of Science and Technology and the Horace H. Rackham School of Graduate Studies during the last year of this work are greatly appreciated. Prior to this period, the author benefited from fellowships given by The Shell Oil Company and The Eastman Kodak Company.

Many thanks go to my wife, Mary Jo Winer, and the Industry Program of the College of Engineering for their help in the preparation of the manuscript.

TABLE OF CONTENTS

TABLE OF CONTENTS (CONT'D)

LIST OF FIGURES

LIST OF FIGURES (CONT'D)

NOMENCLATURE

A, A_i	$(i = 1,2,3,4)$ constants
a	determinant of metric tensor
$a_{\alpha\beta}$	first fundamental metric of flow surface, function of x^α
B	constant
b, b_i	$(i = 1,2,3,\ldots\ldots 17)$ constants
c, c_i	$(i = 1,2,\ldots\ldots\ldots 24)$ constants
$\overline{C}_p$	pitot probe constant for viscous effect
C_p, C_v	specific heats of constant pressure and volume respectively
ds	differential arc length
e	base of natural logarithms
$\overset{\alpha}{F}(\eta)$	function of similarity parameter η, $u^\alpha = U^\alpha \overset{\alpha}{F}'(\eta)$
$g(x^\alpha)$	function of x^α
g_{ij}	fundamental metric space, function of x^i
H	$(\overline{U}^1/\overline{U}^2)^2$
k	Thermal conductivity
K	total or Gaussian curvature of the flow surface
ℓ	constant
m	constant
n	constant
P_a	atmospheric pressure
P_T	total pressure measured at probe tip
p	static pressure
P_R	Prandtl number, $P_R = \frac{C_p \mu}{k}$

R	Reynolds number at probe tip, defined in Equation (B-1)
r	constant
s	constant
T	fluid temperature, function of x^1, x^2, y
T^*	fluid-wall temperature difference, $T^*(x^\alpha) = T_w - T_\infty$
T_s	fluid stagnation temperature
T_w	temperature of flow surface, $T_w(x^\alpha)$
T_∞	temperature of mainstream, $T(x^\alpha)$
U_o	constant
u^α, u_α	contravariant and covariant boundary layer velocity components in x^α direction respectively
U^α, U_α	contravariant and covariant mainstream velocity components in x^α directions respectively
$\bar{U}^\alpha$, $\bar{u}^\alpha$	physical components of mainstream and boundary layer velocities in x^α directions respectively
$\dot{u},\dot{v},\dot{w}$	velocities in $\dot{x},\dot{y},\dot{z}$ directions respectively
V	velocity
v	physical components of boundary layer velocity normal to surface
x^α, $x^{*\alpha}$, $\bar{x}^\alpha$	coordinate systems imbedded on surface, $\alpha = 1,2$
$\mathring{x},\mathring{y},\mathring{z}$	Cartesian coordinates
y^*	physical coordinate normal to flow surface
y	$y^*/\sqrt{\nu}$
$\left\{ {\alpha \atop \beta\gamma} \right\}$, $\left\{ {i \atop jk} \right\}$	Christoffel symbols of the surface and space respectively
α	constant

Δ_1, Δ_2 first and second differential parameters of the surface

η similarity parameter, $\eta = yg(x^\alpha)$

$\theta(\eta)$ function of similarity parameter η, $\theta(\eta) = \frac{T - T_\infty}{T_w - T_\infty}$

μ coefficient of absolute viscosity

ν coefficient of kinematic viscosity

ρ fluid density

σ_1, σ_2 geodesic curvature of coordinate lines, x^1, x^2 respectively

ϕ turning angle of velocity V

ϖ angle between coordinate lines x^α

Subscripts:

$;\alpha$ denotes covariant differentiation with respect to surface coordinates x^α

$,i$ denotes covariant differentiation with respect to space coordinates x^i

m.s. mainstream

Supercripts:

primes denote differentiation with respect to η

Tensor Indices:

Greek letters refer to surface coordinate, range 1,2

Latin letters refer to space coordinates, range 0,1,2

CHAPTER I

INTRODUCTION

Since the introduction of the boundary-layer concept in fluid mechanics in 1904 by Prandtl [1], a great deal of work, both analytical and experimental, has been directed toward its application. The first analytical application of Prandtl's theory was an investigation of the flow of an infinite uniform stream over a thin flat plate at zero incidence by Blausis [2] in 1908. In the intervening years research in boundary-layer theory expanded rapidly. Accounts of the fundamental concepts and the important achievements in the general field of boundary layers can be found in References 3, 4, 5, 6, 7, 8. Cooke & Hall [9] give a general review of some of the recent advances in the theory of three dimensional boundary layers.

To efficiently design various turbomachine configurations it is important to analyze and understand boundary-layer phenomena. In the design of turbomachinery two critical problems arise. They are: (a) the transport of low momentum fluid to undesirable regions in the blade passage and (b) choking of the blade passages due to boundary layer growth (this is particularly critical when operating with flow near mach one in the blade passage). Neither of these problems could be accurately explained nor corrected on the basis of two dimensional boundary-layer concepts. This is due to the fact that two-dimensional boundary layer concepts will only account for boundary layer velocities normal to the surface and parallel to a main stream velocity that consists of a single component directed along a coordinate line which is a

geodesic of the surface.* The effect of the geodesic curvature of the external flow streamline on secondary flows is discussed by Sedney (10).

With three dimensional boundary layers, on the other hand, the boundary layer velocity component parallel to the surface is no longer parallel to the velocity of the potential flow near the surface. This is true whenever the potential flow streamline on the surface has a geodesic curvature with respect to that surface which is different from zero. For instance for flow over a plane surface, the geodesic curvature of any streamline, which is not straight, is different from zero. In three dimensional boundary layers the streamline of the boundary layer flow curves away from the mainstream streamlines (sometimes said to "under cut" the mainstream). This type of boundary layer flow is also referred to as secondary flow. Because three dimensional boundary layer concepts could more readily explain the flow behavior which gives rise to the problems in turbomachinery design, theoretical and experimental investigations of three dimensional boundary layers were initiated.

Theoretical research in three dimensional boundary layers is continually hampered by the inherent complexity of the governing equations. In many practical cases the flow is turbulent, for which case the equations are all but impossible to solve. Considerable analytical work on laminar three dimensional boundary layers has, however met with success. The practical importance of the laminar flow analyses can be

---

*A curve C on the surface S is a geodesic of S if at each point on C the principal normal of C coincides with the normal to S; its geodesic curvature with respect to S vanishes identically. The geodesic curvature of the Curve C on surface S at point P is the curvature of the curve C^1 at P where C^1 is the orthogonal projection of C onto the tangent plane of the surface S at P.

summarized as follows: (a) experimental investigations by Herzig & Hansen [11], Rohlik et al [12], and Kofskey & Allen [13] indicate that laminar boundary-layer flows can provide qualitative information concerning the behavior of turbulent boundary layers, (b) certain boundary layer problems such as external-surface boundary layer flows for high altitude flight might well be encompassed by a laminar flow analysis.

The analytical work in boundary layer investigations has been both of the approximate type and exact type.* The approximate techniques consist mainly of the integral methods and series expansions. Recent reviews of these methods are presented by Cooke & Hall [9] and Cooke [14]. An integral method for compressible flow is presented by Yang [15]. Because the approximate solutions are not rigorously established from physical laws but are devised in such a manner as to readily supply design information, each new approximate method presented must rely on some independent check to establish its domain of validity and usefulness. It is in this respect that the investigations of exact solutions of the boundary layer equations obtain their greatest justification. This fact has been emphasized by Cooke & Hall [9].

Exact solutions of the boundary-layer equations have mainly been found by using the similarity technique. In this technique the partial differential equations of the boundary layer are reduced to ordinary differential equations which are then usually solved numerically. Solutions

---

*The word "exact" here is used in the sense that no further assumptions beyond those of boundary-layer theory have been made.

obtained by similarity techniques are referred to as similar solutions. In this technique flows are restricted to the basic assumption that the velocity profile varies at most by a scale factor along the coordinate lines. In view of this, as might well be expected, the type of coordinate system used governs to a great extent the types of flows for which exact similar solutions can be obtained.

Hansen [16] and Geis [17] present a general approach for obtaining similar solutions. They use this method to establish the classes of mainstream flow components for which the incompressible boundary-layer equations will admit to similar type solutions when the coordinate system is orthogonal. Numerical solutions to two of the types of flows found by Hansen [16] are presented by Yohner and Hansen [18]. A second general method (group theoretic techniques) for obtaining similar solutions for partial differential equations in general is presented by Michal [19] and Morgan [20] and the specific application of this method, by Morgan, to the three dimensional boundary-layer equations is presented as an extensive discussion following Reference 16. The exact solutions for three dimensional compressible flow are not as extensive; the case of the infinite yawed cylinder has been quite thoroughly presented by Reshotko and Beckwith [21].

None of the analytical solutions presented in References 7, 13-18 has been experimentally verified. Although the two-dimensional exact solution of Blausis [2] has been experimentally verified by Burgers [22], van der Hegge Zÿen [23], M. Hansen [24], and Nikuradse [25], no experimental effort has been directed toward the verification of the exact solutions for three-dimensional boundary layers. Visual studies of three-dimensional

boundary-layer behavior are presented by Herzig & Hansen [11], Rohlik et al [12], and Kofskey & Allen [13]. Velocity measurements for three dimensional boundary layers have been carried out for turbulent flow by Gruschwitz [26] and Johnston [27] and for special boundary wall geometries by Kuethe et al [28] and Senoo [29] none of which has corresponding exact solutions.

The work presented here consists of both analytical and experimental studies in three dimensional, incompressible, laminar boundary-layers. In the analytical studies presented, new classes of conditions are found with which the partial differential equations describing the three-dimensional, laminar, incompressible, boundary-layer behavior reduce to ordinary differential equations which yield similar type solutions. The method used in this work is similar to that used by Hansen [16]. The associated boundary layer energy equation for constant properties is also analyzed for the conditions with which it will admit to similar solutions along with the momentum equations.

In the experimental phase of the work presented here two mainstream configurations over developable surfaces (flat plates in both cases) are investigated. Under the conditions of each case the boundary-layer equations admit to a similar-type solution. The mathematical proofs that these flows admit to similar-type solutions both exist; one is from Hansen [16] and the other is one of the class of solutions found in this work. The numerical solutions to the ordinary differential equations in both cases are presented by Yohner and Hansen [18].

The results of the experimental investigations show, that under proper conditions, similarity solutions are physically, as well as

mathematically valid, and that they can be applied with a good degree of accuracy and confidence to finite channel flows.

CHAPTER II

MATHEMATICAL ANALYSIS

Exact solutions of the laminar, incompressible, boundary-layer equations are generally obtained by the use of similarity transformations. By means of such transformations the governing partial differential equations are reduced to ordinary differential equations which can then be solved numerically. Unfortunately, the conditions under which this transformation of the governing equations takes place are such that only very restricted types of mainstream flows, surfaces, and imbedded coordinate systems will satisfy them. It was with the intention of relaxing these restrictions that this work was carried out.

Since the similar solutions assume that the velocity profiles vary, at most, by a scale factor along the coordinate lines, the choice of the coordinate system used is very critical in determining the types of flows which admit similar solutions. The work presented here, therefore, approached the governing partial differential equations in general coordinates, (non-orthogonal curvilinear) imbedded on the surface, using the methods presented by Hansen [16], who considered orthogonal-curvilinear coordinates. It was found, by requiring the angle between the coordinate lines to remain constant (although not $\frac{\pi}{2}$) and with the proper transformation of variables that extensive generalization of the conditions for similarity can be made.

A. Governing Equations

The original derivation of the boundary layer momentum equations by Prandtl [1] was done assuming orthogonal coordinates and using an order

of magnitude argument based on physical intuition. The boundary-layer momentum equations used here are derived in the more mathematically rigorous fashion of a series expansion of the Navier-Stokes equations by Michal [8]. Michal's work was carried out using general coordinates on the surface which makes the form of these equations useful for this work.

The Navier-Stokes equations from which they are derived are restricted to steady motion of a fluid without any external body forces. In addition the fluid is assumed to be homogeneous, i.e. incompressible and constant density ρ.

During the derivation of the boundary-layer momentum equations from the Navier-Stokes equations an additional restriction is imposed. The restriction is that the boundary-layer thickness must be less than the minimum magnitude of the principal radii of curvature over the surface under consideration.

Under these conditions the boundary-layer momentum equations are found to be the first approximation to the Navier-Stokes equations when they are solved by a method of series expansion. The momentum and continuity equations take the following form.

$$u^{\beta} u_{\alpha;\beta} + \frac{v}{\sqrt{\nu}} \frac{\partial u_{\alpha}}{\partial y} = \frac{\partial^2 u_{\alpha}}{\partial y^2} + U^{\beta} U_{\alpha;\beta} \qquad (1)$$

$$\alpha = 1,2$$

$$u^{\alpha}{}_{;\alpha} + \frac{1}{\sqrt{\nu}} \frac{\partial v}{\partial y} = 0 \qquad (2)$$

where the usual indicial notation of tensor calculus is employed. In these equations y is the coordinate normal to the surface which is equal to the actual physical normal distance y^* divided by $\sqrt{\nu}$. The velocity v is the physical component of the boundary layer velocity in the normal direction. The pressure gradient term has been replaced by its equivalent in terms of the mainstream velocities. u^α are the contravariant components of the boundary layer velocity in the x^α directions and U^α are the contravariant components of the mainflow at the surface defined by the joining of the boundary layer flow and the mainflow. The U^α are obtained by evaluating the inviscid solution of the flow configuration at the surface. The metric tensor is $a_{\alpha\beta}(x^1, x^2)$, which is the metric tensor of the surface, and which is equal to the metric tensor of the space evaluated y = 0. The metric tensor defines the element of length on the surface by

$$(ds)^2 = a_{\alpha\beta}\, dx^\alpha\, dx^\beta \tag{3}$$

The metric tensor $a_{\alpha\beta}$ is a double covariant tensor symmetric in α,β. The contravariant components of the metric tensor, $a^{\alpha\beta}$, are defined by

$$a^{\alpha\beta} a_{\beta\gamma} = \delta^\alpha_\gamma \tag{4}$$

where δ^α_γ is the Kronecker delta.

It is assumed throughout that the distance separating the surface over which the flow takes place and the surface defined by the joining of the boundary layer region to the inviscid mainflow is sufficiently small such that the outer surface can be assumed to be a parallel displacement of the flow surface itself.

The surface is considered as a two dimensional Riemannian space and the semicolon denotes surface covariant differentiation, i.e.

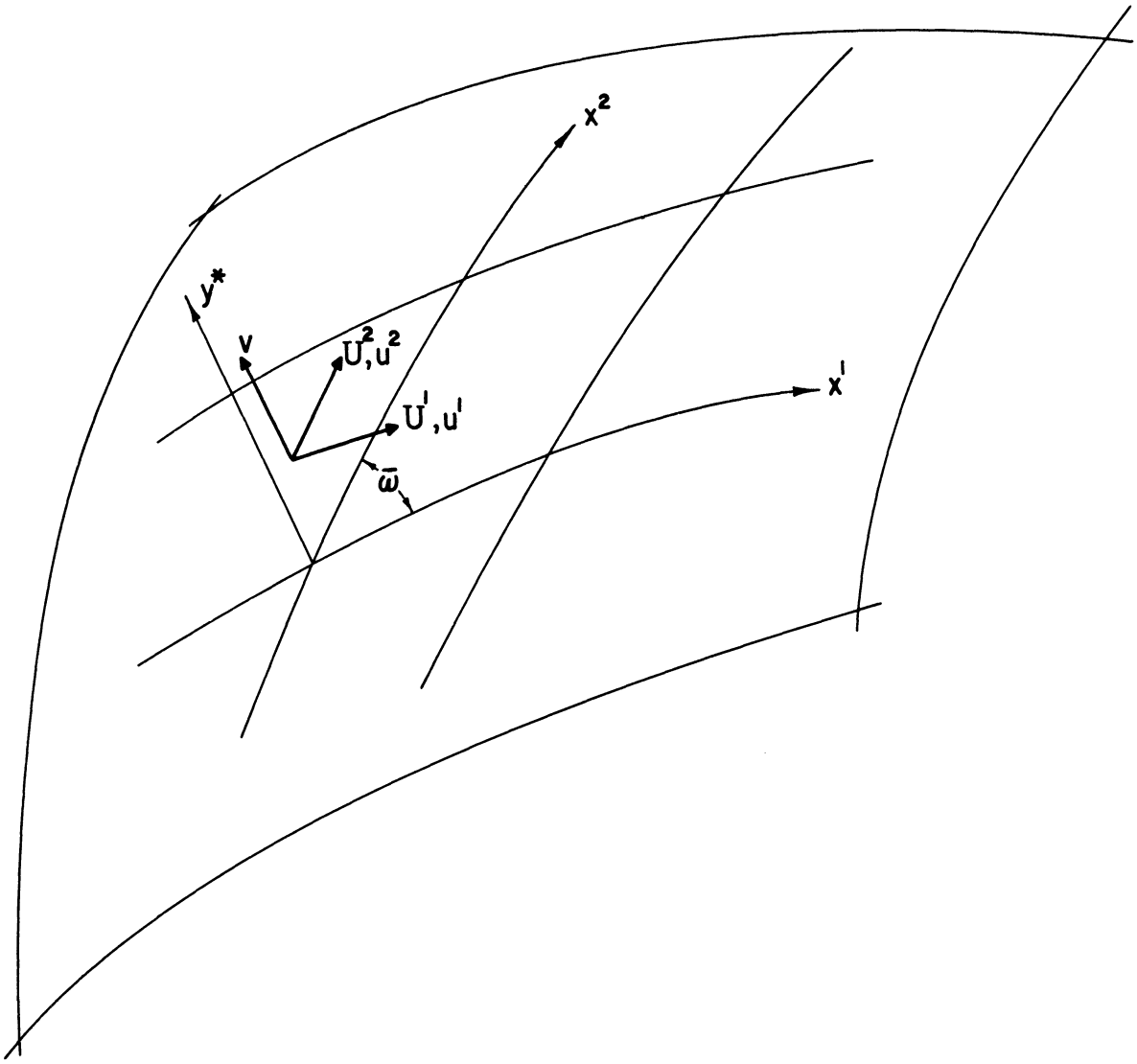

Figure 1. Coordinate System and Orientation of Velocity Components for Flow over a Surface.

$$u^{\alpha}_{;\beta} \equiv \frac{\partial u^{\alpha}}{\partial x^{\beta}} + \left\{ {\alpha \atop \beta\gamma} \right\} u^{\gamma} \tag{5}$$

and

$$u_{\alpha;\beta} \equiv \frac{\partial u_{\alpha}}{\partial x^{\beta}} - \left\{ {\gamma \atop \alpha\beta} \right\} u_{\gamma} \tag{6}$$

The Christoffel symbols are, by definition,

$$\left\{ {\alpha \atop \beta\gamma} \right\} \equiv \frac{a^{\alpha\delta}}{2} \left[\frac{\partial a_{\delta\beta}}{\partial x^{\gamma}} + \frac{\partial a_{\delta\gamma}}{\partial x^{\beta}} - \frac{\partial a_{\beta\gamma}}{\partial x^{\delta}} \right] \tag{7}$$

Equation (1) is in terms of the covariant velocity components u_{α}. The following relations between the covariant velocity component u_{α}, the contravariant velocity component u^{α}, and one set of physical components $\bar{u}^{\alpha}$, exists

$$\left.\begin{aligned} u^{\alpha} &= a^{\alpha\beta} u_{\beta} \\ u_{\alpha} &= a_{\alpha\beta} u^{\beta} \\ \bar{u}^{\alpha} &= \sqrt{a_{\alpha\alpha}}\, u^{\alpha} \end{aligned}\right\} \tag{8}$$

The set of physical components $\bar{u}^{\alpha}$ defined here are summed by the familiar parallelogram rule to obtain the total physical velocity.

If Equation (1) is now multiplied thru by $a^{\alpha\lambda}$ and Ricci's Lemma applied, which states that the covariant derivative of the metric tensor is identically zero, we obtain an equation which is all in terms of the contravariant components of velocity instead of the covariant components. This is desirable because the contravariant components are more readily transformed into physical components. Equations (1) and (2) now take the following form

$$u^\beta u^\lambda_{;\beta} + \frac{v}{\sqrt{\nu}} \frac{\partial u^\lambda}{\partial y} = \frac{\partial^2 u^\lambda}{\partial y^2} + U^\beta U^\lambda_{;\beta} \quad , \lambda = 1,2 \tag{9}$$

$$u^\alpha_{;\alpha} + \frac{1}{\sqrt{\nu}} \frac{\partial v}{\partial y} = 0 \quad , \quad \alpha = 1,2 \tag{10}$$

In the intrinsic geometry of surfaces the first term of the continuity equation, Equation (10), is known as the surface divergence of the contravariant surface vector u^α. It can be shown by the use of Equation (5) and Equation (7) that this invariant takes the form,

$$u^\alpha_{;\alpha} \equiv \frac{1}{\sqrt{a}} \frac{\partial}{\partial x^\alpha} (\sqrt{a}\, u^\alpha) \tag{11}$$

where

$$a = \begin{vmatrix} a_{11} & a_{12} \\ a_{12} & a_{22} \end{vmatrix} \tag{12}$$

Equation (10), the continuity equation, now becomes

$$\frac{1}{\sqrt{a}} \frac{\partial}{\partial x^\alpha} (\sqrt{a}\, u^\alpha) + \frac{1}{\sqrt{\nu}} \frac{\partial v}{\partial y} = 0 \tag{13}$$

The boundary-layer energy equation for steady flow and constant fluid properties can be written in the general coordinates used here as,

$$u^\alpha \frac{\partial T}{\partial x^\alpha} + \frac{v}{\sqrt{\nu}} \frac{\partial T}{\partial y} = \frac{1}{P_R} \frac{\partial^2 T}{\partial y^2} + \frac{1}{c_p} a_{\alpha\beta} \frac{\partial u^\alpha}{\partial y} \frac{\partial u^\beta}{\partial y} \tag{14}$$

The derivation of this form of the energy equation is presented in Appendix A. It should be noted here that, as before, y is not the physical normal distance but that distance divided by $\sqrt{\nu}$ which accounts for the

form of the coefficient on the viscous dissipation term which is the last term on the right hand side of Equation (14). The basic momentum, continuity, and energy equations to be analyzed for similarity solutions are:

$$u^\beta u^\lambda_{;\beta} + \frac{v}{\sqrt{\nu}} \frac{\partial u^\lambda}{\partial y} = \frac{\partial^2 u^\lambda}{\partial y^2} + U^\beta U^\lambda_{;\beta} \quad , \quad \lambda = 1,2 \tag{9}$$

$$\frac{1}{\sqrt{a}} \frac{\partial}{\partial x^\alpha} (\sqrt{a}\, u^\alpha) + \frac{1}{\sqrt{\nu}} \frac{\partial v}{\partial y} = 0 \tag{13}$$

$$u^\alpha \frac{\partial T}{\partial x^\alpha} + \frac{v}{\sqrt{\nu}} \frac{\partial T}{\partial y} = \frac{1}{P_R} \frac{\partial^2 T}{\partial y^2} + \frac{1}{C_p} a_{\alpha\beta} \frac{\partial u^\alpha}{\partial y} \frac{\partial u^\beta}{\partial y} \tag{14}$$

These are subject to the following boundary conditions:

$$\left.\begin{aligned} &@ \quad y = 0 \; ; \quad u^\alpha = v = 0 \quad , \; T = T_w \\ &\text{and} \quad \lim_{y \to \infty} u^\alpha = U^\alpha \\ &\qquad \lim_{y \to \infty} T = T_\infty \end{aligned}\right\} \tag{15}$$

B. Conditions for Similarity

Following the usual approach in obtaining similarity solutions, the boundary layer velocities are assumed expressible as follows:

$$u^\alpha = U^\alpha \overset{\alpha}{F}{}'(\eta) \tag{16}$$

where

$$\eta = \frac{y^*}{\sqrt{\nu}}\, g(x^\alpha) = y\, g(x^\alpha) \tag{17}$$

The dimensionless temperature profile is also assumed to be expressible as a function of the similarity parameter as

$$\Theta(\eta) = \frac{T - T_\infty}{T_w - T_\infty} \tag{18}$$

Substituting Equations (16) and (17) into Equation (13), the continuity equation, yields

$$\frac{\partial v}{\partial \eta} = -\frac{\sqrt{\nu}}{g\sqrt{a}}\left[\overset{\alpha}{F}{}' \frac{\partial \sqrt{a} U^\alpha}{\partial x^\alpha} + \sqrt{a}\, U^\alpha \overset{\alpha}{F}{}'' \eta \frac{\partial \ln g}{\partial x^\alpha}\right] \tag{19}$$

By integrating Equation (19) with respect to η :

$$v = -\frac{\sqrt{\nu}}{g\sqrt{a}}\left[\frac{\partial \sqrt{a} U^\alpha}{\partial x^\alpha}\overset{\alpha}{F} + \sqrt{a}\, U^\alpha \frac{\partial \ln g}{\partial x^\alpha g}\left(\overset{\alpha}{F}{}'\eta - \overset{\alpha}{F}\right)\right] + f(x^\alpha) \tag{20}$$

---

*The superscript on $\overset{\alpha}{F}(\eta)$ or any of its derivatives is not a tensor index and is placed directly over the F to distinguish it from tensor indices. The functions $\overset{\alpha}{F}\,\overset{\alpha}{F}$ etc. always occur as a multiple of U^α and the superscript on F takes the same numerical value as that of U^α.

The arbitrary function $f(x^\alpha)$ will be assumed zero. It has been shown by Hansen [30] that no loss of generality results from this assumption.

Now substituting for u^α, v, η, and T from Equations (16), (20), (17), (18) respectively into the momentum and energy equations, Equations (9) and (14) respectively, gives

$$\left(\frac{1}{F}'\right)^2\left[\frac{\partial U'}{\partial x'}+U'\left\{\begin{matrix}1\\1\,1\end{matrix}\right\}\right]+\frac{1}{F}'\frac{2}{F}'\left[\frac{U^2}{U'}\frac{\partial U'}{\partial x^2}+2U^2\left\{\begin{matrix}1\\1\,2\end{matrix}\right\}\right]$$

$$+\left(\frac{2}{F}'\right)^2\left[\frac{(U^2)^2}{U'}\left\{\begin{matrix}1\\2\,2\end{matrix}\right\}\right]-\frac{1}{F}''\frac{1}{F}\left[\frac{1}{\sqrt{a}}\frac{\partial\sqrt{a}U'}{\partial x'}-U'\frac{\partial \ln g}{\partial x'}\right]$$

$$-\frac{1}{F}''\frac{2}{F}\left[\frac{1}{\sqrt{a}}\frac{\partial\sqrt{a}U^2}{\partial x^2}-U^2\frac{\partial \ln g}{\partial x^2}\right]=\left[g^2\right]\frac{1}{F}'''$$

$$+\left[\frac{\partial U'}{\partial x'}+U'\left\{\begin{matrix}1\\1\,1\end{matrix}\right\}+\frac{U^2}{U'}\frac{\partial U'}{\partial x^2}+2U^2\left\{\begin{matrix}1\\1\,2\end{matrix}\right\}+\left\{\begin{matrix}1\\2\,2\end{matrix}\right\}\frac{(U^2)^2}{U'}\right] \qquad (21)$$

$$\left(\frac{2}{F}'\right)^2\left[\frac{\partial U^2}{\partial x^2}+U^2\left\{\begin{matrix}2\\2\,2\end{matrix}\right\}\right]+\frac{1}{F}'\frac{2}{F}'\left[\frac{U'}{U^2}\frac{\partial U^2}{\partial x'}+2U^2\left\{\begin{matrix}2\\2\,1\end{matrix}\right\}\right]$$

$$+\left(\frac{1}{F}'\right)^2\left[\frac{(U')^2}{U^2}\left\{\begin{matrix}2\\1\,1\end{matrix}\right\}\right]-\frac{2}{F}''\frac{2}{F}\left[\frac{1}{\sqrt{a}}\frac{\partial\sqrt{a}U^2}{\partial x^2}-U^2\frac{\partial \ln g}{\partial x^2}\right]$$

$$-\frac{2}{F}''\frac{1}{F}\left[\frac{1}{\sqrt{a}}\frac{\partial\sqrt{a}U'}{\partial x'}-U'\frac{\partial \ln g}{\partial x'}\right]=\left[g^2\right]\frac{2}{F}'''$$

$$+\left[\frac{U'}{U^2}\frac{\partial U^2}{\partial x'}+\frac{\partial U^2}{\partial x^2}+\frac{(U')^2}{U^2}\left\{\begin{matrix}2\\1\,1\end{matrix}\right\}+2U'\left\{\begin{matrix}2\\2\,1\end{matrix}\right\}+U^2\left\{\begin{matrix}2\\2\,2\end{matrix}\right\}\right] \qquad (22)$$

$$\left[\frac{g^2}{P_R}\right]\theta'' + \left[U'\frac{\partial \ln \sqrt{a}/g}{\partial x'}\right]\theta' \overset{1}{F} + \left[U^2\frac{\partial \ln \sqrt{a}/g}{\partial x^2}\right]\theta' \overset{2}{F}$$

$$-\left[U'\frac{\partial \ln T^*}{\partial x'}\right]\overset{1}{F}'\theta - \left[U^2\frac{\partial \ln T^*}{\partial x^2}\right]\overset{2}{F}'\theta$$

$$+\left[\frac{g^2}{C_p T^*} a_{11} U'U'\right]\left(\overset{1}{F}''\right)^2 + \left[\frac{2g^2}{C_p T^*} a_{12} U'U^2\right]\overset{1}{F}''\overset{2}{F}''$$

$$+\left[\frac{g^2}{C_p T^*} a_{22} U^2U^2\right]\left(\overset{2}{F}''\right)^2 = 0 \qquad (23)$$

It is obvious that if the terms in brackets [ ] are proportional or zero in each of Equations (21), (22), and (23) that these equations will be ordinary differential equations in $\overset{\alpha}{F}(\eta)$, $\theta(\eta)$, and η. This proportionality of the bracketed terms is a sufficient condition for similarity solutions of the equations. No attempt has been made to determine if it is also a necessary condition. Consequently the requirements for similarity obtained in the following work may not be the only requirements with which similarity solutions could be obtained. In the case of x^1, x^2 being orthogonal, if $a_{12} = 0$ in the above equations, it has been shown by Geis [17] that these are the

necessary as well as sufficient conditions for similarity. There is a coefficient g^2 or (const)g^2 in all three equations, therefore the coefficients of all three equations must be mutually proportional or individually zero. This requirement can be expressed as:

$$
\begin{aligned}
g^2 &= b_1\left[\frac{\partial U^1}{\partial x^1} + U^1\left\{{1 \atop 11}\right\}\right] = b_2\left[\frac{U^2}{U^1}\frac{\partial U^1}{\partial x^2} + 2U^2\left\{{1 \atop 12}\right\}\right] \\
&= b_3\left[\frac{(U^2)^2}{U^1}\left\{{1 \atop 22}\right\}\right] = b_4\left[\frac{1}{\sqrt{a}}\frac{\partial \sqrt{a}U^1}{\partial x^1} - U^1\frac{\partial \ln g}{\partial x^1}\right] \\
&= b_5\left[\frac{1}{\sqrt{a}}\frac{\partial \sqrt{a}U^2}{\partial x^2} - U^2\frac{\partial \ln g}{\partial x^2}\right] = b_6\left[\frac{\partial U^1}{\partial x^1} + U^1\left\{{1 \atop 11}\right\}\right. \\
&\left. + \frac{U^2}{U^1}\frac{\partial U^1}{\partial x^2} + 2U^2\left\{{1 \atop 12}\right\} + \frac{(U^2)^2}{U^1}\left\{{1 \atop 22}\right\}\right] \\
&+ b_7\left[\frac{\partial U^2}{\partial x^2} + U^2\left\{{2 \atop 22}\right\}\right] = b_8\left[\frac{U^1}{U^2}\frac{\partial U^2}{\partial x^1} + 2U^1\left\{{2 \atop 21}\right\}\right] \\
&= b_9\left[\frac{(U^1)^2}{U^2}\left\{{2 \atop 11}\right\}\right] = b_{10}\left[\frac{U^1}{U^2}\frac{\partial U^2}{\partial x^1} + \frac{\partial U^2}{\partial x^2} + \frac{(U^1)^2}{U^2}\left\{{2 \atop 11}\right\}\right. \\
&\left. + 2U^1\left\{{2 \atop 21}\right\} + U^2\left\{{2 \atop 22}\right\}\right] = b_{11}\left[U^1\frac{\partial \ln \sqrt{a}/g}{\partial x^1}\right] \\
&= b_{12}\left[U^2\frac{\partial \ln \sqrt{a}/g}{\partial x^2}\right] = b_{13}\left[U^1\frac{\partial \ln T^*}{\partial x^1}\right] = b_{14}\left[U^2\frac{\partial \ln T^*}{\partial x^2}\right] \\
&= b_{15}\left[\frac{g^2}{T^*}a_{11}U^1U^1\right] = b_{16}\left[\frac{g^2}{T^*}a_{12}U^1U^2\right]
\end{aligned}
\tag{24}
$$

$$= b_{17}\left[\frac{g^2}{T^*} a_{22} U^2 U^2\right] \qquad \text{(24) Cont'd.}$$

The following observations can now be made. From Equations (17) we know that g^2 cannot be zero. Therefore if the terms

$$\frac{\partial U^1}{\partial x^1} + U^1\left\{{1 \atop 11}\right\}, \quad \frac{U^2}{U^1}\frac{\partial U^1}{\partial x^2} + 2U^2\left\{{1 \atop 12}\right\},$$

and $\frac{(U^2)^2}{U^1}\left\{{1 \atop 22}\right\}$ are each proportional to g^2 or identically zero, then the term

$$\frac{\partial U^1}{\partial x^1} + U^1\left\{{1 \atop 11}\right\} + \frac{U^2}{U^1}\frac{\partial U^1}{\partial x^2} + 2U^2\left\{{1 \atop 12}\right\} + \frac{(U^2)^2}{U^1}\left\{{1 \atop 22}\right\}$$

is also either proportional to g^2 or identically zero. Similarly if

$$\frac{\partial U^2}{\partial x^2} + U^2\left\{{2 \atop 22}\right\}, \quad \frac{U^1}{U^2}\frac{\partial U^2}{\partial x^1} + 2U^1\left\{{2 \atop 21}\right\},$$

and $\frac{(U^1)^2}{U^2}\left\{{2 \atop 11}\right\}$ are either proportional to g^2 or identically zero then

$$\frac{U^1}{U^2}\frac{\partial U^2}{\partial x^1} + \frac{\partial U^2}{\partial x^2} + \frac{(U^1)^2}{U^2}\left\{{2 \atop 11}\right\} + 2U^1\left\{{2 \atop 21}\right\} + U^2\left\{{2 \atop 22}\right\}$$

is also either proportional to g^2 or identically zero.

Therefore the conditions imposed by Equation (24) reduce to the requirement that sixteen coefficients be mutually proportional or identically zero. These terms are:

$$\textcircled{1} \quad g^2 \qquad (25)$$

(25) Cont'd.

② $\frac{\partial U^1}{\partial x^1} + U^1 \left\{ {1 \atop 11} \right\}$

③ $\frac{U^2}{U^1} \frac{\partial U^1}{\partial x^2} + 2U^2 \left\{ {1 \atop 12} \right\}$

④ $\frac{(U^2)^2}{U^1} \left\{ {1 \atop 22} \right\}$

⑤ $\frac{1}{\sqrt{a}} \frac{\partial \sqrt{a} U^1}{\partial x^1} - U^1 \frac{\partial \ln g}{\partial x^1}$

⑥ $\frac{1}{\sqrt{a}} \frac{\partial \sqrt{a} U^2}{\partial x^2} - U^2 \frac{\partial \ln g}{\partial x^2}$

⑦ $\frac{\partial U^2}{\partial x^2} + U^2 \left\{ {2 \atop 22} \right\}$

⑧ $\frac{U^1}{U^2} \frac{\partial U^2}{\partial x^1} + 2U^1 \left\{ {2 \atop 21} \right\}$

⑨ $\frac{(U^1)^2}{U^2} \left\{ {2 \atop 11} \right\}$

⑩ $U^1 \frac{\partial \ln \sqrt{a}/g}{\partial x^1}$

⑪ $U^2 \frac{\partial \ln \sqrt{a}/g}{\partial x^2}$

⑫ $U^1 \frac{\partial \ln T^*}{\partial x^1}$

⑬ $U^2 \frac{\partial \ln T^*}{\partial x^2}$

⑭ $\frac{g^2}{T^*} a_{11} (U^1)^2$

(15) $\frac{g^2}{T^*} a_{12} U' U^2$

(16) $\frac{g^2}{T^*} a_{22} (U^2)^2$

(25) Cont'd

Conditions (1)→(9) are associated with the momentum equations only and conditions (10)→(16) are the added requirements for the energy equation. Conditions (1)→(16) are the conditions required to make Equations (9) and (14) ordinary differential equations and shall be referred to as O.D.E. conditions.

Through considerations of the intrinsic geometric properties of the surface the Christoffel symbols in Conditions (25) can be explicitly described in terms of properties of the coordinate system imbedded on the surface.

The general equation for the geodesic curvature of a curve imbedded on a surface is (31, p. 186).

$$\frac{d^2 x^\alpha}{ds^2} + \left\{ \begin{matrix} \alpha \\ \beta\gamma \end{matrix} \right\} \frac{dx^\beta}{ds} \frac{dx^\gamma}{ds} = -\sigma \varepsilon^{\alpha\beta} a_{\beta\gamma} \frac{dx^\gamma}{ds} \tag{26}$$

where S is the distance measured along the curve C whose geodesic curvature with respect to the surface is σ. The symbol

$$\varepsilon^{\alpha\beta} = \frac{1}{\sqrt{a}} e^{\alpha\beta} \tag{27}$$

is defined by

$$e^{\alpha\beta} = 0 \quad , \alpha = \beta$$

$$= 1 \quad , \alpha = 1, \beta = 2$$

$$e^{\alpha\beta} = -1 \quad , \quad \alpha = 2 \, , \, \beta = 1$$

Employing Equation (26) the following expressions relating the geodesic curvature of the coordinate lines and the Christoffel symbols are obtained:

$$\left\{ {2 \atop 1\,1} \right\} = \sigma_1 \frac{a_{11}^{3/2}}{\sqrt{a}} \tag{28}$$

and

$$\left\{ {1 \atop 2\,2} \right\} = -\sigma_2 \frac{a_{22}^{3/2}}{\sqrt{a}} \tag{29}$$

Coburn (32, p. 169) gives the relation

$$\frac{\partial \ln \sqrt{a}}{\partial x^\alpha} = \left\{ {\beta \atop \alpha\,\beta} \right\} \tag{30}$$

and Eisenhart (33, p. 153) gives

$$\frac{\partial \bar{\omega}}{\partial x^1} = -\sqrt{a}\left[\frac{1}{a_{11}} \left\{ {2 \atop 1\,1} \right\} + \frac{1}{a_{22}} \left\{ {1 \atop 1\,2} \right\} \right] \tag{31}$$

and

$$\frac{\partial \bar{\omega}}{\partial x^2} = -\sqrt{a}\left[\frac{1}{a_{11}} \left\{ {2 \atop 1\,2} \right\} + \frac{1}{a_{22}} \left\{ {1 \atop 2\,2} \right\} \right] \tag{32}$$

where $\bar{\omega}$ is the angle between the coordinate lines on the surface. By manipulating Equations (28)→(32) the following expressions for the Christoffel symbols can be obtained:

$$\left\{ {1 \atop 1\,1} \right\} = \frac{\partial \ln \sqrt{a}}{\partial x^1} - \frac{\sqrt{a_{11}}}{\sin \bar{\omega}} \left[\sigma_2 - \frac{1}{\sqrt{a_{22}}} \frac{\partial \bar{\omega}}{\partial x^2} \right] \tag{33}$$

$$\left\{ {1 \atop 12} \right\} = -\frac{\sqrt{a_{22}}}{\sin\bar{\omega}}\left[\frac{1}{\sqrt{a_{11}}}\frac{\partial\bar{\omega}}{\partial x^1} + \sigma_1\right]$$

$$\left\{ {1 \atop 22} \right\} = -\sigma_2\frac{a_{22}^{3/2}}{\sqrt{a}}$$

$$\left\{ {2 \atop 11} \right\} = \sigma_1\frac{a_{11}^{3/2}}{\sqrt{a}} \qquad \text{(33) Cont'd.}$$

$$\left\{ {2 \atop 12} \right\} = \frac{\sqrt{a_{11}}}{\sin\bar{\omega}}\left[\sigma_2 - \frac{1}{\sqrt{a_{22}}}\frac{\partial\bar{\omega}}{\partial x^2}\right]$$

$$\left\{ {2 \atop 22} \right\} = \frac{\partial \ln\sqrt{a}}{\partial x^2} + \frac{\sqrt{a_{22}}}{\sin\bar{\omega}}\left[\frac{1}{\sqrt{a_{11}}}\frac{\partial\bar{\omega}}{\partial x^1} + \sigma_1\right]$$

Some additional observations can be made. From conditions (14), (15), and (16) it is seen that

$$C_1 a_{11}(U^1)^2 = C_2 a_{12} U^1 U^2 = C_3 a_{22}(U^2)^2$$

or

$$C_4 = \frac{a_{12}U^2}{a_{11}U^1} \quad , \quad C_5 = \frac{a_{12}U^1}{a_{22}U^2} .$$

Therefore

$$C_6 = C_4 C_5 = \frac{(a_{12})^2}{a_{11}a_{22}} .$$

From the intrinsic geometry of surfaces it is known that this is equal to the square of the cosine of the angle between the coordinate lines,

$$C_6 = \frac{(a_{12})^2}{a_{11}a_{22}} = \cos^2 \bar{\omega} \tag{34}$$

Therefore the coordinates may be non-orthogonal but must be constant angle coordinates.

The requirement for constant angle comes from the viscous dissipation term in the energy equation and if viscous dissipation were neglected may not be required by the remaining conditions. But because of the complexity of the system of O.D.E. conditions, it was necessary to find some means of simplifying them and, still obtain profitable results. In the author's opinion it is doubtful that a meaningful analysis could be made in the more general case. The assumption of constant angle between the coordinate lines was, for this reason, used throughout this work.

From Equations (34) and (12) it follows that

$$a = a_{11}a_{22}\sin^2 \bar{\omega} \tag{35}$$

O.D.E conditions (1)→(9), which are from the momentum equations, are now considered. The application of O.D.E. conditions (10)→(16) will be applied to the results from (1)→(9) to determine T^* and any additional requirements necessary to obtain similarity solutions of the energy equation.

If in Equation (26), the curve C is considered to be the coordinate curves x^1 = constant and x^2 = constant respectively, the

following relations for the geodesic curvature of the coordinate lines are obtained:

$$\sqrt{a}\,\sigma_1 = \frac{\partial}{\partial x^1}\left(\frac{a_{12}}{\sqrt{a_{11}}}\right) - \frac{\partial \sqrt{a_{11}}}{\partial x^2} \tag{36}$$

and

$$\sqrt{a}\,\sigma_2 = -\frac{\partial}{\partial x^2}\left(\frac{a_{12}}{\sqrt{a_{22}}}\right) + \frac{\partial \sqrt{a_{22}}}{\partial x^1} \tag{37}$$

For the constant angle case Equation (34) can be applied to give

$$\sqrt{a}\,\sigma_1 = \cos\bar{\omega}\,\frac{\partial \sqrt{a_{22}}}{\partial x^1} - \frac{\partial \sqrt{a_{11}}}{\partial x^2} \tag{38}$$

and

$$\sqrt{a}\,\sigma_2 = -\cos\bar{\omega}\,\frac{\partial \sqrt{a_{11}}}{\partial x^2} + \frac{\partial \sqrt{a_{22}}}{\partial x^1} \tag{39}$$

Multiplying Equation (38) by $\cos\bar{\omega}$ and subtracting it from Equation (39), it follows that,

$$\frac{1}{\sqrt{a}}\,\frac{\partial \sqrt{a_{22}}}{\partial x^1} = \frac{1}{\sin^2\bar{\omega}}\left[\sigma_2 - \cos\bar{\omega}\,\sigma_1\right] \tag{40}$$

In similar manner

$$\frac{1}{\sqrt{a}}\,\frac{\partial \sqrt{a_{11}}}{\partial x^2} = -\frac{1}{\sin^2\bar{\omega}}\left[\sigma_1 - \cos\bar{\omega}\,\sigma_2\right] \tag{41}$$

Under the conditions of constant angle coordinates, applying Equations (8), (28), (29) and (33-41), O.D.E. conditions (1)→(9) of Conditions (25) become

$$
\begin{aligned}
&① \quad g^2 \\
&② \quad \frac{1}{\sqrt{a_{11}}}\frac{\partial \bar{U}^1}{\partial x^1} - \bar{U}^1 \cot\bar{\omega}\,\sigma_1 \\
&③ \quad \frac{\bar{U}^2}{\sqrt{a_{22}}}\frac{\partial \ln \bar{U}^1}{\partial x^2} - \bar{U}^2\left[\frac{\sigma_1}{\sin\bar{\omega}} + \cot\bar{\omega}\,\sigma_2\right] \\
&④ \quad \frac{(\bar{U}^2)^2}{\bar{U}^1}\frac{\sigma_2}{\sin\bar{\omega}} \\
&⑤ \quad \bar{U}^1\frac{\sigma_2}{\sin\bar{\omega}} - \frac{\bar{U}^1}{\sqrt{a_{11}}}\frac{\partial \ln g}{\partial x^1} \\
&⑥ \quad \bar{U}^2\frac{\sigma_1}{\sin\bar{\omega}} + \frac{\bar{U}^2}{\sqrt{a_{22}}}\frac{\partial \ln g}{\partial x^2} \\
&⑦ \quad \frac{1}{\sqrt{a_{22}}}\frac{\partial \bar{U}^2}{\partial x^2} + \bar{U}^2\cot\bar{\omega}\,\sigma_2 \\
&⑧ \quad \frac{\bar{U}^1}{\sqrt{a_{11}}}\frac{\partial \ln \bar{U}^2}{\partial x^1} + \bar{U}^1\left[\frac{\sigma_2}{\sin\bar{\omega}} + \cot\bar{\omega}\,\sigma_1\right] \\
&⑨ \quad \frac{(\bar{U}^1)^2}{\bar{U}^2}\frac{\sigma_1}{\sin\bar{\omega}}
\end{aligned}
\tag{42}
$$

An additional equation from the geometry of surfaces can also be employed. Laguerre's formula, McConnell (31 p.191), relates the Gaussian or total curvature, K, of the surface to the coordinate system imbedded on it. Laguerre's formula is

$$K = \frac{1}{\sqrt{a}}\left[\frac{\partial^2 \bar{\omega}}{\partial x' \partial x^2} - \frac{\partial}{\partial x'}(\sigma_2 \sqrt{a_{22}}) + \frac{\partial}{\partial x^2}(\sigma_1 \sqrt{a_{11}})\right] \tag{43}$$

The term $\frac{\partial^2 \bar{\omega}}{\partial x' \partial x^2}$ is zero for the constant angle case under consideration. By using the O.D.E. Conditions (42), in Equation (43) it will be shown that for certain Gaussian curvatures the mainstream velocity components must be proportional if the O.D.E. conditions are to be satisfied.

Under the condition of constant coordinate angle Laguerre's formula, Equation (43), becomes

$$\sqrt{a}\, K = \frac{\partial}{\partial x^2}(\sigma_1 \sqrt{a_{11}}) - \frac{\partial}{\partial x'}(\sigma_2 \sqrt{a_{22}})$$

or

$$K = \frac{\sigma_1}{\sqrt{a}} \frac{\partial \sqrt{a_{11}}}{\partial x^2} + \frac{\sqrt{a_{11}}}{\sqrt{a}} \frac{\partial \sigma_1}{\partial x^2} - \frac{\sigma_2}{\sqrt{a}} \frac{\partial \sqrt{a_{22}}}{\partial x'} - \frac{\sqrt{a_{22}}}{\sqrt{a}} \frac{\partial \sigma_2}{\partial x'} \tag{44}$$

From Equations (40) and (41), $\frac{1}{\sqrt{a}} \frac{\partial \sqrt{a_{22}}}{\partial x'}$ and $\frac{1}{\sqrt{a}} \frac{\partial \sqrt{a_{11}}}{\partial x^2}$ respectively can be substituted to obtain,

$$K = -\frac{\sigma_1}{\sin^2 \bar{\omega}}(\sigma_1 - \cos \bar{\omega}\, \sigma_2) - \frac{\sigma_2}{\sin^2 \bar{\omega}}(\sigma_2 - \cos \bar{\omega}\, \sigma_1)$$

$$+ \frac{\sqrt{a_{11}}}{\sqrt{a}} \frac{\partial \sigma_1}{\partial x^2} - \frac{\sqrt{a_{22}}}{\sqrt{a}} \frac{\partial \sigma_2}{\partial x'} \tag{45}$$

From O.D.E. (1) and (4), Conditions (42),

$$\sigma_2 = C_7 g^2 \frac{\bar{U}'}{(\bar{U}^2)^2}$$

so

$$\frac{\partial \sigma_2}{\partial x'} = C_7 \frac{\partial}{\partial x'}\left(g^2 \frac{\bar{U}'}{(\bar{U}^2)^2}\right)$$

$$= \sigma_2\left[\frac{\partial \ln g^2}{\partial x'} + \frac{\partial \ln \bar{U}'}{\partial x'} - 2\frac{\partial \ln \bar{U}^2}{\partial x'}\right] \tag{46}$$

This can be further evaluated. From O.D.E. (4) and (5),

$$\frac{\partial \ln g^2}{\partial x'} = 2C_8 \frac{(\bar{U}^2)^2}{(\bar{U}')^2} \frac{\sigma_2 \sqrt{a_{11}}}{\sin \bar{\omega}} - 2\frac{\sigma_2 \sqrt{a_{11}}}{\sin \bar{\omega}} \tag{47}$$

From O.D.E. (2) and (9),

$$\frac{\partial \ln \bar{U}'}{\partial x'} = C_9 \frac{\bar{U}'}{\bar{U}^2} \frac{\sqrt{a_{11}}\sigma_1}{\sin \bar{\omega}} + \sigma_1 \sqrt{a_{11}} \cot \bar{\omega} \tag{48}$$

From O.D.E. (8) and (9),

$$\frac{\partial \ln \bar{U}^2}{\partial x'} = C_{10} \frac{\bar{U}'}{\bar{U}^2} \frac{\sqrt{a_{11}}\sigma_1}{\sin \bar{\omega}} - \sqrt{a_{11}}\left[\cot \bar{\omega}\,\sigma_1 + \frac{\sigma_2}{\sin \bar{\omega}}\right] \tag{49}$$

Substituting Equations (47, 48, 49) into Equation (46),

$$\frac{\partial \sigma_2}{\partial x'} = \frac{2C_8}{\sin \bar{\omega}}\left(\frac{\bar{U}^2}{\bar{U}'}\right)^2 \sigma_2^2 \sqrt{a_{11}} - 2\frac{\sigma_2^2 \sqrt{a_{11}}}{\sin \bar{\omega}}$$

$$+ C_9 \frac{\bar{U}'}{\bar{U}^2} \frac{\sqrt{a_{11}}\sigma_1\sigma_2}{\sin \bar{\omega}} + \sqrt{a_{11}}\,\sigma_1\sigma_2 \cot \bar{\omega} \tag{50}$$

$$-\frac{2C_{10}}{\sin\bar{\omega}}\frac{\bar{U}'}{\bar{U}^2}\sqrt{a_{11}}\,\sigma_1\sigma_2-2\sqrt{a_{11}}\left[\cot\bar{\omega}\,\sigma_1\sigma_2+\frac{\sigma_2^2}{\sin\bar{\omega}}\right] \quad (50)\ \text{Cont'd.}$$

In the same manner $\frac{\partial\sigma_1}{\partial x^2}$ can be evaluated. From O.D.E. (1) and (9),

$$\sigma_1 = C_{11}\sin\bar{\omega}\,g^2\frac{\bar{U}^2}{(\bar{U}')^2} \quad (51)$$

Hence,

$$\frac{\partial\sigma_1}{\partial x^2} = \sigma_1\frac{\partial\ln g^2}{\partial x^2}+\sigma_1\frac{\partial\ln\bar{U}^2}{\partial x^2}-2\sigma_1\frac{\partial\ln\bar{U}'}{\partial x^2} \quad (52)$$

And from O.D.E. (6) and (9),

$$\frac{\partial\ln g^2}{\partial x^2} = C_{12}\left(\frac{\bar{U}'}{\bar{U}^2}\right)^2 2\sqrt{a_{22}}\frac{\sigma_1}{\sin\bar{\omega}}-2\frac{\sqrt{a_{22}}\,\sigma_1}{\sin\bar{\omega}} \quad (53)$$

From O.D.E. (7) and (9),

$$\frac{\partial\ln\bar{U}^2}{\partial x^2} = C_{13}\left(\frac{\bar{U}'}{\bar{U}^2}\right)^2\frac{\sigma_1\sqrt{a_{22}}}{\sin\bar{\omega}}-\sqrt{a_{22}}\,\sigma_2\cot\bar{\omega} \quad (54)$$

From O.D.E. (3) and (9),

$$\frac{\partial\ln\bar{U}'}{\partial x^2} = C_{14}\left(\frac{\bar{U}'}{\bar{U}^2}\right)^2\frac{\sqrt{a_{22}}\sigma_1}{\sin\bar{\omega}}+\sqrt{a_{22}}\left[\frac{\sigma_1}{\sin\bar{\omega}}+\sigma_2\cot\bar{\omega}\right] \quad (55)$$

Therefore Equation (52) becomes,

$$\frac{\partial\sigma_1}{\partial x^2} = C_{12}\frac{2\sqrt{a_{22}}\sigma_1^2}{\sin\bar{\omega}}\left(\frac{\bar{U}'}{\bar{U}^2}\right)^2-\frac{2\sqrt{a_{22}}\,\sigma_1^2}{\sin\bar{\omega}}+C_{13}\frac{\sigma_1^2\sqrt{a_{22}}}{\sin\bar{\omega}}\left(\frac{\bar{U}'}{\bar{U}^2}\right)^2$$

$$-\sqrt{a_{22}}\,\sigma_1\sigma_2\cot\bar{\omega}-2C_{14}\frac{\sqrt{a_{22}}\,\sigma_1^2}{\sin\bar{\omega}}\left(\frac{\bar{U}'}{\bar{U}^2}\right)^2 \quad (56)$$

$$-2\sigma_1\sqrt{a_{22}}\left[\frac{\sigma_1}{\sin\bar{\omega}}+\cot\bar{\omega}\,\sigma_2\right] \tag{56}$$

With Equations (50), (55) & (35), Equation (45) becomes,

$$K\sin^2\bar{\omega}=\left[(2C_{12}+C_{13}-2C_{14})\left(\frac{\bar{U}'}{\bar{U}^2}\right)^2-5\right]\sigma_1^2$$

$$-\left[2C_8\left(\frac{\bar{U}^2}{\bar{U}'}\right)^2-3\right]\sigma_2^2+\left[2C_{12}-C_9\right]\frac{\bar{U}'}{\bar{U}^2}\sigma_1\sigma_2 \tag{57}$$

If this is now divided through by σ_1^2 (division by σ_2^2 would also be acceptable), Equation (57) becomes,

$$\frac{K}{\sigma_1^2}\sin^2\bar{\omega}=-5+\left[3-2C_8\left(\frac{\bar{U}^2}{\bar{U}'}\right)^2\right]\left(\frac{\sigma_2}{\sigma_1}\right)^2$$

$$+\left[2C_{10}-C_9\right]\left(\frac{\bar{U}'}{\bar{U}^2}\right)\left(\frac{\sigma_2}{\sigma_1}\right)$$

$$+\left[2C_{12}+C_{13}-2C_{14}\right]\left(\frac{\bar{U}'}{\bar{U}^2}\right)^2 \tag{58}$$

From O.D.E. (4) and (9) .

$$\frac{\sigma_2}{\sigma_1}=C_{15}\left(\frac{\bar{U}'}{\bar{U}^2}\right)^3 \tag{59}$$

and if H is defined as

$$\left(\frac{\bar{U}'}{\bar{U}^2}\right)^2\equiv H \tag{60}$$

Equation (58) becomes

$$\frac{K}{\sigma_1^2}\sin^2\bar{\omega} = 3C_{15}^2H^3 + (2C_{10} - C_9 - 2C_8C_{15})C_{15}H^2 \qquad (61)$$

$$+ (2C_{12} + C_{13} - 2C_{14})H - 5$$

From Equation (61) and the definition of H, Equation (60), it is seen that H must be a positive constant whenever $\frac{K}{\sigma_1^2}$ or $\frac{K}{\sigma_2^2}$ is a constant or identically zero. The same result is obtained when either one of the coordinate line geodesic curvatures is zero and the other non-zero. In this case, any time the ratio of the Gaussian curvature of the surface to the square of the non-zero geodesic curvature of a coordinate line is constant H must be a positive constant. This includes any developable surface ($K \equiv 0$) where either one of the coordinate line geodesic curvatures is non-zero. This does not include surfaces where the coordinate lines are constant angle and both have zero geodesic curvatures. By Laguerre's formula, Equation (43), the Gaussian curvature is zero and this formula cannot be applied.

Consequently, two conditions of constant angle coordinate systems will now be considered: (1) systems where $\frac{K}{\sigma_1^2}$ or $\frac{K}{\sigma_2^2}$ is constant, and (2) systems where $K = \sigma_1 = \sigma_2 = 0$.

In the following two sections, it will be shown that the O.D.E. conditions for the case of constant angle coordinates have the same form as those obtained for orthogonal coordinates by Geis[17] and

Hansen (34). Consequently the systems presented in (34), which satisfy the O.D.E. conditions, can be extended to the more general constant angle case by simply referring them to the constant angle coordinate system.

1. Coordinate Systems for which $\frac{K}{\sigma_1^2}$ or $\frac{K}{\sigma_2^2}$ is constant.

From Equations (60) and (61), it is known that

$$\bar{U}^2 = (\text{const.})\,\bar{U}^1 \tag{62}$$

and then from O.D.E. (4) and (9) or Equation (59),

$$\sigma_2 = (\text{const.})\,\sigma_1 \tag{63}$$

With Equations (62) and (63), O.D.E. (4) or (9), can be written in the following forms

$$\begin{aligned} &(4)^* \quad (\text{const.}) \quad \bar{U}^2\sigma_2 \\ &(4)^* \quad (\text{const.}) \quad \bar{U}^1\sigma_1 \end{aligned} \tag{64}$$

Since Conditions (64), O.D.E. (4) and (9), must be either proportional to g^2 or identically zero, it is assured that in Conditions (42) the second terms of O.D.E. (2) and (7) and the third terms of O.D.E. (3) and (8) will also be proportional to g^2 or identically zero. Consequently these terms can be removed from the O.D.E. conditions as written in Conditions (42). The O.D.E. conditions now become,

$$
\begin{aligned}
&① \quad g^2 \\
&② \quad \frac{1}{\sqrt{a_{11}}} \frac{\partial \bar{U}'}{\partial x'} \\
&③ \quad \frac{\bar{U}^2}{\sqrt{a_{22}}} \frac{\partial \ln \bar{U}'}{\partial x^2} - \bar{U}^2 \frac{\sigma_1}{\sin \bar{\omega}} \\
&④ \quad \frac{(\bar{U}^2)^2}{\bar{U}'} \frac{\sigma_2}{\sin \bar{\omega}} \\
&⑤ \quad \bar{U}' \frac{\sigma_2}{\sin \bar{\omega}} - \frac{\bar{U}'}{2\sqrt{a_{11}}} \frac{\partial \ln g^2}{\partial x'} \qquad (65) \\
&⑥ \quad \bar{U}^2 \frac{\sigma_1}{\sin \bar{\omega}} + \frac{\bar{U}^2}{2\sqrt{a_{22}}} \frac{\partial \ln g^2}{\partial x^2} \\
&⑦ \quad \frac{1}{\sqrt{a_{22}}} \frac{\partial \bar{U}^2}{\partial x^2} \\
&⑧ \quad \frac{\bar{U}'}{\sqrt{a_{11}}} \frac{\partial \ln \bar{U}^2}{\partial x'} + \bar{U}' \frac{\sigma_2}{\sin \bar{\omega}} \\
&⑨ \quad \frac{(\bar{U}')^2}{\bar{U}^2} \frac{\sigma_1}{\sin \bar{\omega}}
\end{aligned}
$$

Further terms could be removed by the above argument but instead of removing the terms it will be noted that each term in the O.D.E. conditions must be individually proportional and not just proportional in the added combinations shown. The form shown above has considerable advantage. This will become obvious in the next few paragraphs.

Some observations concerning the nature of the coordinate geodesic curvatures under the conditions imposed on the problem can now be made. Equations (38) and (39) are the equations for the coordinate geodesic curvatures under the condition of constant angle. It has been found that the condition of constant angle imposes the condition of proportional mainstream velocity components which in turn requires proportional geodesic curvatures of the coordinate lines. Therefore Equations (38) and (39) give

$$\cos\bar{\omega}\,\frac{\partial\sqrt{a_{22}}}{\partial x^1} - \frac{\partial\sqrt{a_{11}}}{\partial x^2} = C_{16}\left[-\cos\bar{\omega}\,\frac{\partial\sqrt{a_{11}}}{\partial x^2} + \frac{\partial\sqrt{a_{22}}}{\partial x^1}\right]$$

or

$$\frac{\partial\sqrt{a_{22}}}{\partial x^1} = \frac{1-C_{16}\cos\bar{\omega}}{\cos\bar{\omega}-C_{16}}\;\frac{\partial\sqrt{a_{11}}}{\partial x^2} \tag{66}$$

$$C_{16} \neq \cos\bar{\omega}$$

Consequently the coordinate geodesic curvatures from Equations (38) and (39) can now be written as,

$$\sigma_1 = -\frac{\sin\bar{\omega}}{1-\dfrac{\cos\bar{\omega}}{C_{16}}}\;\frac{1}{\sqrt{a_{11}\,a_{22}}}\;\frac{\partial\sqrt{a_{11}}}{\partial x^2} \tag{67}$$

and

$$\sigma_2 = \frac{\sin\bar{\omega}}{1-C_{16}\cos\bar{\omega}} \frac{1}{\sqrt{a_{11}a_{22}}} \frac{\partial\sqrt{a_{22}}}{\partial x'} \tag{68}$$

where $C_{16} \neq \cos\bar{\omega}$ and $C_{16}\cos\bar{\omega} \neq 1$.
The following definitions will now be made,

$$C_{17} = \frac{1}{1-\frac{\cos\bar{\omega}}{C_{16}}} \quad ; \quad C_{16} \neq \cos\bar{\omega}$$

$$C_{18} = \frac{1}{1-C_{16}\cos\bar{\omega}} \quad ; \quad C_{16} \neq \frac{1}{\cos\bar{\omega}} \tag{69}$$

Substituting Equations (67), (68) and (69) into the O.D.E. Conditions (65) they become,

$$\textcircled{1} \quad q^2$$

$$\textcircled{2} \quad \frac{1}{\sqrt{a_{11}}} \frac{\partial\bar{U}'}{\partial x'}$$

$$\textcircled{3} \quad \frac{\bar{U}^2}{\sqrt{a_{22}}} \frac{\partial \ln\bar{U}'}{\partial x^2} - C_{17}\bar{U}^2 \frac{1}{\sqrt{a_{11}a_{22}}} \frac{\partial\sqrt{a_{11}}}{\partial x^2} \tag{70}$$

$$\textcircled{4} \quad \frac{(\bar{U}^2)^2}{\bar{U}'} C_{18} \frac{1}{\sqrt{a_{11}a_{22}}} \frac{\partial\sqrt{a_{22}}}{\partial x'}$$

$$\textcircled{5} \quad \bar{U}' C_{18} \frac{1}{\sqrt{a_{11}a_{22}}} \frac{\partial\sqrt{a_{22}}}{\partial x'} - \frac{\bar{U}'}{2\sqrt{a_{11}}} \frac{\partial \ln q^2}{\partial x'}$$

$$⑥ \quad -\bar{U}^2 C_{17} \frac{1}{\sqrt{a_{11}a_{22}}} \frac{\partial \sqrt{a_{11}}}{\partial x^2} + \frac{\bar{U}^2}{2\sqrt{a_{22}}} \frac{\partial \ln g^2}{\partial x^2}$$

$$⑦ \quad \frac{1}{\sqrt{a_{22}}} \frac{\partial \bar{U}^2}{\partial x^2}$$

$$⑧ \quad \frac{\bar{U}'}{\sqrt{a_{11}}} \frac{\partial \ln \bar{U}^2}{\partial x'} + \bar{U}' C_{18} \frac{1}{\sqrt{a_{11}a_{22}}} \frac{\partial \sqrt{a_{22}}}{\partial x'}$$

(70) Cont'd.

$$⑨ \quad -\frac{(\bar{U}')^2}{\bar{U}^2} C_{17} \frac{1}{\sqrt{a_{11}a_{22}}} \frac{\partial \sqrt{a_{11}}}{\partial x^2}$$

These O.D.E. conditions are now compared with those found by Hansen [34] for the orthogonal curvilinear case. The O.D.E. conditions for the orthogonal curvilinear case (34) are

$$① \quad g^2$$

$$② \quad \frac{1}{h_1} \frac{\partial \bar{U}'}{\partial x'}$$

$$③ \quad \frac{\bar{U}^2}{h_2} \frac{\partial \ln \bar{U}'}{\partial x^2} + \bar{U}^2 \frac{1}{h_1 h_2} \frac{\partial h_1}{\partial x^2}$$

$$④ \quad \frac{(\bar{U}^2)^2}{\bar{U}'} \frac{1}{h_1 h_2} \frac{\partial h_2}{\partial x'}$$

$$⑤ \quad \bar{U}' \frac{1}{h_1 h_2} \frac{\partial h_2}{\partial x'} - \frac{\bar{U}'}{2h_1} \frac{\partial h_1 q^2}{\partial x'}$$

$$⑥ \quad \bar{U}^2 \frac{1}{h_1 h_2} \frac{\partial h_1}{\partial x^2} - \frac{\bar{U}^2}{2h_2} \frac{\partial h_1 q^2}{\partial x^2}$$

$$⑦ \quad \frac{1}{h_2} \frac{\partial \bar{U}^2}{\partial x^2}$$

$$⑧ \quad \frac{\bar{U}'}{h_1} \frac{\partial h_1 \bar{U}^2}{\partial x'} + \bar{U}' \frac{1}{h_1 h_2} \frac{\partial h_2}{\partial x'}$$

$$⑨ \quad \frac{(\bar{U}')^2}{\bar{U}^2} \frac{1}{h_1 h_2} \frac{\partial h_1}{\partial x^2}$$

In Reference [34] the h_α by definition is

$$h_\alpha = \left(\frac{\partial S}{\partial x^\alpha}\right)$$

where S is the distance measured along the curve x^α equals a variable on the surface. This is by definition precisely equal to $\sqrt{a_{\alpha\alpha}}$ in this analysis. Therefore the two sets of O.D.E. conditions are equivalent except for the constants C_{17} and C_{18} in O.D.E. conditions ③ , ⑤ , ⑥ , and ⑧ . Although it was not done so in Reference 34, it can be established, by the same argument as was used proceeding Conditions (65), that under the conditions of (34) the individual terms of each

O.D.E. conditions must be proportional. In view of this, the constants C_{17} and C_{18} do not constitute real differences between the two sets of O.D.E. conditions because they can always be absorbed in the proportionality constant. Hence the requirements for similarity which are obtained from the solution of the O.D.E. conditions in Reference 33 are precisely the requirements for similarity needed in this analysis when the requirements from (33) are referred to a constant angle curvilinear coordinate system.

No restrictions have been placed on the magnitude of the angle $\bar{\omega}$ between the coordinate lines. The special case of $\bar{\omega} = \frac{\pi}{2}$, of the analysis presented here, is the orthogonal coordinate case.

The additional O.D.E. conditions (10) → (16) from the energy equation can be reduced under the conditions of constant angle coordinates and $\frac{K}{\sigma_1^2}$ or $\frac{K}{\sigma_2^2}$ being constant.

O.D.E. conditions (10) and (11) can be expanded using Equations (35) and (8) becoming,

$$(10)\quad \bar{U}' \frac{\sin\bar{\omega}}{\sqrt{a}} \frac{\partial\sqrt{a_{22}}}{\partial x'} + \frac{\bar{U}'}{\sqrt{a_{11}}} \frac{\partial \ln\sqrt{a_{11}}}{\partial x'} - \frac{\bar{U}'}{\sqrt{a_{11}}} \frac{\partial \ln q}{\partial x'}$$

$$(11)\quad \bar{U}^2 \frac{\sin\bar{\omega}}{\sqrt{a}} \frac{\partial\sqrt{a_{11}}}{\partial x^2} + \frac{\bar{U}^2}{\sqrt{a_{22}}} \frac{\partial \ln\sqrt{a_{22}}}{\partial x^2} - \frac{\bar{U}^2}{\sqrt{a_{22}}} \frac{\partial \ln q}{\partial x^2}$$

By Equations (40) and (41), O.D.E. (10) and (11) become,

$$(10)\ \bar{U}'\frac{\sigma_2}{\sin\bar{\omega}} - \bar{U}'\cot\bar{\omega}\,\sigma_1 + \frac{\bar{U}'}{\sqrt{a_{11}}}\frac{\partial \ln\sqrt{a_{11}}}{\partial x'} - \frac{\bar{U}'}{\sqrt{a_{11}}}\frac{\partial \ln q}{\partial x'}$$

$$(11)\ -\frac{\bar{U}^2\sigma_1}{\sin\bar{\omega}} + \bar{U}^2\cot\bar{\omega}\,\sigma_2 + \frac{\bar{U}^2}{\sqrt{a_{22}}}\frac{\partial \ln\sqrt{a_{22}}}{\partial x^2} - \frac{\bar{U}^2}{\sqrt{a_{22}}}\frac{\partial \ln q}{\partial x^2} \qquad (71)$$

The first and last terms of O.D.E. (10) and (11) are exactly equal to O.D.E. (5) and (6) respectively and hence are already satisfied and need not be included. The second terms in each O.D.E. (10) and (11) are of the same form as O.D.E. (4) or (9), as shown in Conditions (64) and therefore may be removed here. Hence O.D.E. (10) and (11) reduce to

$$(10)\ \frac{\bar{U}'}{a_{11}}\frac{\partial\sqrt{a_{11}}}{\partial x'}$$

$$(11)\ \frac{\bar{U}^2}{a_{22}}\frac{\partial\sqrt{a_{22}}}{\partial x^2} \qquad (72)$$

Upon changing to physical components, it is clear that with constant angle coordinates and proportional mainstream components that O.D.E. Conditions (14), (15) and (16) differ only by a constant and therefore may be reduced to only one condition,

(14) $\frac{g^2}{T^*}(\bar{U}')^2$.

Therefore the O.D.E. conditions from the energy equation for $\frac{K}{\sigma_1^2}$ or $\frac{K}{\sigma_2^2}$ equal to a constant are,

$$
\begin{aligned}
&(10)\quad \frac{\bar{U}'}{a_{11}}\frac{\partial\sqrt{a_{11}}}{\partial x'}\\
&(11)\quad \frac{\bar{U}^2}{a_{22}}\frac{\partial\sqrt{a_{22}}}{\partial x^2}\\
&(12)\quad \frac{\bar{U}'}{\sqrt{a_{11}}}\frac{\partial \ln T^*}{\partial x'}\\
&(13)\quad \frac{\bar{U}^2}{\sqrt{a_{22}}}\frac{\partial \ln T^*}{\partial x^2}\\
&(14)\quad \frac{g^2}{T^*}(\bar{U}')^2
\end{aligned}
\qquad (73)
$$

If viscous dissipation is neglected O.D.E. condition (14) of Conditions (73) need not be satisfied.

Therefore Conditions (65) and (73) constitute the O.D.E. conditions for the boundary layer momentum and energy equations when the surface and imbedded constant angle coordinate system are such that $\frac{K}{\sigma_1^2}$ or $\frac{K}{\sigma_2^2}$ are constant.

2. Coordinate Systems for which $K = \sigma_1 = \sigma_2 = 0$.

Again the assumption of constant angle coordinates is made and in addition it will be assumed that at most a constant change of scale occurs along a coordinate line. In this system, where the Gaussian curvature is zero, the two dimensional Riemmanian space is said to be developable or isometric with the Euclidean plane. When the surface is the Euclidean plane the constant angle geodesic coordinate lines consist of two coplanar sets of equally spaced lines parallel, in the Euclidean sense, and intersecting at any angle $\bar{\omega}$. When the angle $\bar{\omega}$ is $\frac{\pi}{2}$ this is the common Cartesian coordinate system of the plane.

If, to O.D.E. Conditions (42), which arise from the momentum equations with constant angle coordinates, the additional restriction of $\sigma_1 = \sigma_2 = 0$ is applied, the following O.D.E. conditions are obtained:

$$\textcircled{1} \quad g^2$$

$$\textcircled{2} \quad \frac{1}{\sqrt{a_{11}}} \frac{\partial \bar{U}'}{\partial x'} \tag{74}$$

$$\textcircled{3} \quad \frac{\bar{U}^2}{\sqrt{a_{22}}} \frac{\partial \ln \bar{U}'}{\partial x^2}$$

$$⑤ \quad \frac{\bar{U}'}{\sqrt{a_{11}}} \frac{\partial \ln q}{\partial x'}$$

$$⑥ \quad \frac{\bar{U}^2}{\sqrt{a_{22}}} \frac{\partial \ln q}{\partial x^2}$$

(74) Cont'd.

$$⑦ \quad \frac{1}{\sqrt{a_{22}}} \frac{\partial \bar{U}^2}{\partial x^2}$$

$$⑧ \quad \frac{\bar{U}'}{\sqrt{a_{11}}} \frac{\partial \ln \bar{U}^2}{\partial x'}$$

Under the conditions that $K = \sigma_1 = \sigma_2 = 0$ and at most a constant scale change is allowed to occur along a coordinate line, the metric components a_{11} and a_{22} are constant. Therefore the following coordinate transformation can be made

$$\bar{x}^\alpha = \sqrt{a_{\alpha\alpha}}\, x^\alpha \qquad \text{(No sum on } \alpha\text{)} \tag{75}$$

Then O.D.E. Conditions (74) become,

$$① \quad q^2$$

$$② \quad \frac{\partial \bar{U}'}{\partial \bar{x}'} \tag{76}$$

③ $\bar{U}^2 \frac{\partial \ln \bar{U}'}{\partial \bar{X}^2}$

⑤ $\bar{U}' \frac{\partial \ln g}{\partial \bar{X}'}$

⑥ $\bar{U}^2 \frac{\partial \ln g}{\partial \bar{X}^2}$ (76) Cont'd.

⑦ $\frac{\partial \bar{U}^2}{\partial \bar{X}^2}$

⑧ $\bar{U}' \frac{\partial \ln \bar{U}^2}{\partial \bar{X}'}$

These O.D.E. conditions are exactly the same as those found and solved by Hansen [34] for the case of rectangular coordinates. Therefore the above O.D.E. conditions show that the requirements for similarity in rectangular coordinates found in Reference 34 are also the requirements for similarity when referred to constant angle geodesic coordinates on a developable surface.

O.D.E. conditions ⑩→⑯ , for the energy equation are now considered for this case. O.D.E. conditions ⑩ and ⑪ for constant angle are found in condition (71). Applying the conditions of $\sigma_1 = \sigma_2 = 0$, the metric tensor components equal to a constant,

and the change of coordinates shown in Equation (75), they become,

$$(10) \quad -\bar{U}' \frac{\partial \ln g}{\partial \bar{x}'}$$

$$(11) \quad -\bar{U}^2 \frac{\partial \ln g}{\partial \bar{x}^2}$$

From O.D.E. conditions (5) and (6), (76), it is noted that both (10) and (11) are required to be proportional to g^2 or identically zero and therefore O.D.E. conditions (10) and (11) are already satisfied and may be dropped.

Now, with O.D.E. (12)→(16) written in terms of physical velocity components and the new coordinates $\bar{x}^1$ and $\bar{x}^2$ the energy equation O.D.E. conditions become,

$$(12) \quad \bar{U}' \frac{\partial \ln T^*}{\partial \bar{x}'}$$

$$(13) \quad \bar{U}^2 \frac{\partial \ln T^*}{\partial \bar{x}^2}$$

$$(14) \quad \frac{g^2}{T^*} (\bar{U}')^2$$

$$(15) \quad \frac{g^2}{T^*} \cos\bar{\omega}\, \bar{U}' \bar{U}^2$$

(16) $\frac{g^2}{T^*}(\bar{U}^2)^2$

It is clear from O.D.E. (14) and (16) that the mainstream velocity components must be proportional if similarity solutions of the energy equation are to be obtained. But, because of the type surface and coordinate system in this section, if the mainstream velocity components are proportional there would be no three dimensional boundary layers generated. That is, the mainstream streamlines would be straight lines when the surface is the Euclidean plane and a simple rotation of the coordinate system to aline one coordinate line with the mainstream streamline will show this to be a two dimensional problem. O.D.E. Conditions (14)→(16), from which this requirement is obtained, are from the viscous dissipation term in the energy equation. Consequently to obtain similarity solutions to the energy equation for three dimensional boundary layer flows on developable surfaces and constant angle geodesic coordinates, viscous dissipation must be neglected.

In this case the O.D.E. conditions for the energy equation become,

$$\begin{aligned} &(12)\quad \bar{U}^1 \frac{\partial \ln T^*}{\partial \bar{x}^1} \\ &(13)\quad \bar{U}^2 \frac{\partial \ln T^*}{\partial \bar{x}^2} \end{aligned} \tag{77}$$

Therefore Conditions (76) and (77) constitute the O.D.E. conditions for the boundary-layer momentum and energy equations (neglecting viscous dissipation) when the surface is developable and the imbedded coordinate system is constant angle and geodesic.

C. Solutions of the Conditions for Similarity

Proportionality between the various O.D.E. conditions presented in the last two sections constitute systems of partial differential equations which, when solved, yield the requirements for the existence of similarity solutions of the boundary-layer momentum and energy equations.

1. Coordinate System for which $\frac{K}{\sigma_1^2}$ or $\frac{K}{\sigma_2^2}$ is constant.

Conditions (65) constitute the O.D.E. conditions for the momentum equations in this case. As was shown in Conditions (70) these O.D.E. conditions are identical to those already analyzed in Reference 34 for the orthogonal case.

It has been shown in Reference 34 that the most general form of the metric components in Conditions (65) is

$$\sqrt{a_{11}} = (b_1 x' + b_2 x^2)^n$$
$$\sqrt{a_{22}} = (b_1 x' + b_2 x^2)^n \qquad (78)$$

For the constant angle case it is known from Equation (34) that $a_{12} = \sqrt{a_{11} a_{22}} \cos \bar{\omega}$, therefore in this general metric tensor the a_{12} is

$$a_{12} = \cos\varpi\,(b_1 x^1 + b_2 x^2)^{2n} \tag{79}$$

Therefore the differential quadric

$$(ds)^2 = a_{11}(dx^1)^2 + a_{22}(dx^2)^2 + 2a_{12}\,dx^1\,dx^2$$

becomes

$$(ds)^2 = (b_1x^1+b_2x^2)^{2n}\left[(dx^1)^2 + (dx^2)^2 + 2\cos\varpi\,dx^1\,dx^2\right]$$

Now perform the following orthogonal transformation

$$x^1 = x^{1*}\sin\alpha - x^{2*}\cos\alpha$$

$$x^2 = x^{1*}\cos\alpha + x^{2*}\sin\alpha$$

where α is constant. The differential quadric becomes,

$$(ds)^2 = \left[(b_1\sin\alpha+b_2\cos\alpha)\,x^{1*} + (b_2\sin\alpha-b_1\cos\alpha)x^{2*}\right]^{2n}$$

$$\left[(1+2\cos\varpi\sin\alpha\cos\alpha)(dx^{1*})^2 + (1-2\cos\varpi\sin\alpha\cos\alpha)(dx^{2*})^2\right.$$

$$\left.+2\cos\varpi(\sin^2\alpha-\cos^2\alpha)\,dx^{1*}\,dx^{2*}\right]$$

Since α was arbitrary it is possible to choose α such that

$$b_1 \sin\alpha + b_2 \cos\alpha = 0$$

Then

$$(ds)^2 = c^2 (x^{2*})^{2n} \Big[(1+\ell)(dx^{1*})^2 + (1-\ell)(dx^{2*})^2$$

$$+ 2\cos\bar{\omega} (\sin^2\alpha - \cos^2\alpha)\, dx^{1*} dx^{2*} \Big]$$

where $c = (b_2 \sin\alpha - b_1 \cos\alpha)^n$ and

$$\ell = 2\cos\bar{\omega} \sin\alpha \cos\alpha .$$

If the following transformation is performed,

$$\bar{x}^1 = c \left(\frac{n+1}{c}\right)^{\frac{n}{n+1}} (1+\ell)^{1/2}\, x^{1*}$$

$$\bar{x}^2 = \left(\frac{c}{n+1}\right)^2 (1-\ell)^{1/2} (x^{2*})^{n+1}$$

where $n \neq -1$, the differential quadric becomes,

$$(ds)^2 = \left(\frac{c}{n+1}\right)^{-\frac{2n}{n+1}} (1-\ell)^{-\frac{n}{n+1}} (\bar{x}^2)^{\frac{2n}{n+1}} (d\bar{x}^1)^2$$

$$+ (d\bar{x}^2)^2$$

$$+\frac{2\cos\bar{\omega}\,(\sin^2\alpha-\cos^2\alpha)\left(\frac{c}{n+1}\right)^{-\frac{n}{n+1}}(1-\ell)^{-\frac{n}{2n+2}}(\bar{\chi}^2)^{\frac{n}{n+1}}}{\left[(1+\ell)(1-\ell)\right]^{1/2}}\,d\bar{\chi}^1 d\bar{\chi}^2 \qquad (80)$$

From the above it is noted that the general metric components obtained from the O.D.E. Conditions (65) can always be transformed, without loss of generality to systems for which a_{22} is unity. This fact was also proven and used in Reference 34 for orthogonal systems.

Because $a_{22} = 1$ in Reference 34 and here, the results of (34) may be extrapolated. In Reference 34 three sets of solutions of the conditions for similarity were found to exist. They are:

Case I: $\dfrac{K}{\sigma_1^2} = \dfrac{K}{\sigma_2^2}$ = constant

$$\sqrt{a_{11}} = (\chi^2)^n \;,\; \sqrt{a_{22}} = 1 \;,\; n \neq 0,1$$

$$\bar{U}^1 = A_1\bar{U}^2 = A_2(\chi^2)^m$$

$$q^2 = A_3\frac{\bar{U}^1}{\chi^2}$$

Case II: K = constant (nonzero) and σ_1 and σ_2 constants,

$$\sqrt{a_{11}} = e^{n\chi^2} \;,\; \sqrt{a_{22}} = 1 \;,\; n \neq 0$$

$$\bar{U}^1 = A_1\bar{U}^2 = A_2 e^{m\chi^2}$$

$$g^2 = A_3 \bar{U}'$$

Case III: $K = 0$, $\sigma_1^2 + \sigma_2^2 = 0$,

$$\sqrt{a_{11}} = x^2 \quad , \quad \sqrt{a_{22}} = 1$$

$$\bar{U}' = A_1 \bar{U}^2 = A_2 (x^2)^n e^{m x^1}$$

$$g^2 = A_3 \frac{\bar{U}'}{x^2} .$$

To obtain the requirements for similarity solutions of the energy equation, for each of the above cases, O.D.E. conditions (10)→(14), of Conditions (73), must be satisfied. O.D.E. Conditions (10) and (11) are identically zero for each case because a_{11} is not a function of x^1 and a_{22} is not a function of x^2 in any of the cases.

O.D.E. (14), of Conditions (73), when set proportional to O.D.E. (1), requires that

$$T^* = A_4 (\bar{U}')^2 \tag{81}$$

If this is substituted into O.D.E. (12) and (13) of Conditions (73) these reduce identically to O.D.E. (2) and (7) of Conditions (70) respecitvely and are therefore satisfied.

Therefore Equation (81) constitutes the only additional requirement needed to obtain similarity solutions of the energy equation in

in Cases I, II, III, when viscous dissipation is included.

When viscous dissipation is neglected O.D.E. condition (14) no longer needs to be satisfied. Hence O.D.E. (12) and (13) must be proportional to, say, g^2 (O.D.E. (1)), where g^2 is obtained from each of the above cases. Solving these for each of Cases I→III relations for T^*, the wall-fluid temperature difference, are obtained. They are:

Case I:

$$T^* = A_4(\chi^2)^b \tag{82}$$

Case II:

$$T^* = A_4 e^{b\chi^2} \tag{83}$$

Case III:

$$T^* = A_4(\chi^2)^r e^{s\chi'} \tag{84}$$

It should be noted that when viscous dissipation is neglected a condition of constant T^*, constant wall-fluid temperature difference, will always yield a similarity solution of the energy equation if the momentum equation yields a similarity solution, whereas when viscous dissipation is included this is only true if the mainstream velocity components $\bar{U}^1$ and $\bar{U}^2$ are also constant.

2. Coordinate Systems for which $K = \sigma_1 = \sigma_2 = 0$.

Conditions (76) constitute the O.D.E. conditions for the momentum equations of these systems. These are exactly the same conditions that have been completely analyzed by Hansen [34] for the

rectangular coordinate case. Therefore it has been shown that the requirements for similarity obtained in Reference 34 are also the requirements for similarity when these requirements and the governing equations are referred to the non orthogonal constant angle coordinate system.

In Reference 34 four sets of requirements for similarity were obtained. In the notation used here they are:

Case IV: $\sqrt{a_{11}} = \sqrt{a_{22}} = 1$

$$\bar{U}' = A_1 e^{n\chi'} (\chi^2)^{m-1}$$

$$\bar{U}^2 = A_2 e^{n\chi'} (\chi^2)^{m}$$

$$g^2 = A_3 \bar{U}'$$

Case V: $\sqrt{a_{11}} = \sqrt{a_{22}} = 1$

$$\bar{U}' = A_1 (\chi')^n (\chi^2)^{m-1}$$

$$\bar{U}^2 = A_2 (\chi')^{n-1} (\chi^2)^{m}$$

$$g^2 = A_3 \frac{\bar{U}'}{\chi'}$$

Case VI: $\sqrt{a_{11}} = \sqrt{a_{22}} = 1$

$$\bar{U}' = A_1 (\chi')^n$$

$$\bar{U}^2 = A_2 (\chi')^m$$

$$g^2 = A_3 \frac{\bar{U}^1}{\chi'}$$

Case VII $\sqrt{a_{11}} = \sqrt{a_{22}} = 1$

$$\bar{U}^1 = A_1 e^{n\chi'}$$

$$\bar{U}^2 = A_2 e^{m\chi'}$$

$$g^2 = A_3 \bar{U}^1$$

To obtain the requirements for similarity solutions of the energy equation, for each of the above cases, O.D.E. conditions (12) and (13), Conditions (77), must be satisfied. Setting these conditions proportional to g^2 in each of Cases IV→VII will give equations which can be solved for T^*.

The results are:

Case IV:

$$T^* = A_4 e^{r\chi'} (\chi^2)^s$$

Case V:

$$T^* = A_4 (\chi')^r (\chi^2)^s$$

Case VI:

$$T^* = A_4 (\chi')^r e^{s\chi^2}$$

where S = 0 if $m \neq n - 1$,

Case VII:

$$T^* = A_4 e^{r\chi'}.$$

Again it is noted that $T^* = \text{const.}$ will always yield similarity solutions of the energy equation when viscous dissipation is neglected and when the momentum equation admits to a similarity solution.

3. Comments on Mainstream Velocity Components

The mainstream velocity components $[\ \bar{U}^1,\ \bar{U}^2\ ]$ are the values of the non-viscous solution evaluated at the surface. These components are the only quantities of the non-viscous flow which this analysis will specify explicitly. To determine the non-viscous mainflow the surface shape must be specified completely but, as will be seen in the following section, this analysis only demands that the surfaces be of a given class. The determination of the classes of non-viscous flows which have surface components of the form required over the general classes of surfaces required is an investigation in its own right and has not been attempted here. In such an investigation the analyticity of the non-viscous flow may place further restrictions on the above systems which admit the boundary layer equations to similarity solutions.

In the required forms of the mainflow velocity components at the surface, a negative exponent would correspond to a decelerating flow or flow with an adverse pressure gradient. In such systems there is a strong tendency toward separation in which case neither the boundary layer assumptions nor the assumed similarity transformations are valid and the analysis can't be used.

D. Classes of the Admissible Surfaces and Imbedded Coordinate Systems

Knowing the metric coefficients for each case, the admissible types of surfaces and imbedded coordinate systems can be obtained through the use of the intrinsic differential geometry of surfaces.

1. Case I, $\sqrt{a_{11}} = (\chi^2)^n$, $\sqrt{a_{22}} = 1$.

The differential quadric of the coordinate system is

$$(ds)^2 = \left[(\chi^2)^n d\chi^1\right]^2 + \left[d\chi^2\right]^2 + 2\cos\bar{\omega}\,(\chi^2)^n d\chi^1 d\chi^2 \tag{85}$$

If the coordinates are transformed by,

$$\chi^1 = \frac{\cos\bar{\omega}}{1-n}\left[\frac{\sin\bar{\omega}}{\cos\bar{\omega}}\,\bar{\chi}^1 - \bar{\chi}^2\right]$$

$$\chi^2 = (\bar{\chi}^2)^{\frac{1}{1-n}} \qquad n \neq 0,1 \tag{86}$$

the differential quadric on the surface in the new coordinate system becomes,

$$(ds)^2 = \left[\frac{\sin\bar{\omega}}{1-n}(\bar{\chi}^2)^{\frac{n}{1-n}}\right]^2\left[(d\bar{\chi}^1)^2 + (d\bar{\chi}^2)^2\right], \quad n \neq 0,1 \tag{87}$$

A theorem from Eisenhart (33, p. 108) states;

When the linear element of a surface is reducible to the form

$$(ds)^2 = \lambda\left[(du)^2 + (dv)^2\right] \tag{88}$$

where λ is a function of u or v alone, the surface is applicable to a surface of revolution.

The significance of the term "applicable" is that the portion of one surface in the neighborhood of every point can be so bent as to

be made to coincide with the corresponding portion of the other surface without stretching or duplication. The application of one surface upon another necessitates a continuous array of surfaces applicable to both surfaces. The process of transformation is called deformation and one surface is called the deform of the other.

Another theorem from Eisenhart (33, p. 156) states:

> Two applicable surfaces have the same total curvature, K, at corresponding points.

Two surfaces with the same quadric differential form (or linear element, i.e. Equation (88) in this case) are applicable, but the fact that the quadric differentials of two surfaces are unlike is not a sufficient condition to prove that they are not applicable. An example of this fact is the difference in the quadric differential forms of the polar and Cartesian coordinates of the plane.

The problem of determining the necessary and sufficient conditions for two surfaces to be applicable is known as the "Problem of Minding" (33, p. 321), being named for the man who first proposed it. The results of the "Problem of Minding" which pertain to surfaces of revolution with variable Gaussian curvature are given in the following theorem (33, p. 326);

The equations

$$\Delta_1 K = f(K) \quad , \quad \Delta_2 K = \phi(K) \tag{89}$$

constitute a necessary and sufficient condition that a surface be applicable to a surface of revolution.

In Equation (89) f(K) and $\phi(K)$ represent arbitrary functions of K, the Gaussian curvature of the surface, and Δ_1 and Δ_2 represent the first and second order differential parameters,

$$\Delta_1 K \equiv \frac{a_{11}\left(\frac{\partial K}{\partial x^2}\right)^2 - 2a_{12}\frac{\partial K}{\partial x^1}\frac{\partial K}{\partial x^2} + a_{22}\left(\frac{\partial K}{\partial x^1}\right)^2}{a}$$

$$\Delta_2 K \equiv \frac{1}{\sqrt{a}}\left[\frac{\partial}{\partial x^1}\left(\frac{a_{22}\frac{\partial K}{\partial x^1} - a_{12}\frac{\partial K}{\partial x^2}}{\sqrt{a}}\right) + \frac{\partial}{\partial x^2}\left(\frac{a_{11}\frac{\partial K}{\partial x^2} - a_{12}\frac{\partial K}{\partial x^1}}{\sqrt{a}}\right)\right]$$

which are invariants of the surface.

Therefore the necessary and sufficient conditions for a surface to be admissible in this case are:

$$\begin{aligned} \Delta_1 K &\equiv -\frac{4}{n(n-1)} K^3 \\ \Delta_2 K &\equiv \frac{2(n-3)\sin^2\bar{\omega}}{n(n-1)} K^2 \end{aligned} \tag{90}$$

A particular example of a class of surfaces which are applicable to surfaces of revolution are the helicoids. The theorem of Bour (33, p. 147) states:

> Every helicoid is applicable to some surface of revolution, and helices on the first correspond to the parallels on the latter.

Helicoids are generated by revolving a space curve about a fixed line axis and at the same time translating the curve along the axis at a velocity which is in a constant ratio with the velocity of rotation. For the differential quadratic of the form of Equation (88) on a

helicoid the lines of constant u would be the helices and the lines of constant v would be the orthogonal trajectories of the helices. A section of the helicoid by a plane through the axis of rotation is called the meridian. The meridians of a helicoid and the surface of revolution to which it is applicable are not the same unless the surfaces are also developable in which case the meridian curves are straight lines.

In the following analysis only the surface of revolution itself will be discussed without considering other applicable surfaces.

The surface of revolution corresponding to a differential quadric of the form of Equation (88) is analyzed in Reference 33, p. 109. For the particular differential quadric under consideration, namely Equation (87), the equation of the meridian curve or generatrix in three dimensional space is

$$z = \int \left\{ \left[\frac{(1-n)^{1/n}}{n} \left(\frac{r}{\sin\bar{\omega}} \right)^{\frac{1-n}{n}} \right]^2 - 1 \right\}^{1/2} dr \quad , n \neq 0,1 \tag{91}$$

where z is the axis of revolution and r the distance from the meridian to the z axis. Also the following relation exists between r and the coordinates on the surface

$$r = \sqrt{\lambda} \tag{92}$$

where $\lambda = \lambda(u)$ in Equation (88) and in the particular case under consideration

$$r = \frac{\sin\bar{\omega}}{1-n} \left(\bar{\chi}^2 \right)^{\frac{n}{1-n}} \quad , n \neq 0,1 \tag{93}$$

Consequently the lines $\bar{x}^2$ = constant, the $\bar{x}^1$ coordinate lines, are the parallels of the surface. That is, the circles described by a point on the generatrix as the generatrix is rotated about the axis of revolution. The $\bar{x}^1$ = constant lines, the $\bar{x}^2$ coordinate lines, are the meridians or generatrices of the surface.

Returning to the original coordinates (x^1, x^2), at constant angle $\bar{\omega}$, by the transformation, Equation (86), it is now known that the lines of x^2 = constant, the x^1 coordinate lines, are also the parallels of the surface. The lines x^1 = constant, the x^2 coordinate lines, must intersect the x^1 coordinate lines at constant angle $\bar{\omega}$. These must be, by definition, the loxodromic curves of the surface of revolution. The equation of the x^2 coordinate lines, the loxodromes, as a function of the orthogonal $\bar{x}^1$, $\bar{x}^2$ coordinates on the surface is

$$b_1 \bar{\chi}^1 + b_2 \bar{\chi}^2 + b_3 = 0 \tag{94}$$

where b_1, b_2, b_3 are constants. When the coordinate angle $\bar{\omega}$ is $\frac{\pi}{2}$ the x^2 coordinate lines coincide with the meridians of the surface.

Combining Equation (93) and the second of Equations (86) the relation between the x^2 coordinate and the distance r from the axis of revolution to the surface is

$$r = \frac{\sin \bar{\omega}}{1-n} (\chi^2)^n \quad , n \neq 0,1 \tag{95}$$

By consideration of the metric components and the relation for the Gaussian curvature of the surface, it is known that

$$K = -\frac{n(n-1)}{\sin^2 \bar{\omega} \, (\chi^2)^2} \quad , n \neq 0,1 \tag{96}$$

From this the following can be noted: if (a) $n > 1$ or $n < 0$ the surface is one of negative total curvature, and if (b) $0 < n < 1$ the surface is one of positive total curvature. The possibility of $n = 0$ or 1 has already been excluded because the analysis of this case assumed from the beginning that the surface was nondevelopable.

Consideration of the derivative of Equation (91) with respect to r, which is

$$\frac{dz}{dr} = \left\{ \left[\frac{(1-n)^{\frac{1}{n}}}{n} \left(\frac{r}{\sin\bar{\omega}} \right)^{\frac{1-n}{n}} \right]^2 - 1 \right\}^{1/2} \quad , n \neq 0,1 \tag{97}$$

gives some indication of the shapes of the surfaces of revolution involved. Figure (2) depicts the shapes of the generatrices of the surfaces.

In Figure (2), r^* are those values of r at which the quantity under the radical of Equation (91) becomes zero.

That is

$$r^* = \sin\bar{\omega} \left(\frac{n}{(1-n)^{\frac{1}{n}}} \right)^{\frac{n}{1-n}} \quad , n \neq 0,1 \tag{98}$$

The surfaces only exist for values of r where the integrand of Equation (91) is real. Therefore for values of n such that $n < 0$ or $n > 1$, $r < r^*$ and for values of n such that $0 < n < 1$, $r > r^*$ give the ranges of r for which the surface exists. Also, because this integrand must be real, it is noted that only specific values of n are allowable in the range $n > 1$. These values are all the odd integers in this range. That is $n = 2m + 1$, $m = 1, 2, 3, \ldots\ldots\ldots$. In the other range of values of n there are no restrictions; n can have any real value, integral or not.

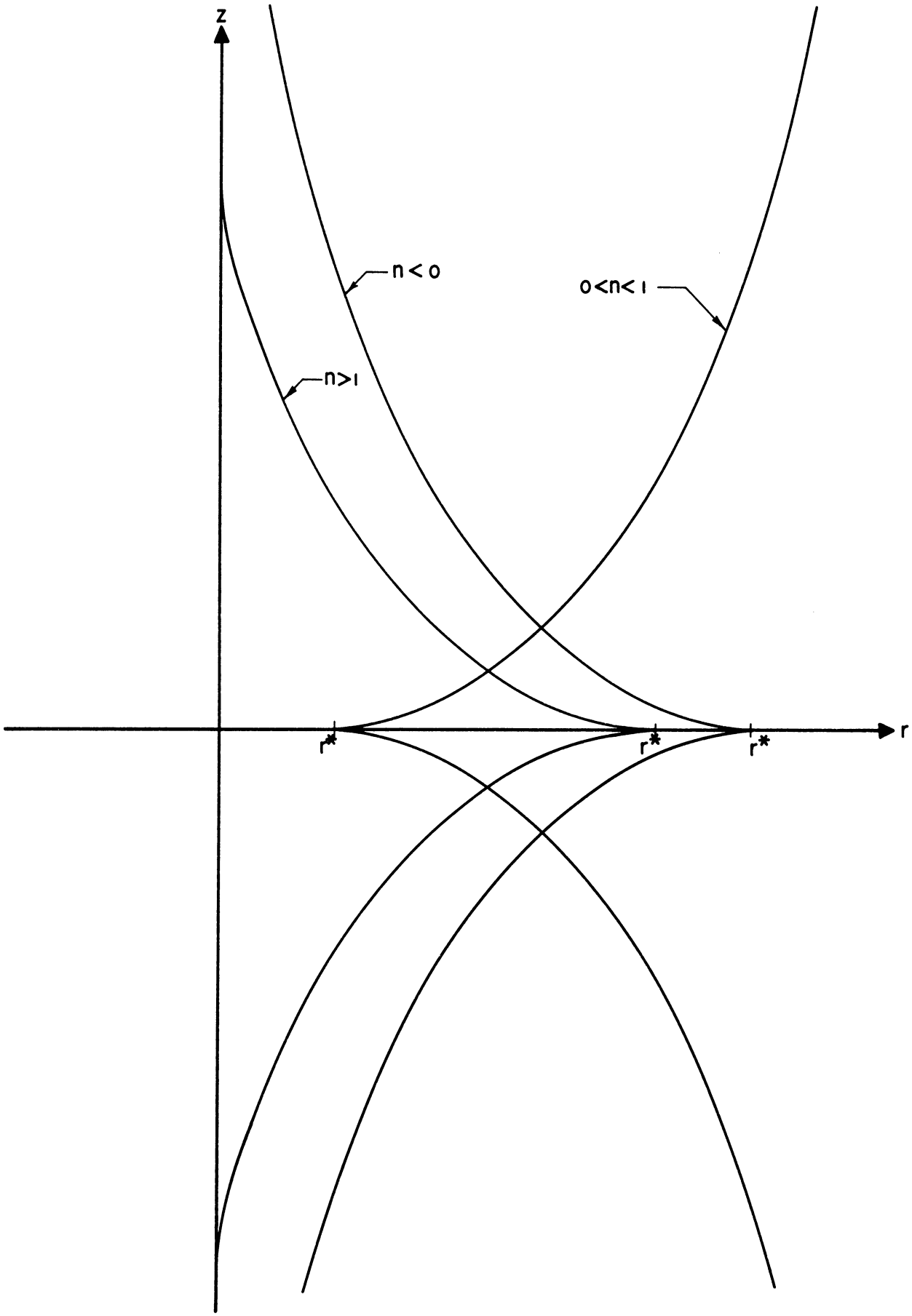

Figure 2. Generatrix Shapes for Surfaces of Revolution for Case I.

From the above restrictions on r for the various ranges of n, and Equation (95), relating r to the x^2 coordinate, it is clear that for $n < 0$ and $0 < n < 1$ that the location of the x^2 origin ($x^2 = 0$) is not on the surface. This may raise serious doubt, for physical reasons, as to whether or not these surfaces are acceptable. But this difficulty may not be encountered on other surfaces which are applicable to these. For the case of $n > 0$, n being any of the old integers beginning with three, the integration of Equation (91) gives a relation for which r is zero for periodic values of z. Hence the x^2 origin is on the z axis.

2. Case II, $\sqrt{a_{11}} = e^{nx^2}$, $\sqrt{a_{22}} = 1$.

The differential quadric is

$$(ds)^2 = (e^{nx^2}dx')^2 + (dx^2)^2 + 2\cos\bar{\omega}\, e^{nx^2}dx'dx^2 \tag{99}$$

If the coordinates are transformed by

$$x' = \frac{\cos\bar{\omega}}{n}\left(\bar{x}^2 + \frac{\sin\bar{\omega}}{\cos\bar{\omega}}\,\bar{x}'\right) \qquad n \neq 0 \tag{100}$$

$$x^2 = -\frac{\ln\bar{x}^2}{n}$$

the differential quadric becomes

$$(ds)^2 = \left(\frac{\sin\bar{\omega}}{n\bar{x}^2}\right)^2\left[(d\bar{x}')^2 + (d\bar{x}^2)^2\right] \tag{101}$$

By the theorem from Eisenhart, quoted in the last section it is known that the admissible surfaces in this case must also be applicable to a surface of revolution.

The equation for the generatrix of the surface revolution being,

$$z = \int \left\{ \left(\frac{\sin \bar{\omega}}{nr} \right)^2 - 1 \right\}^{1/2} dr \quad , \; n \neq 0 \tag{102}$$

Again, the coordinate lines are the parallels and the loxodromes. The following relation exists between the x^2 coordinate and r, the distance from the surface to the axis of revolution,

$$r = \frac{\sin \bar{\omega}}{n} \, e^{n x^2} \quad , \; n \neq 0 \tag{103}$$

With the given metric components the Gaussian curvature is,

$$K = -\frac{n^2}{\sin^2 \bar{\omega}} \quad , \; n \neq 0 \tag{104}$$

Therefore the surface is one of constant negative Gaussian curvature. A surface of revolution with constant negative Gaussian curvature is known as a pseudospherical surface. Equation (102), the equation of the generatrix, is known to be the equation of a tractrix (33, p. 274) and therefore the surface of revolution is a pseudospherical surface of the parabolic type, or a pseudosphere. The tractrix is shown in Figure 3 . In Figure 3 r^* corresponds to the value of r for which the radical in Equation (102) becomes zero, namely

$$r^* = \frac{\sin \bar{\omega}}{n}$$

By Equation (103) it is known that the x^2 origin in this case corresponds to the parallel described by the point r^* on the tractrix.

The necessary and sufficient condition that a surface S^1 be applicable to a surface S of constant total curvature is that the total

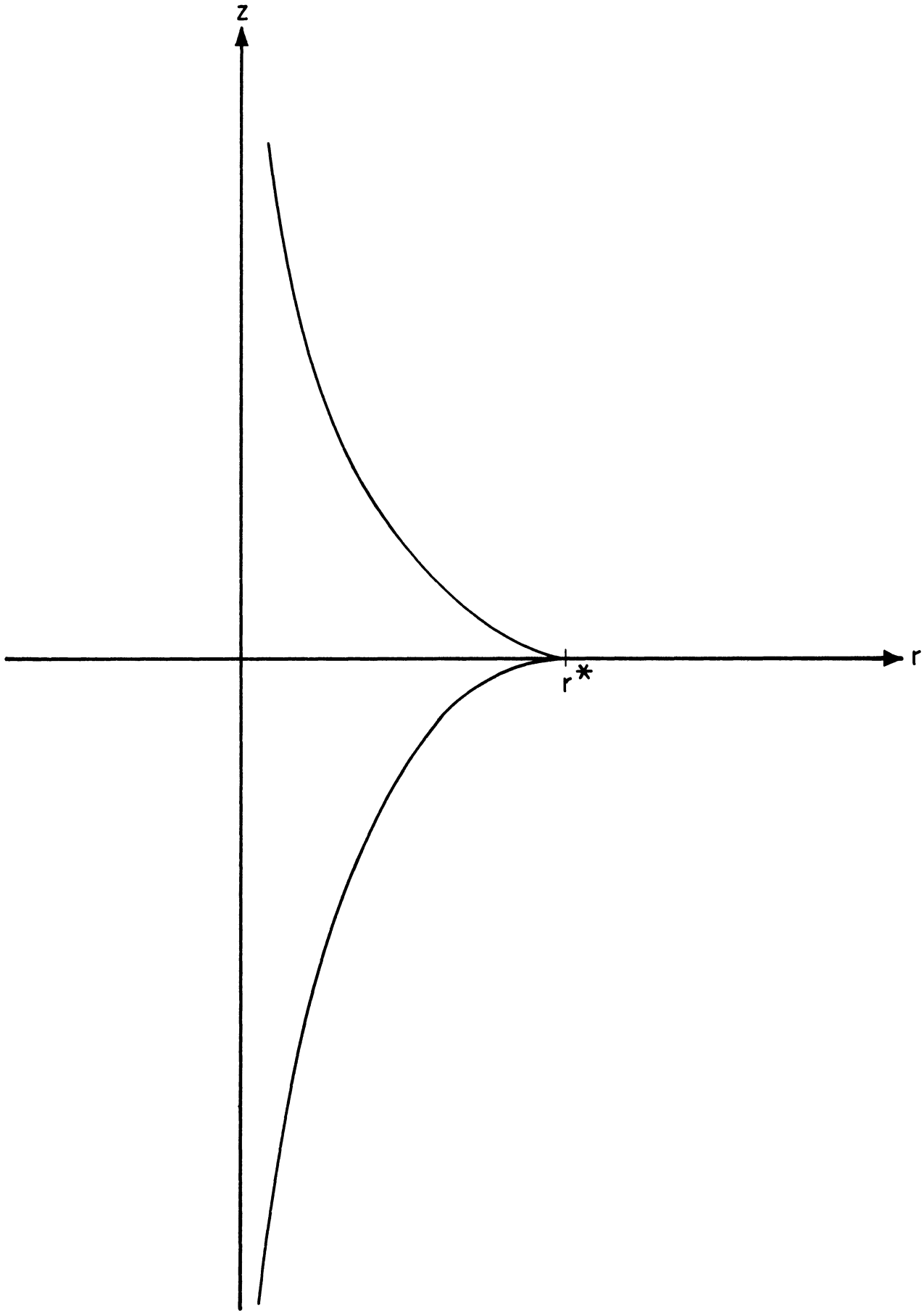

Figure 3. The Tractrix, Generatrix for Case II.

curvature of S^1 is constant and equal to the total curvature of S (33, p. 321). Therefore the necessary and sufficient condition for a surface to be admissible in this case is that its total curvature satisfy Equation (104).

3. Case III, $\sqrt{a_{11}} = x^2$, $\sqrt{a_{22}} = 1$.

The differential quadric is

$$(ds)^2 = (x^2 dx')^2 + (dx^2)^2 + 2\cos\omega\, x^2 dx' dx^2 \qquad (105)$$

Consideration of metric coefficients and Equation (43) shows that the Gaussian curvature is zero. That is, the surface is developable or is said to be applicable to the Euclidean plane. Consequently it is sufficient to consider this case as being represented by a plane surface.

If the coordinates are transformed by

$$x' = \frac{-\ln r + m\theta}{\sqrt{m^2+1}}$$
$$x^2 = \frac{\sqrt{m^2+1}}{m} r \qquad (106),$$

the differential quadric becomes

$$(ds)^2 = (dr)^2 + (r d\theta)^2 \qquad (107),$$

where r, θ are the ordinary polar coordinates of the plane. Therefore from the transformation, Equation (106), the equations of the x^1 and x^2 coordinate lines can be obtained as a function of the polar coordinates r, θ.

The x^1 coordinate lines are lines of x^2 = const. hence are circles. The x^2 coordinate lines are lines of x^1 = const. hence satisfy the relation,

$$r = B e^{m\theta} \tag{108}$$

This is the equation of logarithmic spirals in polar coordinates. If a scale change of r is made such that $\bar{r} = \ell nr$, the $\{\bar{r}, \theta\}$ coordinates are orthogonal and are circles and radial lines. In terms of this set of coordinates the x^1 coordinate lines are represented by $\bar{r}$ equal a constant but the x^2 coordinate lines are represented by the linear relationship.

$$\bar{r} - m\theta + C = 0 \tag{108a}$$

This is pointed out because in the last two sections it was seen that the x^2 coordinate lines were loxodromes of the surface of revolution and could be represented by a linear relation between the orthogonal set of coordinates on the surface and it will be seen in the following sections that in all cases the new admissable coordinates can always be represented by a linear relationship of an orthogonal set of coordinates.

The angle $\bar{\omega}$ between the x^1, x^2 coordinates determines the constant m in Equation (108) by the relation

$$\cos \bar{\omega} = \frac{1}{\sqrt{m^2+1}} \tag{109}$$

This system becomes the polar system as $m \to \infty$, i.e. $\bar{\omega} = \frac{\pi}{2}$. The coordinate system is shown in Figure 4.

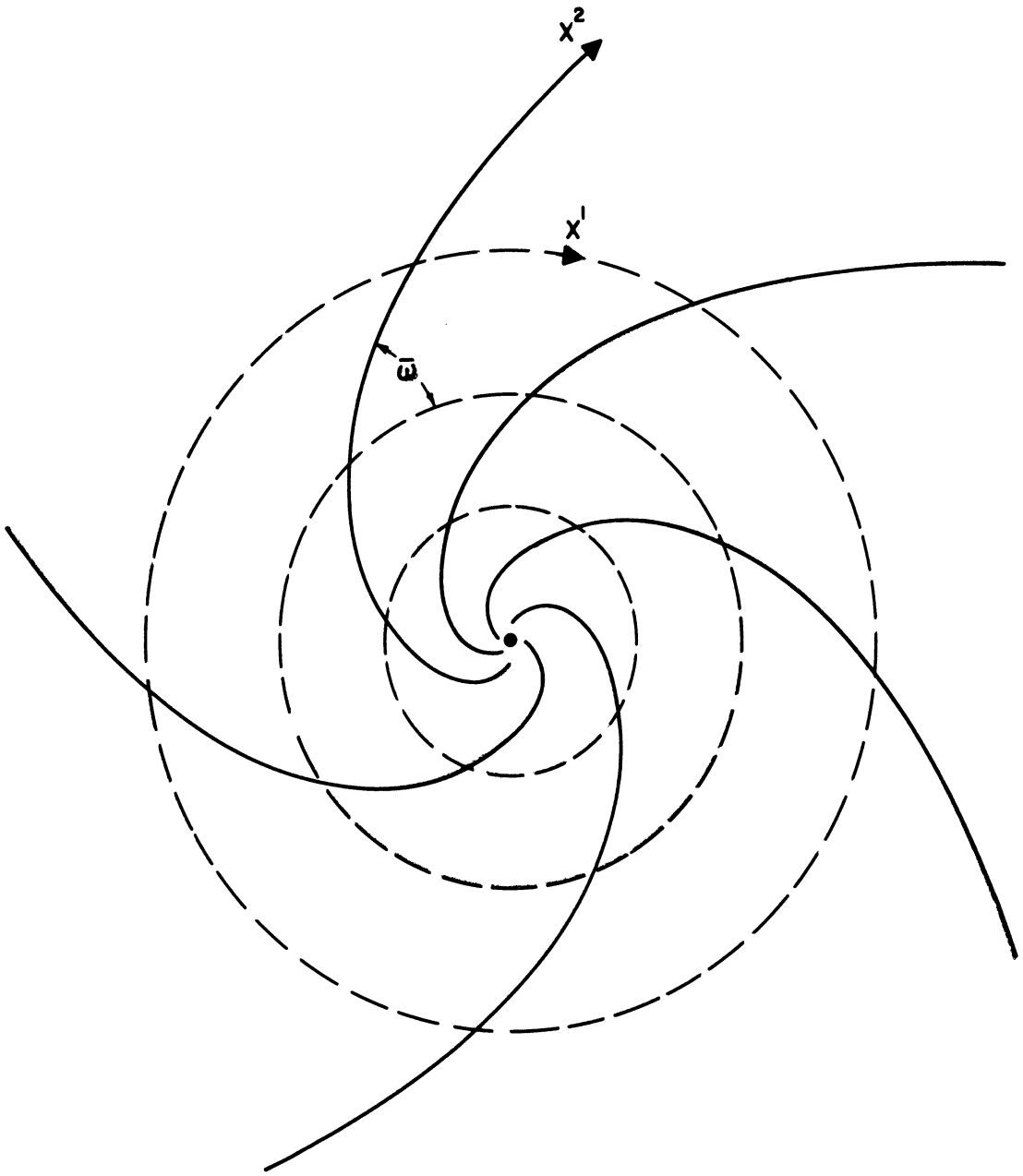

Figure 4. Circle-Log-Spiral Coordinate System Case III.

4. Cases IV → VII, $\sqrt{a_{11}} = \sqrt{a_{22}} = 1$.

In cases IV → VII the surface must be developable, and the admissible coordinate systems are all of the same class. Again, because the surface must be applicable to the Euclidean plane, it is sufficient to consider this case with respect to a plane surface.

When referred to the plane surface the coordinate lines must be straight lines because their geodesic curvature is zero. The differential quadric for the coordinate lines is

$$(ds)^2 = (dx^1)^2 + (dx^2)^2 + 2\cos\bar{\omega}\, dx^1 dx^2 \tag{110}$$

If the coordinates are transformed by

$$\begin{aligned} x^1 &= \operatorname{cosec}\bar{\omega}\ \bar{x}^1 \\ x^2 &= \bar{x}^2 - \cot\bar{\omega}\ \bar{x}^1 \end{aligned} \tag{111}$$

the differential quadric becomes,

$$(ds)^2 = (d\bar{x}^1)^2 + (d\bar{x}^2)^2 \tag{112}$$

Hence the system $\{\bar{x}^1, \bar{x}^2\}$ is the ordinary Cartesian coordinate system in the plane, and the system $\{x^1, x^2\}$ consists of any two sets of parallel straight lines intersecting at a constant angle $\bar{\omega}$. The special case of $\bar{\omega} = \frac{\pi}{2}$ is the ordinary Cartesian system. As in Cases I → III, the constant angle coordinates can be described by linear relationships of orthogonal coordinates on the surface. Figure 5 shows the coordinate system $\{x^1, x^2\}$.

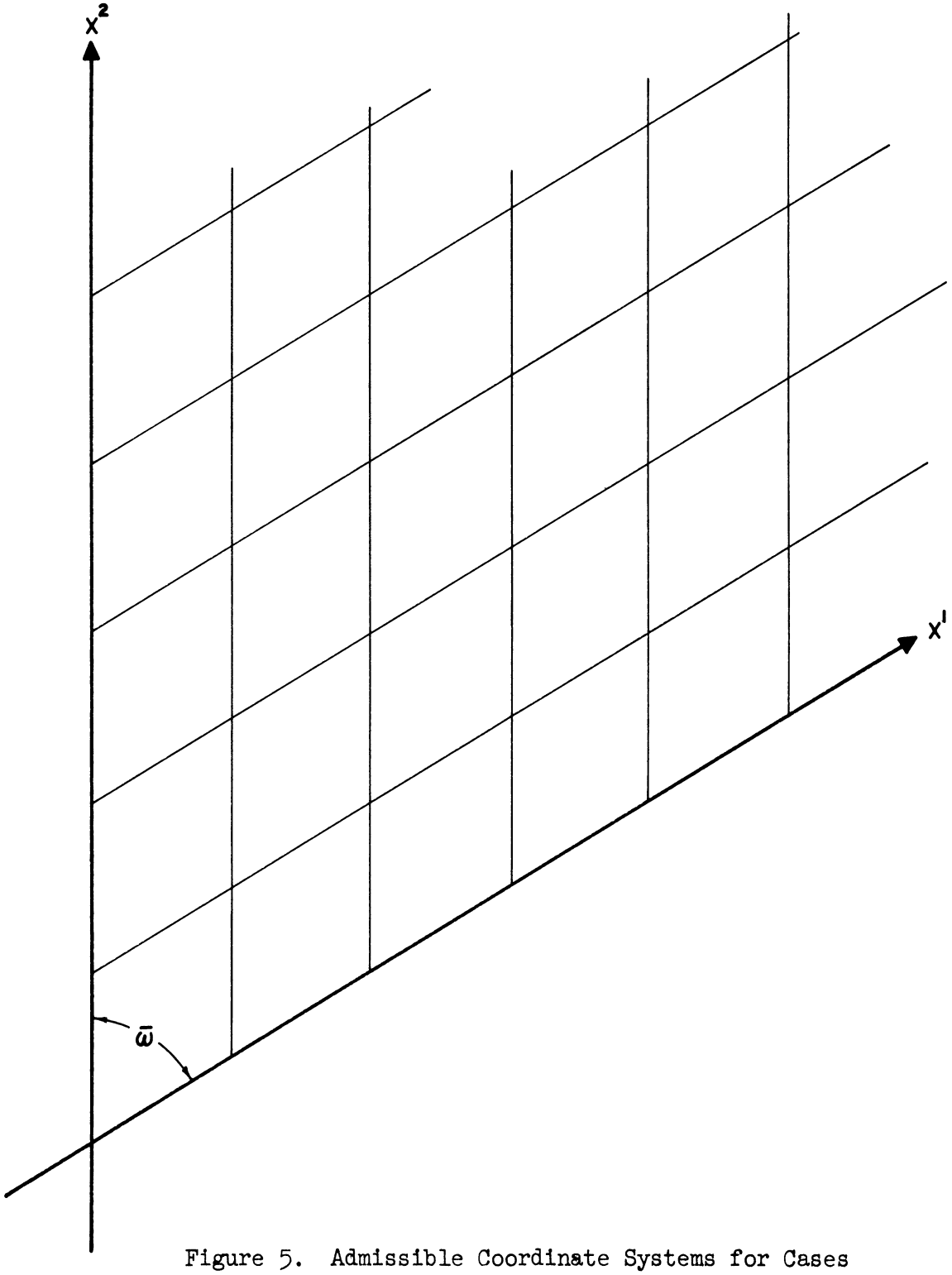

Figure 5. Admissible Coordinate Systems for Cases IV - VII.

E. Summary of the Systems which Admit to Similarity and the Associated Ordinary Differential Equations.

In the last section the admissible types of surfaces and coordinate systems were listed. In this section the required systems of mainstream velocities and the similarity parameters will be repeated along with the ordinary differential equations which result from them. The requirements and ordinary differential equations are in each case referred to the admissible coordinate systems of that case.

To obtain the ordinary differential equations the requirements for similarity in each case are substituted into Equations (21), (22) and (23). The boundary conditions are the same in each case. They are:

$$\overset{\alpha}{F}(\eta) = \overset{\alpha}{F}'(\eta) = 0 \quad @\ \eta = 0 \quad , \alpha = 1,2$$

$$\lim_{\eta \to \infty} \overset{1}{F}'(\eta) = 1$$

$$\lim_{\eta \to \infty} \overset{2}{F}'(\eta) = 1 \quad \text{if } \bar{U}^2 \neq 0 \qquad (113)$$

$$= 0 \quad \text{if } \bar{U}^2 = 0$$

$$\Theta(\eta) = 1 \quad @\ \eta = 0$$

$$\lim_{\eta \to \infty} \Theta(\eta) = 0$$

where

$$\eta = y\, g(x', x^2) \tag{17}$$

(The following abbreviations will be used in this section in connection with the similarity requirements on T^*, the wall-fluid temperature difference, and the ordinary differential forms of the energy equation: (I.V.D.) - including viscous dissipation, and (N.V.D.) - neglecting viscous dissipation.)

1. Case I $\sqrt{a_{11}} = (x^2)^n$, $\sqrt{a_{22}} = 1$.

$$n \neq 0, 1$$

$$\bar{U}' = A_1 \bar{U}^2 = A_2 (x^2)^m$$

$$g^2 = A_3 \frac{\bar{U}'}{x^2}$$

$$T^* = A_4 (\bar{U}')^2 \qquad \text{(I.V.D.)}$$

$$T^* = A_4 (x^2)^b \qquad \text{(N.V.D.)}$$

Momentum Equations

$$n\cos\bar{\omega}\left[(A_1\bar{F}')^2 + (\bar{F}')^2 - (A_1)^2 - 1\right] + A_1\left[(m-n)\sin^2\bar{\omega} + 2n\right]\left[\bar{F}'\bar{F}' - 1\right]$$

$$-(m+2n+1)A_1\sin^2\bar{\omega}\frac{\bar{F}''\bar{F}}{2} - (A_1)^2 A_3 \sin^2\bar{\omega}\,\bar{F}''' = 0 \tag{114}$$

$$\left[m\sin^2\bar{\omega} - n\cos^2\bar{\omega}\right]\left[(\bar{F}')^2 - 1\right] - 2A_1 n\cos\bar{\omega}\left[\bar{F}'\bar{F}' - 1\right] - (A_1)^2 n\left[(\bar{F}')^2 - 1\right] \tag{115}$$

$$-(m+2n+1)\sin^2\bar{\omega}\frac{\bar{F}''^2\bar{F}^2}{2}-A_1A_3\sin^2\bar{\omega}\bar{F}'''=0 \qquad \text{(115) Cont'd.}$$

Energy Equations:

$$\frac{A_1A_3}{P_R}\theta''+(2n-m+1)\frac{\theta'\bar{F}^2}{2}-2m\bar{F}'^2\theta$$
$$+\frac{(A_2)^2A_3}{C_pA_4}\left[A_1(\bar{F}'')^2+2\cos\bar{\omega}\bar{F}''\bar{F}''+\frac{(\bar{F}''^2)^2}{2}\right]=0 \qquad (116)$$

(N.V.D.) $$\frac{A_1A_3}{P_R}\theta''+(2n-m+1)\frac{\theta'\bar{F}^2}{2}-b\bar{F}^2\theta=0 \qquad (117)$$

2. Case II, $\sqrt{a}_{11}=e^{nx^2}$, $\sqrt{a}_{22}=1$.

$$n\neq 0$$

$$\bar{U}'=A_1\bar{U}^2=A_2e^{mx^2}$$

$$g^2=A_3\bar{U}'$$

$$T^*=A_4(\bar{U}')^2 \qquad \text{(I.V.D.)}$$

$$T^*=A_4e^{bx^2} \qquad \text{(N.V.D.)}$$

Momentum Equations:

$$n\cos\bar{\omega}\left[(\bar{F}^{2\prime})^2+(A_1\bar{F}^{1\prime})^2-(A_1)^2-1\right]+\left[(m-n)\sin^2\bar{\omega}+2n\right]A_1\left[\bar{F}^{1\prime}\bar{F}^{2\prime}-1\right]$$
$$-(m+2n)A_1\sin\bar{\omega}\frac{\bar{F}^{1\prime\prime}\bar{F}^{2}}{2}-A_3(A_1)^2\sin^2\bar{\omega}\,\bar{F}^{1\prime\prime\prime}=0 \tag{118}$$

$$(m\sin^2\bar{\omega}-n\cos^2\bar{\omega})\left[(\bar{F}^{2\prime})^2-1\right]-2nA_1\cos\bar{\omega}\left[\bar{F}^{1\prime}\bar{F}^{2\prime}-1\right]$$
$$-(m+2n)\sin^2\bar{\omega}\frac{\bar{F}^{2\prime\prime}\bar{F}^{2}}{2}-A_3A_1\sin^2\bar{\omega}\,\bar{F}^{2\prime\prime\prime}=0 \tag{119}$$

Energy Equation:

(I.V.D.)
$$\frac{A_1A_3}{P_R}\theta''+\frac{2n-m}{2}\theta'\bar{F}^{2}-2m\bar{F}^{2\prime}\theta$$
$$+\frac{(A_2)^2A_3}{C_pA_4}\left[A_1(\bar{F}^{1\prime\prime})^2+2\cos\bar{\omega}\,\bar{F}^{1\prime\prime}\bar{F}^{2\prime\prime}+\frac{(\bar{F}^{2\prime\prime})^2}{2}\right]=0 \tag{120}$$

(N.V.D.)
$$\frac{A_1A_3}{P_R}\theta''+\frac{2n-m}{2}\theta'\bar{F}^{2}-b\bar{F}^{2\prime}\theta=0 \tag{121}$$

3. Case III, $\sqrt{a_{11}}\,x^2$, $\sqrt{a_{22}}=1$.

$$\bar{U}^{1}=A_1\bar{U}^{2}=A_2(\chi^2)^n\,e^{m\chi^1}$$

$$g^2 = A_3 \frac{\bar{U}'}{\chi^2}$$

$$T^* = A_4 (\bar{U}')^2 \qquad \text{(I.V.D.)}$$

$$T^* = A_4 (\chi^2)^r e^{s\chi'} \qquad \text{(N.V.D.)}$$

Momentum Equations:

$$(A_1)^2 \left[m \sin^2 \bar{\omega} + \cos \bar{\omega} \right] \left[(\bar{F}')^2 - 1 \right] + A_1 \left[(n-1) \sin^2 \bar{\omega} + 2 \right] \left[\bar{F}' \bar{\bar{F}}' - 1 \right]$$

$$+ \cos \bar{\omega} \left[(\bar{\bar{F}}') - 1 \right] - A_1 \sin^2 \bar{\omega} \frac{\bar{F}''}{2} \left[m A_1 \bar{F} + (n+3) \bar{\bar{F}} \right]$$

$$- (A_1)^2 A_3 \sin^2 \bar{\omega} \, \bar{F}''' = 0 \qquad (122)$$

$$(n \sin^2 \bar{\omega} - \cos^2 \bar{\omega}) \left[(\bar{\bar{F}}')^2 - 1 \right] + A_1 (m \sin^2 \bar{\omega} - 2 \cos \bar{\omega}) \left[\bar{F}' \bar{\bar{F}}' - 1 \right]$$

$$(123)$$

$$- \left[(\bar{F}')^2 - 1 \right] - \sin^2 \bar{\omega} \, \frac{n+3}{2} \, \bar{\bar{F}}'' \bar{\bar{F}} - \frac{1}{2} A_1 m \sin^2 \bar{\omega} \, \bar{\bar{F}}'' \bar{F}$$

$$- A_3 (A_1)^2 \sin^2 \bar{\omega} \, \bar{\bar{F}}''' = 0$$

Energy Equation:

$$\text{(I.V.D.)}\quad \frac{A_1A_3}{P_R}\theta'' - \frac{mA_1}{2}\theta'\bar{F}^1 - \frac{n}{2}\theta'\bar{F}^2 - 2mA_1\bar{F}^{1\prime}\theta$$

$$-2n\bar{F}^{2\prime}\theta + \frac{(A_2)^2A_3}{C_pA_4}\left[A_1(\bar{F}^{1\prime\prime})^2 + 2\cos\omega\,\bar{F}^{1\prime\prime}\bar{F}^{2\prime\prime} + \frac{(\bar{F}^{2\prime\prime})^2}{A_1}\right] = 0 \qquad (124)$$

$$\text{(N.V.D.)}\quad \frac{A_1A_3}{P_R}\theta'' - \frac{m}{2}A_1\theta'\bar{F}^1 - \frac{n}{2}\theta'\bar{F}^2 - sA_1\bar{F}^{1\prime}\theta - r\bar{F}^{2\prime}\theta = 0 \qquad (125)$$

Case IV, $\underline{\sqrt{a_{11}} = \sqrt{a_{22}} = 1}$.

$$\bar{U}^1 = A_1 e^{nx'}(\chi^2)^{m-1}$$

$$\bar{U}^2 = A_2 e^{nx'}(\chi^2)^{m}$$

$$g^2 = A_3\bar{U}^1$$

$$T^* = A_4 e^{rx'}(\chi^2)^{s} \qquad \text{(N.V.D.)}$$

Momentum Equations:

$$\left(\overset{1}{F}'\right)^2 - \frac{\overset{1}{F}''\overset{1}{F}}{2} - 1 + \frac{A_2}{A_1 n}(m-1)\left[\overset{1}{F}'\overset{2}{F}' - 1\right]$$

$$- \frac{A_2}{2A_1 n}(m+1)\overset{1}{F}''\overset{2}{F} - \frac{A_3}{n}\overset{1}{F}''' = 0 \qquad (126)$$

$$\left(\overset{2}{F}'\right)^2 + \frac{A_1 n}{A_2 m}\left[\overset{1}{F}'\overset{2}{F}' - \frac{\overset{2}{F}''\overset{1}{F}}{2} - 1\right] - \frac{m+1}{2m}\overset{2}{F}''\overset{2}{F} - 1$$

$$- \frac{A_1 A_3}{A_2 m}\overset{2}{F}''' = 0 \qquad (127)$$

Energy Equation:

$$\text{(N.V.D.)} \quad \frac{A_1 A_3}{P_R}\theta'' - \left[\frac{A_1 n}{2}\overset{1}{F} + \frac{A_2(m-1)}{2}\overset{2}{F}\right]\theta'$$

$$- \left[A_1 r\overset{1}{F}' + A_2 s\overset{2}{F}'\right]\theta = 0 \qquad (128)$$

5. Case V, $\sqrt{a_{11}} = \sqrt{a_{22}} = 1$.

$$\overline{U}^1 = A_1(\chi')^n(\chi^2)^{m-1}$$

$$\overline{U}^2 = A_2(\chi')^{n-1}(\chi^2)^m$$

$$q^2 = A_3 \frac{\overline{U}'}{\chi'}$$

$$T^* = A_4 (\chi')^r (\chi^2)^s \qquad \text{(N.V.D.)}$$

Momentum Equations:

$$(\overset{1}{F}')^2 - \left(\frac{n+1}{n}\right)\frac{\overset{1}{F}''\overset{1}{F}}{2} + \frac{A_2(m-1)}{A_1 n}\left[\overset{1}{F}'\overset{2}{F} - 1\right] - \frac{A_2(m+1)}{2A_1 n}\overset{1}{F}''\overset{2}{F}$$

$$-1 - \frac{A_3}{n}\overset{1}{F}''' = 0 \qquad (129)$$

$$(\overset{2}{F}')^2 + \frac{A_1}{A_2 m}(n-1)\left[\overset{1}{F}'\overset{2}{F}' - \frac{\overset{2}{F}''\overset{1}{F}}{2} - 1\right] - \frac{m+1}{2m}\overset{2}{F}''\overset{2}{F} - 1$$

$$-\frac{A_1 A_3}{A_2 m}\overset{2}{F}''' = 0 \qquad (130)$$

Energy Equation:

$$\text{(N.V.D.)}\quad \frac{A_1 A_3}{P_R}\theta'' - \left[\frac{A_1(n-1)}{2}\overset{1}{F} + \frac{A_2(m-1)}{2}\overset{2}{F}\right]\theta'$$

$$-\left[A_1 r \overset{1}{F}' - A_2 s \overset{2}{F}'\right]\theta = 0 \qquad (131)$$

6. Case VI, $\sqrt{a_{11}} = \sqrt{a_{22}} = 1$.

$$\overline{U}' = A_1 (\chi')^n$$

$$\bar{U}^2 = A_2(\chi')^m$$

$$g^2 = A_3 \frac{\bar{U}'}{\chi'}$$

$$T^* = A_4(\chi')^r e^{s\chi^2} \qquad \text{(N.V.D.)}$$

where S = 0 if m ≠ n - 1

Momentum Equations:

$$(\overset{1}{F}')^2 - \frac{n+1}{2n}\overset{1}{F}''\overset{1}{F} - 1 - \frac{A_3}{n}\overset{1}{F}''' = 0 \qquad (132)$$

$$\overset{1}{F}'\overset{2}{F}' - \frac{n+1}{2m}\overset{2}{F}''\overset{1}{F} - 1 - \frac{A_3}{m}\overset{2}{F}''' = 0 \qquad (133)$$

Energy Equations:

(N.V.D.) if m ≠ n - 1

$$\frac{A_1A_3}{P_R}\theta'' - \frac{A_1(n-1)}{2}\overset{1}{F}\theta' - A_1 r\overset{1}{F}'\theta = 0 \qquad (134)$$

(N.V.D.) if m = n - 1

$$\frac{A_1A_3}{P_R}\theta'' - \frac{A_1(n-1)}{2}\overset{1}{F}\theta' - \left[A_1 r\overset{1}{F}' + A_2 s\overset{2}{F}'\right]\theta = 0 \qquad (135)$$

7. Case VII, $\sqrt{a_{11}} = \sqrt{a_{22}} = 1$.

$$\bar{U}^1 = A_1 e^{nx'}$$

$$\bar{U}^2 = A_2 e^{mx'}$$

$$g^2 = A_3 \bar{U}^1$$

$$T^* = A_4 e^{rx'} \qquad \text{(N.V.D.)}$$

Momentum Equations:

$$\left(\overset{1}{F}'\right)^2 - \frac{\overset{1}{F}''\overset{1}{F}}{2} - 1 - \frac{A_3}{n}\overset{1}{F}''' = 0 \tag{136}$$

$$\overset{1}{F}'\overset{2}{F}' - \frac{n}{2m}\overset{2}{F}''\overset{1}{F} - 1 - \frac{A_3}{m}\overset{2}{F}''' = 0 \tag{137}$$

Energy Equations:

$$\text{(N.V.D.)} \quad \frac{A_1 A_3}{P_R}\theta'' - \frac{A_1 n}{2}\overset{1}{F}\theta' - A_1 r\overset{1}{F}'\theta = 0 \tag{138}$$

8. Comments on Ordinary Differential Equations.

Except for special cases the above ordinary differential equations must be solved by numerical methods, preferably by a computer program. No attempt has been made here to make such calculations.

It is interesting to note that Equations (126 → 138), for Cases IV → VII, are independent of the angle between the coordinate lines.

Consequently the numerical solutions to these equations are valid for a coordinate system at any angle when the mainstream velocity components and the wall-fluid temperature difference satisfy the requirements in that coordinate system. Yohner and Hansen [18] have presented solutions for the momentum equations of Cases V & VI, Equations (129, 130) and (132, 133), for orthogonal coordinates and a wide range of m and n. These solutions can now be used when referred to nonorthogonal coordinates.

CHAPTER III

EXPERIMENTAL INVESTIGATION

A. Introduction

The experimental program consisted of the direct measurements of three-dimensional boundary-layer velocities of two physical systems, for each of which exact similarity solutions exist. This program was carried out to determine the applicability of exact similarity-type solutions for flows of infinite extent to finite channel flows and to experimentally test the similarity solutions of the three-dimensional boundary-layer equations in general. The experimental program was conducted in the Mechanical Engineering Department's Fluid Flow Laboratory in the Fluids Engineering Building.

B. Experimental Apparatus

Basically the experimental equipment consisted of an open-circuit wind tunnel operating with compressed air, two test channels, and the necessary associated instrumentation. A general view of the experimental equipment is shown in Figure 6.

1. Basic Equipment

The wind tunnel had a settling plenum obtained from the Aeronautical and Astronautical Engineering Department which was installed with the necessary piping, control valve, filter, and contraction section.

The settling plenum had an aluminum frame and covering and a wooden liner supporting eleven screens. The air entered the plenum through a two inch pipe. A diverging section from the inlet pipe to the main settling

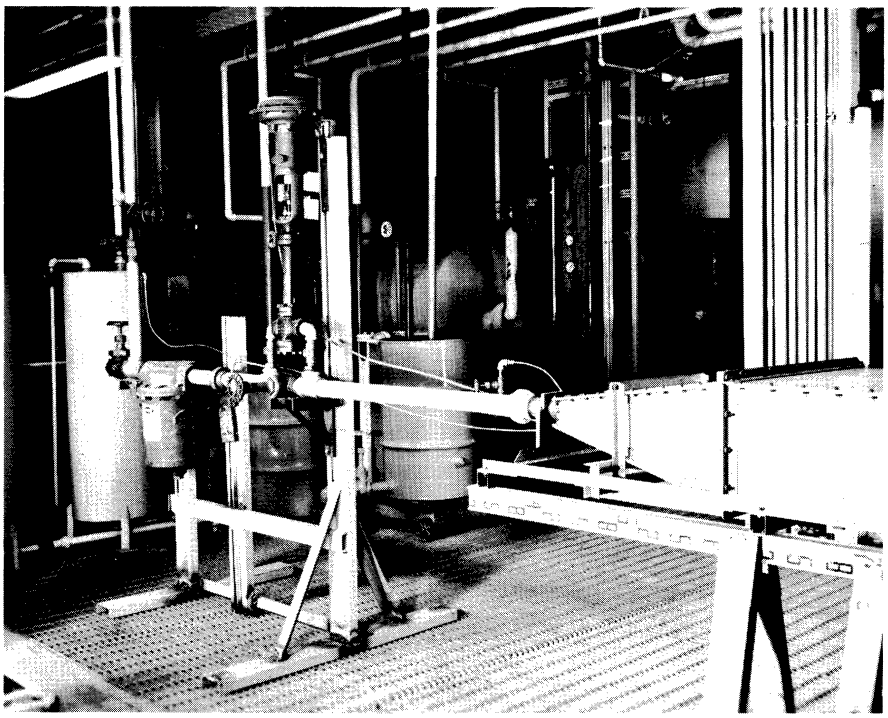

Figure 6a. Filter and Control Valve at Plenum Entrance.

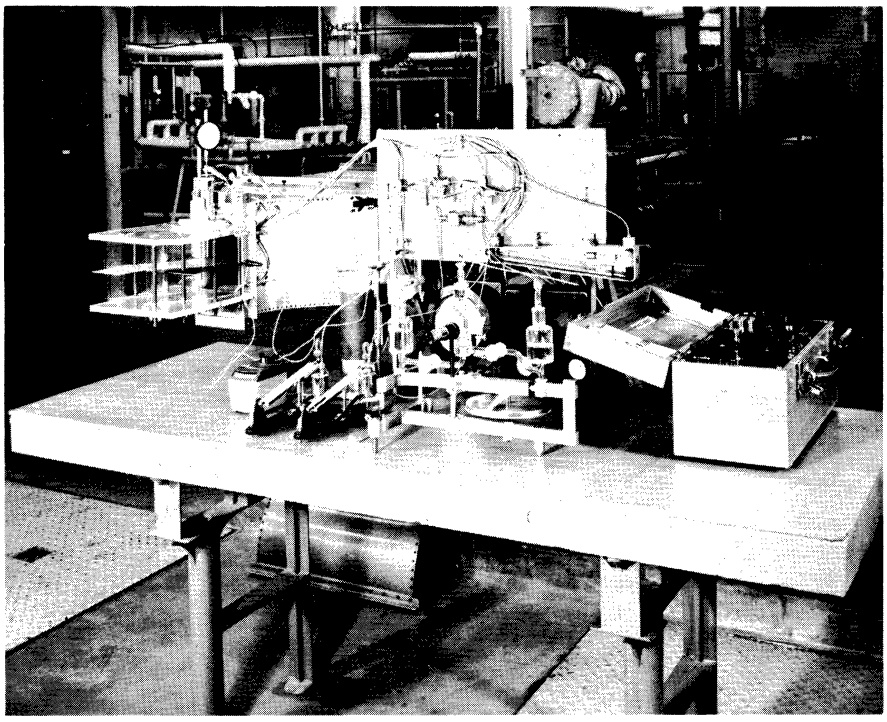

Figure 6b. General View of Test Channels and Associated Instrumentation.

chamber was 32" long and contained four of the eleven screens. The screens in the diverging section had 150 wires to the inch. The main settling chamber had a rectangular crossectional flow area of 23" x 10" and was 78" long. Seven equally spaced screens in the chamber had 50 wires to the inch.

A contraction section was built with a 7.66 to 1 contraction ratio. This contraction section was 18" long and had an outlet cross section of 5" x 6". The outlet of the contraction section was designed such that the test channels could be attached directly to it.

Four feet upstream of the plenum entrance was mounted a Fischer-Governor control valve. It was initially thought that this control valve would maintain steady volumetric flow rates through the system but due to the poor dynamic response of this control unit relative to supply fluctuations this was not possible. Instead, all experimental runs were made with the control valve in a full-open position and the air compressor operating continuously. The contraction section had been designed to give the desired velocities in the test channel with the compressor operating continuously at full load. Fortunately the losses in the system were such that with the control valve fully open the compressor would run continuously and maintain a constant supply pressure. Precautions were taken to insure that during the programmed tests no other laboratory equipment was supplied with air from the compressor. This insured steady flow conditions.

Just upstream of the control valve was a Cuno Model No. 6F1G air filter to remove the fine particles of dirt, water, and oil from the compressed air.

The plenum, filter, and control valve were connected to the receiver of the air compressor with approximately 100 feet of three inch pipe and

20 feet of two inch pipe. The receiver, which had a volume of approximately 750 cubic feet, served to remove the fluctuations in the flow due to the reciprocating nature of the air compressor.

The air compressor was a Joy Model B with a 100 hp drive producing 550 cfm of free air.

2. Test Channels

The curved test channels were shaped to cause the flow to have predetermined streamlines for which exact similarity solutions exist. The two channels used are shown in Figure 7.

The channels were made with 1/2" plexiglass tops and bottoms, and 1/4" curved plexiglass sidewalls. The flat 18 gauge sheet steel plates on which the boundary layer grows were mounted in the center of each channel. The surfaces of the flat plates were polished and a sharp leading edge formed on each.

The exact shapes of the side walls were determined during visualization studies using smoke. Since only specific types of flow fields have similarity solutions, it was necessary for the walls to direct the flow in such a manner that its streamlines coincided with streamlines of flows for which similarity solutions existed. One set of streamlines for which similarity solutions exist was choosen for each test channel and white dots describing the streamlines were superimposed on the buff-black surface of the flat plate of the channel. The smoke in the visualization studies traced out the streamlines of the flow in the channel and the walls were adjusted until the smoke traces coincided with the white dots on the plate. This insured that the streamlines of the flow in the channel were known and were for

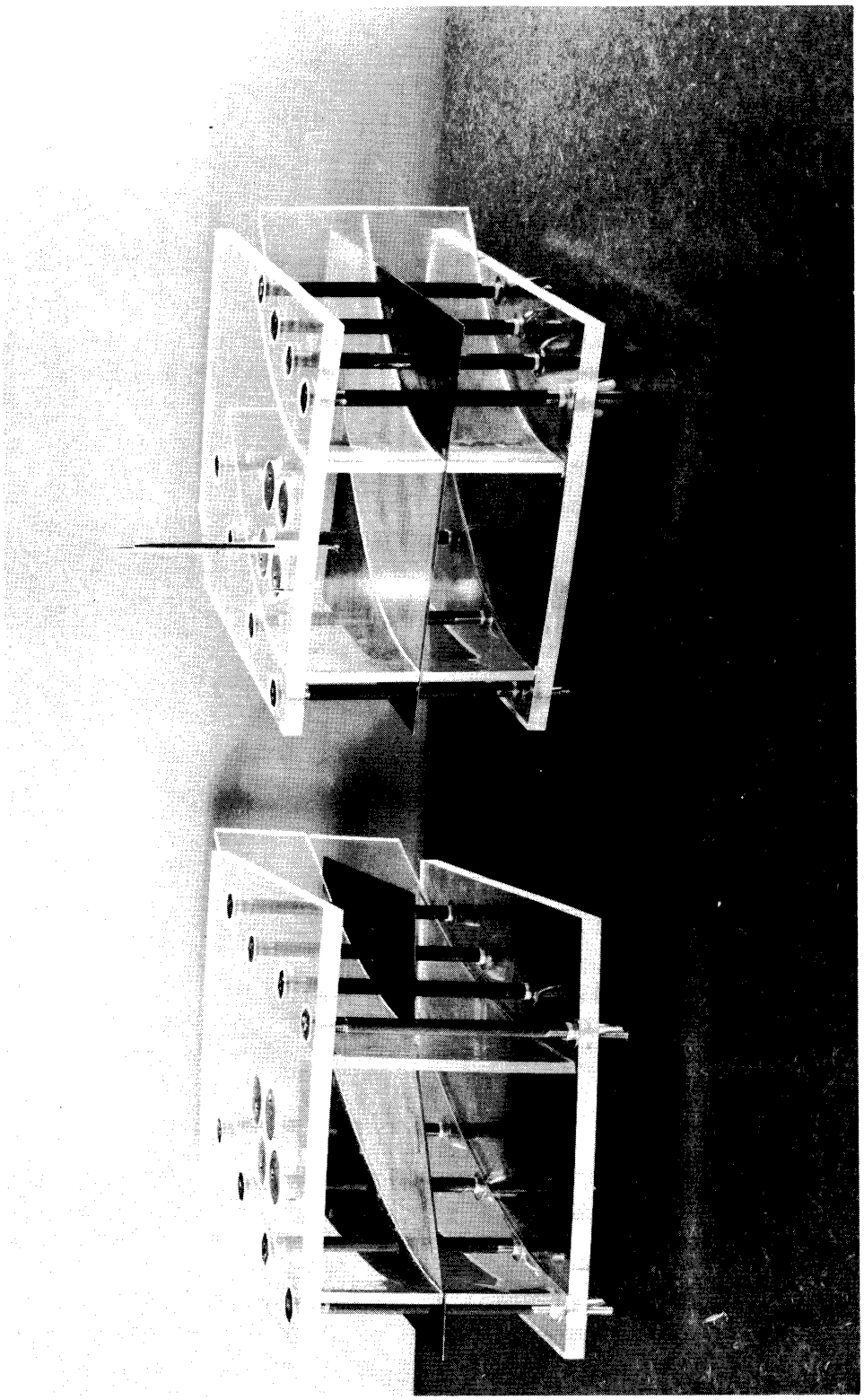

Figure 7. Test Channels.

flows which admit similarity solutions of the boundary layer equations. The paint was cleaned off the plates after the smoke studies to make it possible to use an electrical contact method for determining the probe location accurately.

The channels were held together by using eight tie bolts in each connecting the top and bottom plates forming a clamp which held the side walls in place. The holes in the top of the channels for mounting the probe holder were made after the smoke studies to allow unobstructed views during these studies.

3. Smoke Generator

A schematic diagram of the smoke generator used in the visualization studies is shown in Figure 8. A white smoke was generated by blowing low pressure compressed air through two cigars in a steel tube. The cigars were each injected with approximately 5 cc. of No. 15 lubricating oil prior to insertion in the tube. The smoke from the cigars was directed immediately into the bottom of a 1000 cc. flask with about 1" - 2" of water in the bottom. The flask served three purposes: (1) to settle and filter out drops of tars and unburned oil, (2) to accumulate smoke, (3) to condense some of the water vapor in the products of combustion from the burning cigar. The partial condensing process was necessary to make the smoke more opaque so that a better contrast existed between the buff-black plate and the smoke for photographic purposes. The condensation was brought about by immersing the 1000 cc. flask in an ice water bath which cooled the flask and its contents down to such a temperature that the water vapor in the combustion products would tend to condense.

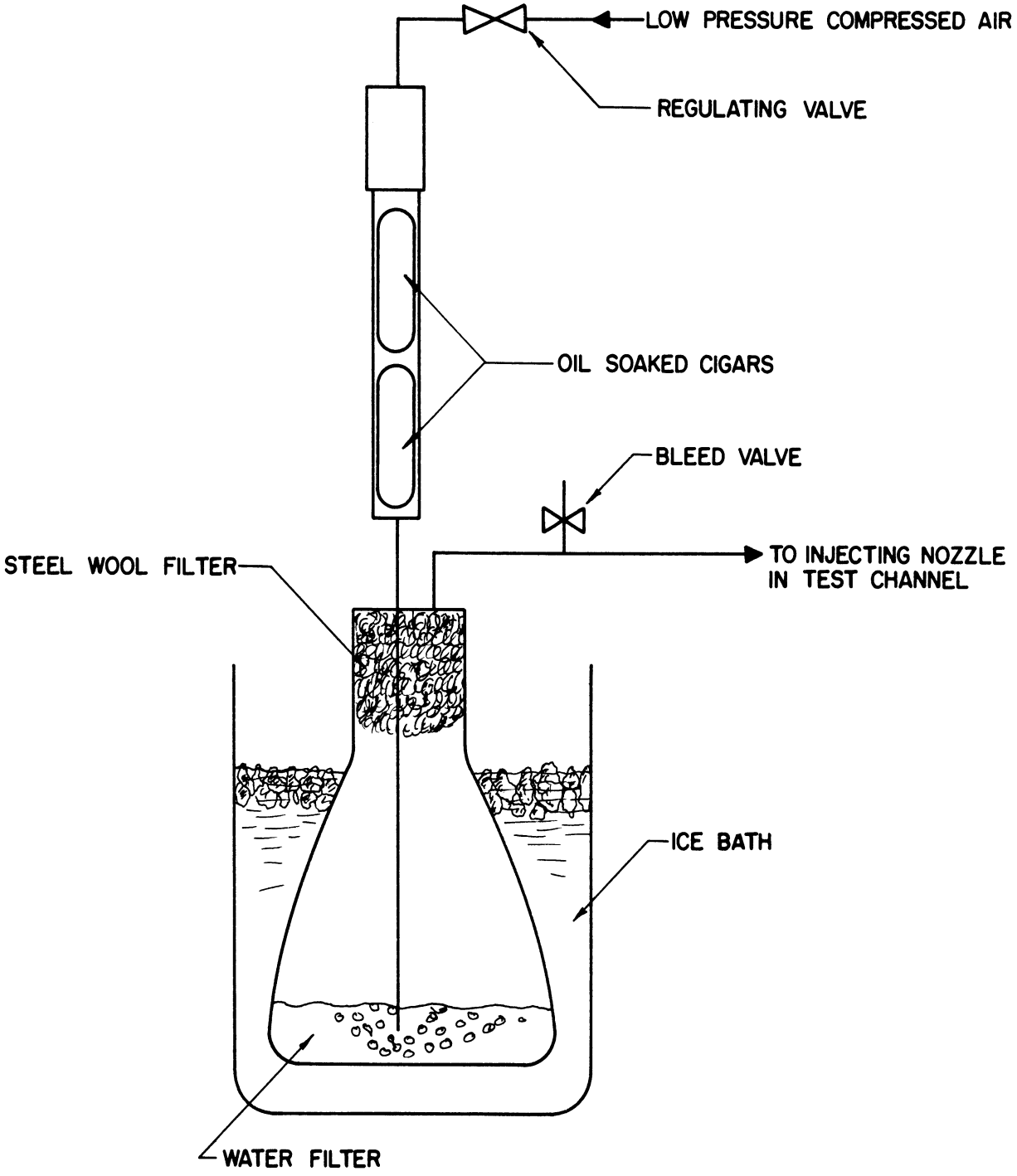

Figure 8. Schematic of Smoke Generator.

In the neck of the flask was a steel wool filter through which the smoke passed. Upon leaving the flask the smoke could either be bled off into the atmosphere or directed to the nozzle in the test channel. The bleed was used when the flow rate of smoke into the nozzle in the test section was too low to keep the cigars burning.

The nozzle for injecting the smoke in the test channels was made of 1/16" O.D. by 1/64" wall thickness brass tubing.

4. Instrumentation

The instrumentation in the visual observation program was a photographic system while in the velocity measurement program it was a system of pressure and temperature probes and their respective sensing devices.

A 3" x 5" graphic press camera, mounted above the channel, was used to photograph the smoke studies. The area of interest in the test channels was the only area visable to the camera, all other areas being masked off with black cardboard to eliminate undesired glare and reflection. In conjunction with the camera, a small "source light" was directed into the exit of the channel and axially down the smoke trace. The entrance velocity to the test section was continually monitored during the visual observations for both its level and steadiness.

Air velocities and pertinent physical quantities were measured by pressure and temperature probes and their respective sensing devices. All velocities were determined by measuring the impact pressure at the location of interest.

The principal instrumentation was the boundary-layer combination total head and yaw probe, its positioning apparatus, and pressure sensing gauge.

A photograph of the combination probe is shown in Figure 9a. The probe was constructed by threading three 1/32" O.D. copper tubes through a piece of 13 gauge stainless steel hypodermic tubing. The stainless steel hypodermic tubing served as a rigid housing for the probe stem. The yaw portion of the probe was made by bending two of the copper tubes at right angles with the stem and soldering them together. The tip was then flattened and sheared off with an included angle of 60°. This angle was recommended in Reference 35 to give the best pressure-difference sensitivity between openings to the angle of alinement with the flow. The total head probe was formed by bending the third copper tube at right angle to the stem so that the impact and yaw probes form a tee with the stem.

The tip of the total head probe was formed by a method developed by Bradfield and Yale (36). The copper tube was put under tension so that it would neck down and yield at the position where the tip was to be placed. After inserting a piece of shim stock steel 0.001 in. thick by 0.030 in. wide the end was flattened. The wall thickness at the probe mouth was further reduced by using the probe tip as an anode in an electrolytic cell with a copper sulfate solution. Care was taken to insure that all sulfate deposits were removed from the inside of the probe, for they could seriously lengthen the response time of the probe if not plug the probe. The final operation in forming the stagnation pressure probe

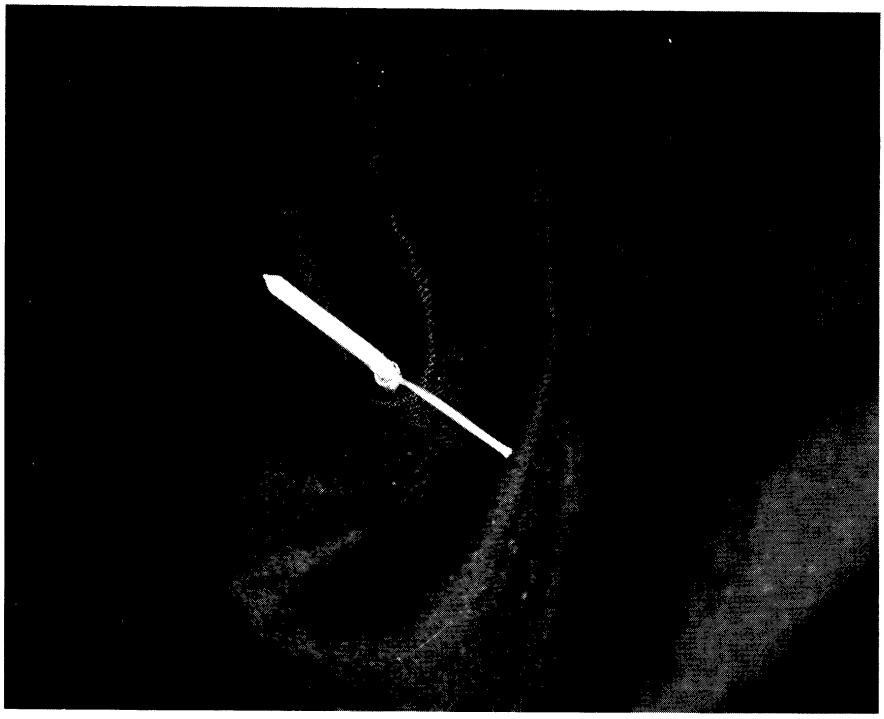

Figure 9a. Boundary Layer Combination Pitot and Yaw Probe.

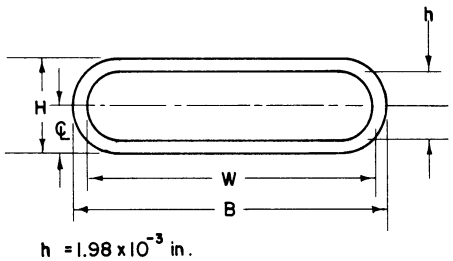

h = 1.98×10^{-3} in.
H = 6.79×10^{-3} in.
B = 34.0×10^{-3} in.
℄ = 3.25×10^{-3} in.
B/h ≅ 17

Figure 9b. Dimensions of Pitot Probe Opening.

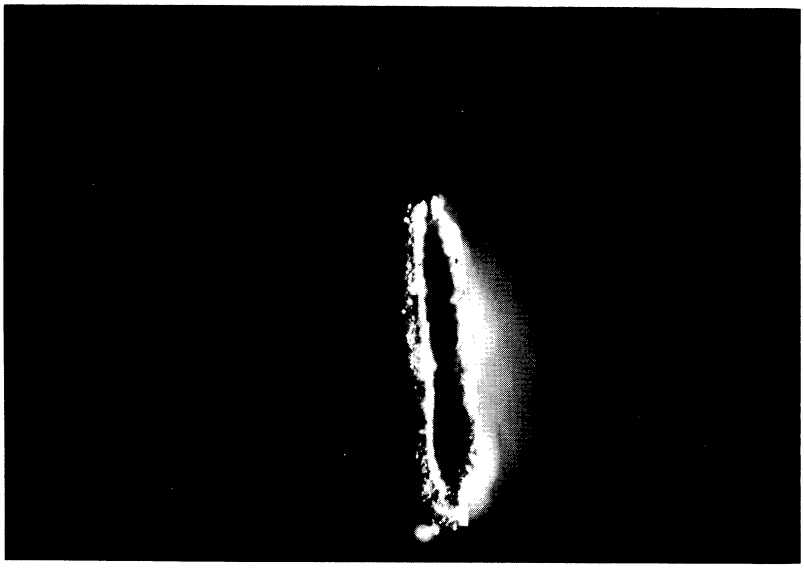

Figure 9c. Photomicrograph of Pitot Probe Opening (Approximate magnification X48).

tip was to hand hone the tip with a fine hone and lapping compound to insure that the plane of the tip face was oriented parallel to the probe stem and perpendicular to the line between the tip and the yaw probe tip. The work on the tip was continually checked under a X30 microscope.

The important dimensions of the probe were measured with the aid of a Bausch and Lomb microscope. This microscope had a scale in the occular eye piece which was calibrated with a standard etched scale. The microscope magnifications available were X35, X100, X430. Only the X35 was used because at the higher magnifications the loss of definition was too great to make meaningful measurements. The measurements of the probe are shown in Figure 9b. In addition to the dimensions of the probe, other geometric features of the probe were checked. These were: (1) the perpendicularity between the stem and a line between the two tips, (2) the perpendicularity between the normal to the impact probe opening and the stem, (3) the apposition of the probe tips.

Because of the small dimensions of the total head probe tip and the low velocities to be measured in the boundary layer, the probe pressure measurements could be expected to display a so-called, viscous effect. This phenomena is manifested by the fact that the pressure the probe tip detects is no longer equal to the static pressure of the stream plus the dynamic pressure, $\frac{1}{2}\rho|V|^2$. No theoretical work on this phenomena has been carried out for the tip shape used here, but some experimental work for this shape has been done by Macmillan [37]. The total head probe was calibrated for the viscous effect following the methods used by

Macmillan. The results of the calibration are shown in Figure 10, and the calibration procedure is described in Appendix B.

Because of the steep velocity gradients existing in the relatively thin boundary layer which was observed, the location of the geometric center of the probe tips must be established with a high degree of accuracy. This was accomplished with the traversing mechanism as shown mounted in a test channel in Figure 11. This traversing mechanism was designed and constructed so that it could be rotated about the center of the brass plug which was inserted in a hole in the upper surface of the channel. The center of the hole in the upper surface of the channel was then put at the lateral location where the traverse was to be made. The tap for the static pressure was located at the center of the brass plug. The hole in which the probe stem was inserted was located so that the tip of the probe was directly opposite the channel wall static pressure tap and on the center line of rotation of the complete assembly. With this construction the complete assembly could be rotated to aline the probe with the flow at any given distance from the surface without changing the lateral location of either the probe tip or the static pressure tap. The probe stem was clamped in a spindle which, in conjunction with two stops, allowed the probe to be rotated exactly 180° at any given height from the surface. When the probe stem was properly clamped in the spindle and the spindle held against one of the stops the yaw probe would be on the center of rotation directly below the static tap. Rotating the spindle 180° against the other stop would put the total head probe in the same desired location.

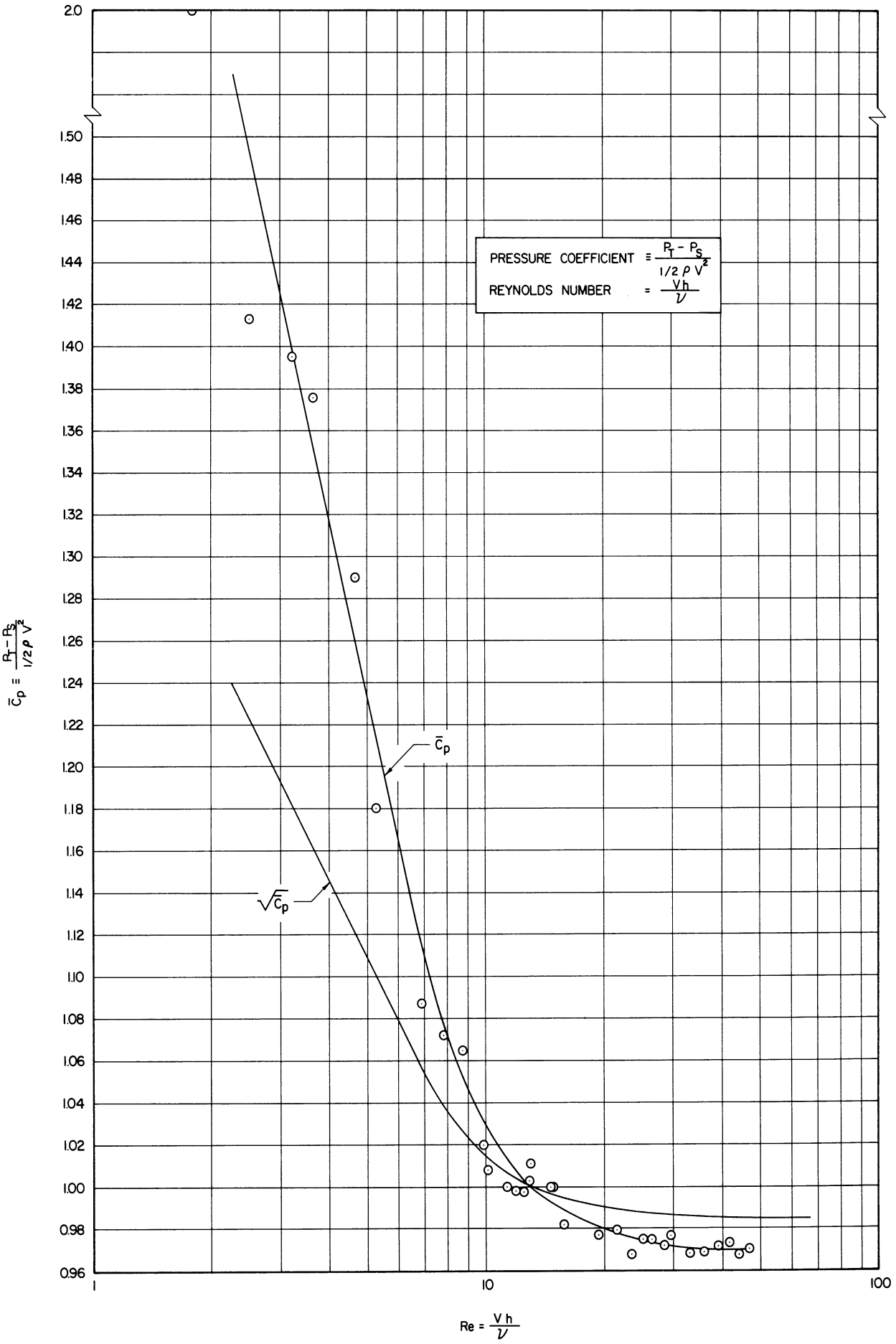

Figure 10. Boundary Layer Probe Calibration.

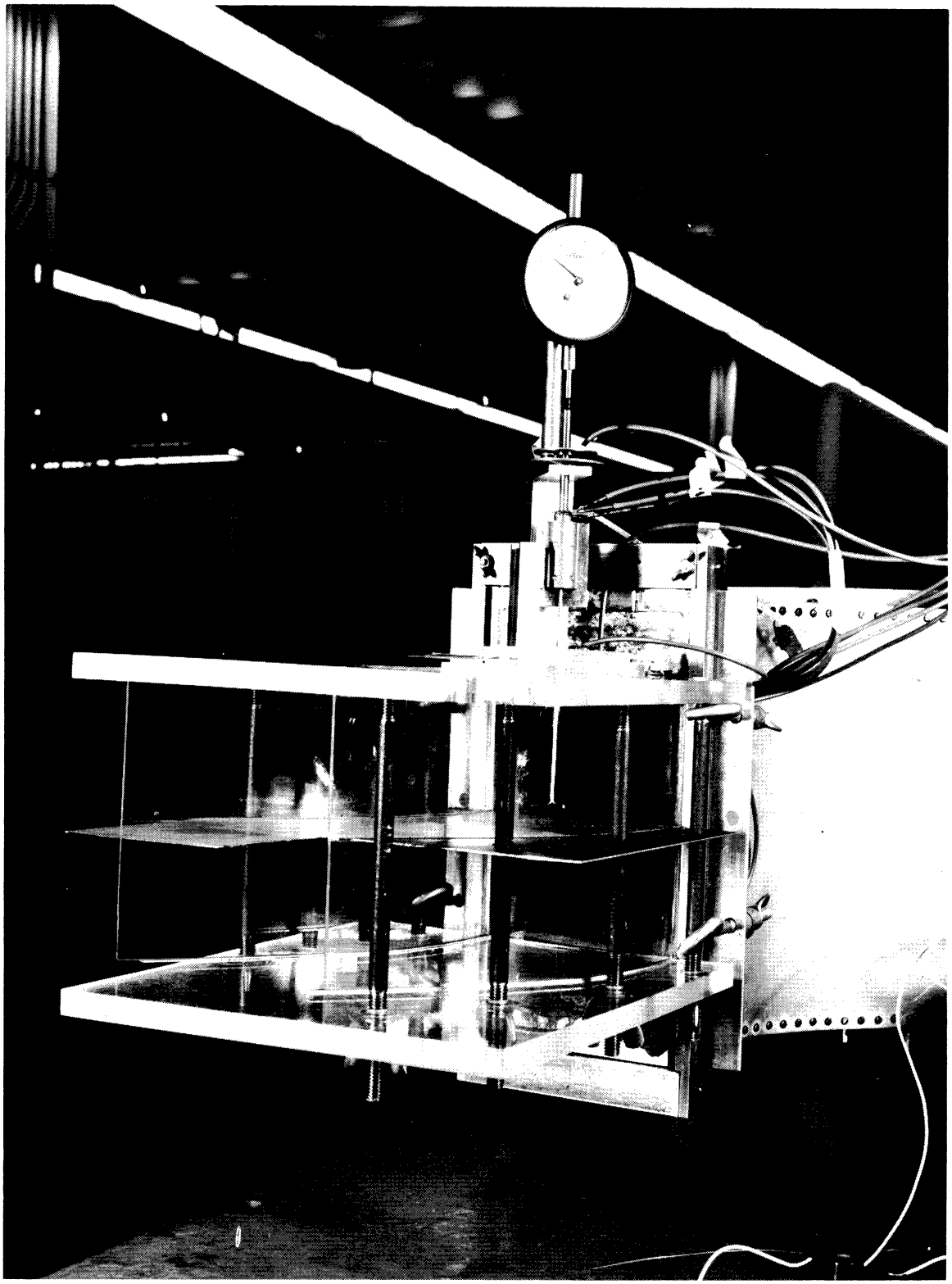

Figure 11. Traversing Mechanism Mounted in Test Channel.

The angular measurement was made with the yaw probe at a given location by rotating the positioning mechanism until no pressure difference could be detected between the two yaw probe openings. The angle measured was that between the actual flow and the direction of the uniform flow entering the test channel. The traversing mechanism had an eight inch protractor mounted on it with a vernier scale scribed on the mounting plate. This arrangement made possible angular readings of 1/10 degree. It is believed that the differences between angle readings are reliable to this accuracy. However, due to the difficulty in making the yaw probe tip symmetric on such a small scale and in mounting the probe in the holder the angle reading itself may be in error by as much as 1 1/2 to 2 degrees. This error would, of course, be constant and always have the same sign.

The position of the probe normal to the plate was determined with a dial indicator mounted on the traversing mechanism. The traveling foot of the dial indicator rested on the top of the spindle which clamps the probe stem. The top portion of this spindle was threaded so that the probe could be moved normal to the plate by turning an adjusting wheel. A lock wheel was provided to lock the adjusting wheel in any location.

The determination of the zero position, i.e., that position where the probe just touches the surface, was very critical in obtaining accurate data. In order to adequately check analytical results the position of the probe tip must be known within, at least, a half of one thousandth of an inch. It was possible to read the dial indicator to 0.2×10^{-3} inches. Consequently the accuracy with which the probe location was known depended on the accurate determination of the zero position or some position whose distance from the plate is accurately known.

A fixed position of the probe tips was determined by placing a gauge block 0.100 in. thick on the plate surface directly below the probe tip. A low voltage circuit, was connected from the plate to the probe stem with two flashlight batteries in series with a highly sensitive galvanometer. Contact of the probe tip with the gauge block was indicated by deflection of the galvanometer. When contact of the impact tip was detected the dial reading was set at 0.100". When contact of the yaw tip was detected the dial reading was recorded.

The dial indicator scale was marked in thousandths of an inch and could easily be estimated to one fifth this value. The procedure used to locate the probes at the 0.100" position could be reproduced to within the accuracy of the dial indicator readings. For these reasons it is believed that the probe location was accurately known to within 0.2×10^{-3} in., within the accuracy necessary to make a meaningful check with the analytical results.

The dynamic head of the uniform stream entering the test channel was continually monitored on a slant gauge by observing the difference between the total pressure as sensed by a NACA Keil-type probe and a static pressure tap located one inch across the channel from the Keil probe. The Keil-type probe was chosen because of its relative insensitivity to alinement with the flow. The main purpose for monitoring the flow at this point was to establish its steadiness during the time in which a boundary-layer traverse was made.

Boundary-layer impact pressure and yaw pressure differences were also continuously monitored on slant gauges. The reason for monitoring the boundary-layer impact and yaw pressures was to obtain an estimate of those pressures to preset a Chattock-Fry tilting manometer before applying the

pressure to the nulling chamber of that gauge. This presetting was necessary to insure accurate readings from the gauge.

Final pressure measurements for boundary-layer traverses of both yaw and impact probes were made on a Chattock-Fry tilting manometer Figure 12 (often referred to simply as a Chattock gauge). The connections between probes and the gauge were made with a system of 1/32 inches I.D. rubber tubing, tee connectors, and four-way valves (3 inlets on the valve, each of which could be connected to one outlet by rotation of the valve stem). This system made it possible to connect any one set of the probes simultaneously to the monitoring slant gauge and the Chattock-Fry gauge.

The Chattock-Fry gauge, shown in Figure 12, consists of two glass cups of 2 inches diameter with centers 13 inches apart. The tube leading from the base of one cup is joined to the central vessel which surrounds a vertical tube joined to the base of the other cup. The latter tube is ground flat on the top surface. Both tubes from the cups are fitted with taps to isolate the central vessel from the cups. The gauge is filled with distilled and deaerated water up to about half way in each cup with the exception of the central vessel which is filled with mineral oil. There are thus two surfaces of separation between water and oil. One is arranged to be immediately above the central tube and the other about half way down the outer part of the central vessel. The former interface has the appearance of a bubble resting on the central tube. The upper surface of this bubble, observed through the microscope, gives a sensitive indication of any displacement of the liquid due to a pressure change in the cups. The bubble is clearly shown in Figure 12. In order to make the

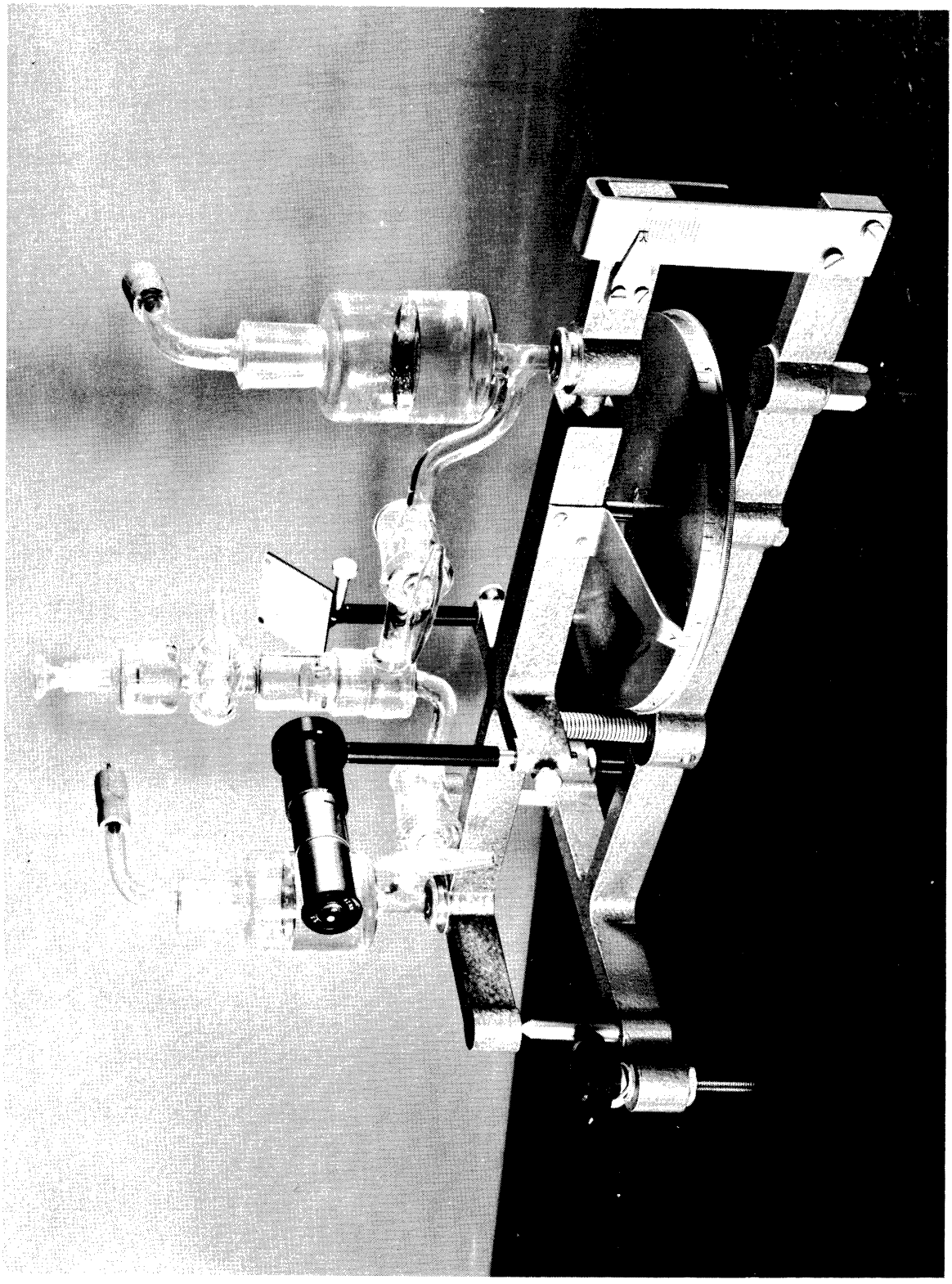

Figure 12. Chattock-Fry Tilting Pressure Manometer.

calibration dependent only on the dimensions of the gauge and the manometric liquid the null method is employed, that is, the glass-work is mounted on a frame which is tilted so that the bubble is always brought back to its zero position. The frame is tilted by a micrometer screw mounted in the base. The micrometer screw has 20 threads per inch and is fitted with a large wheel marked in 100 divisions. The distance between the pivot points and the point on the micrometer screw is 10 inches. Thus, one division on the wheel corresponds to a change in pressure of 13/10 x 1/2000 inches or 0.00065 inches of water. It is possible to estimate readings to one-tenth this value. The maximum range of the gauge is 0.65 inches water. A complete description and evaluation of the Chattock-Fry gauge can be found in the reports by either Pannell (38) or Falkner (39).

The temperature of the air passing through the test channel was determined by means of a stagnation thermocouple at the entrance to the channel. The thermocouple was made of 30-gauge copper-constantan wires. An ice-bath was used as a reference junction. The thermocouple wire was calibrated using the ice point and steam point and was found to be within 1/4 of a percent of the standard copper-constantan thermocouple tables for this temperature difference. The thermocouple e.m.f. was measured with a Leeds and Northrup Potentiometer Model 8662. No correction was applied to the stagnation temperature measured to obtain the static temperature of the stream because under the conditions of the experiment this correction would amount to somewhat less than the uncertainty of the measurement itself.

C. Experimental Program

1. Physical Systems.

The two physical systems chosen for investigation correspond with Case VI of the analytical solutions. The two systems are identical in their mathematical formulation and solution but differ by being referred to different coordinate systems. The first system is referred to an orthogonal coordinate system and the second is referred to a coordinate system with the coordinate angle $\varpi = 60°$.

The constants in Case VI were choen so that the mainstream comonents were

$$\bar{U}^1 = U_0 = \text{const.}$$
$$\bar{U}^2 = U_0 \chi^1 \tag{139}$$

the similarity parameter was

$$\eta = y g = y^* \sqrt{\frac{\bar{U}^1}{\chi^1 \nu}} \tag{140}$$

and the governing momentum equations were

$$\frac{1}{2} F^{1} F^{1\prime\prime} + F^{1\prime\prime\prime} = 0 \tag{141}$$

$$-F^{1} F^{2\prime} + \frac{1}{2} F^{2} F^{1\prime\prime} + F^{2\prime\prime\prime} + 1 = 0 \tag{142}$$

These equations have been solved by Yohner and Hansen [18] for the orthogonal case. In light of the analytical analysis presented in Chapter II these solutions are also valid when referred to a coordinate system with

the coordinate angle $\bar{\omega} = 60°$. The numerical solutions to these equations are reproduced in Appendix C from Reference 18.

From the mainstream velocity components, the equation for the mainstream streamline is

$$\chi^2 = \frac{(\chi')^2}{2} + \text{const.} \tag{143}$$

Reference 18 gives the limiting streamline of the boundary-layer on the surface as

$$\chi^2 = 4.270(\chi')^2 + \text{const.} \tag{144}$$

Figure 13a - 13b show the mainstream and limiting streamlines for $\bar{\omega} = 90°$ and $\bar{\omega} = 60°$, respectively. As seen from Figure 13 the system of $\bar{\omega} = 90°$ corresponds to a uniform flow crossing the leading edge of the surface at right angles and the system of $\bar{\omega} = 60°$ corresponds to a uniform flow crossing the leading edge of the surface at an angle of inclination.

In both systems the analytical model has no x^2 dependency. That is, the flow is a translate flow. Since the physical system requires side walls and hence a finite x^2 dimension, wall effects might be expected. Therefore it was necessary to shape the test channel walls so that the physical system sufficiently approximated the analytical model over a region large enough to make meaningful measurements to compare with the analytical solutions.

To accomplish the shaping of the channel walls and determine the region in which the physical system closely approximated the analytical model, smoke studies were executed. In each system the desired mainstream

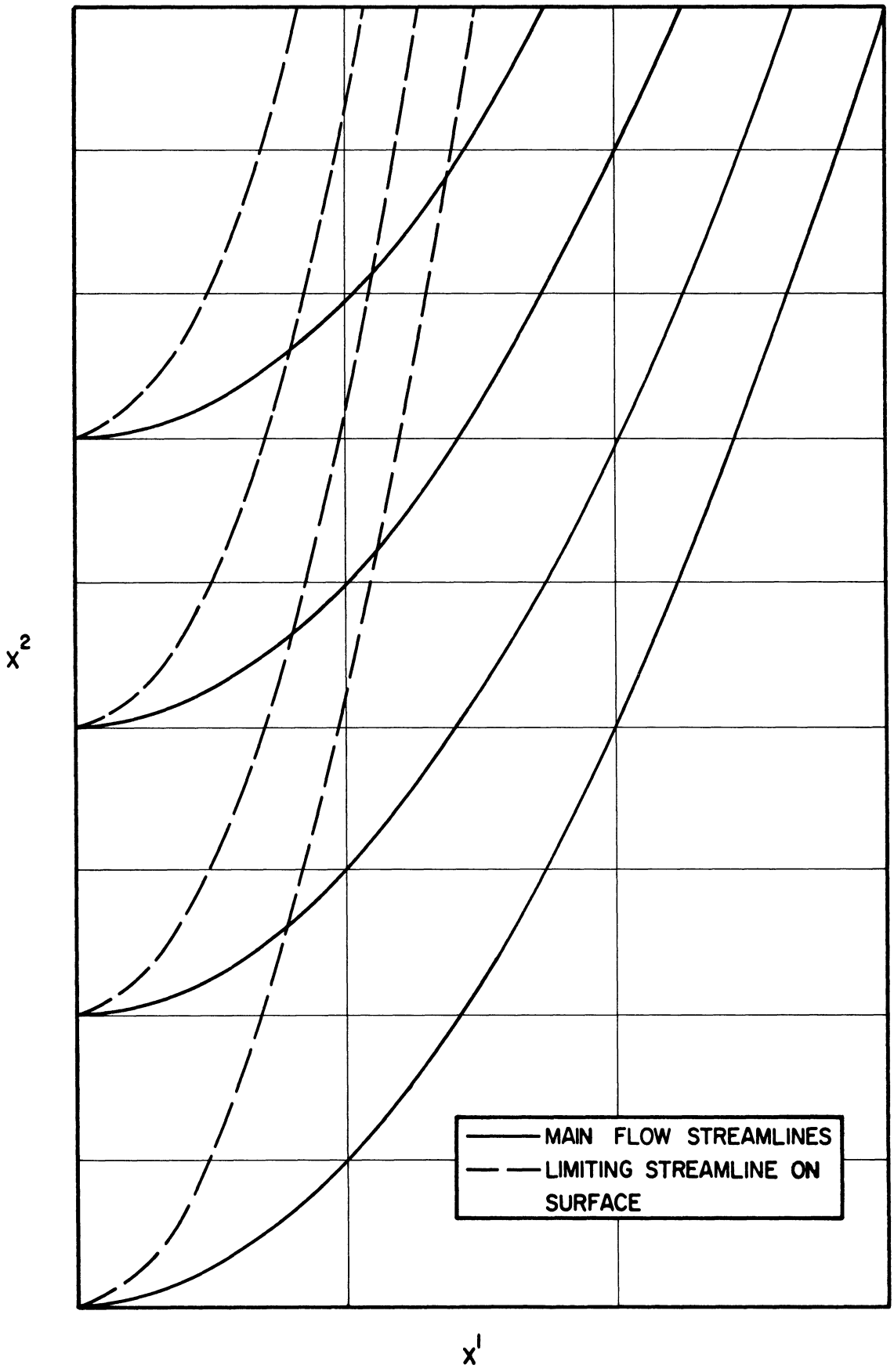

Figure 13a. Mainstream and Limiting Streamlines of Analytical Model - $\varpi = 90°$.

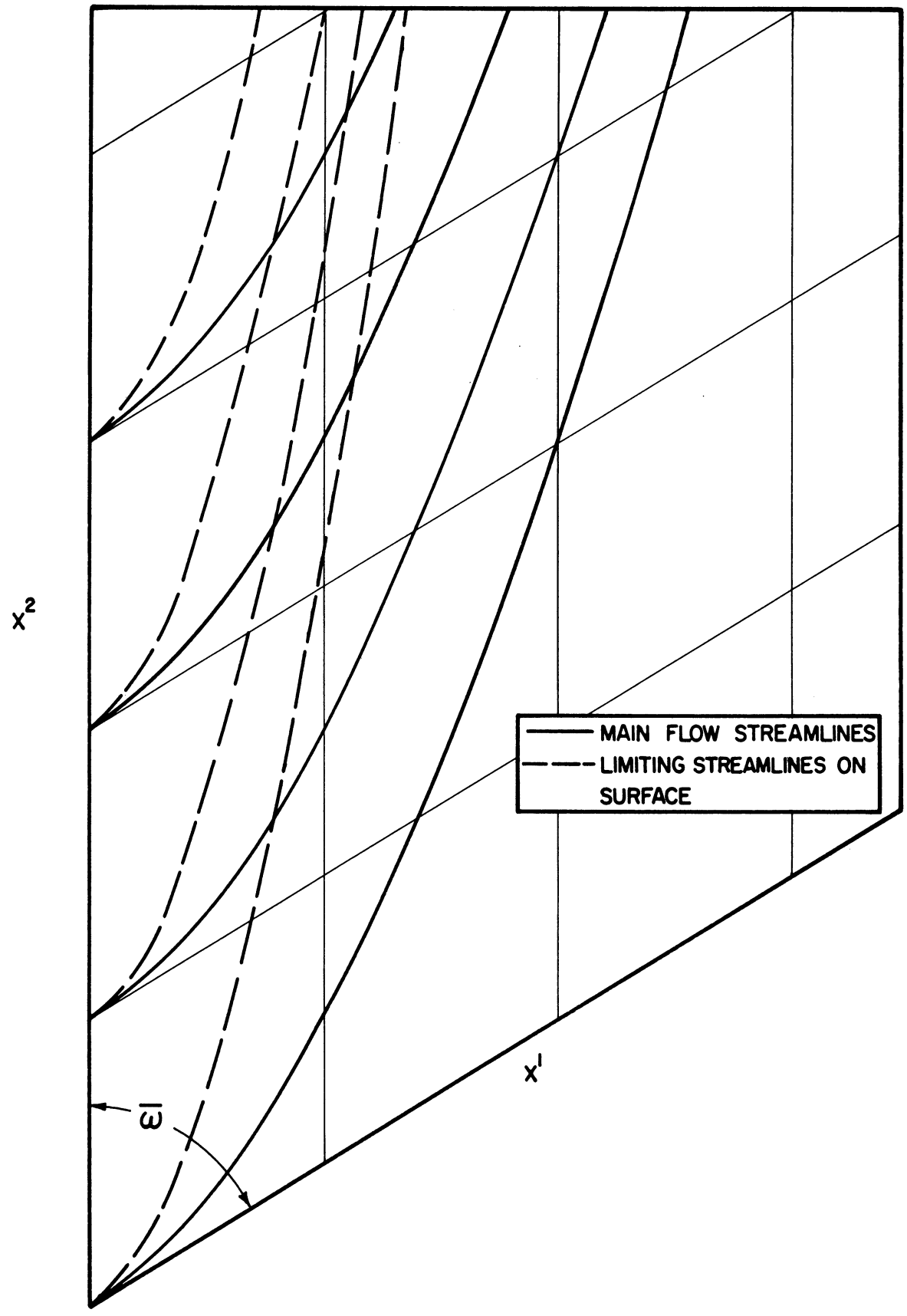

Figure 13b. Mainstream and Limiting Streamlines of Analytical Model - $\bar{\omega} = 60°$.

and limiting streamlines were painted on the plate and the channel walls adjusted until the main-flow streamline, traced out with smoke, coincided with the paint markings. Figure 14a - 14b show the smoke traces coinciding with the paint markings when the walls were properly adjusted for $\bar{\omega} = 90°$ and $\bar{\omega} = 60°$ respectively.

Although the coincidence of the smoke trace and the streamlines painted on the surface is necessary, it is not sufficient to insure that the physical system corresponds to the analytical model formulated above. For instance mainstream components of $\bar{U}_1 = A(x^1)^n$ and $\bar{U}^2 = A(x^1)^{n+1}$ would give the same shape mainstream streamlines.

From the smoke studies it is known that within the accuracy of the visualization methods the flow in the major portion of the channel is independent of x^2. And because the channel neither diverges nor converges in the direction normal to the plate there is no mainstream component in the y direction. With these two facts, if the continuity equation is applied with the above mainstream component combination, which for any value of n will yield the desired streamlines, it can be seen that the only value of n that will satisfy the continuity equation is n=0, that is, the system of mainstream velocity components chosen, Equations (139). The above argument is true on the average throughout the channel but does not, of course, exclude the possibility of small nonuniformities in the flow field.

With the above argument, it can be said that for this channel configuration the smoke studies are sufficient to establish a correspondence between the physical system and the analytical model which has a similarity solution.

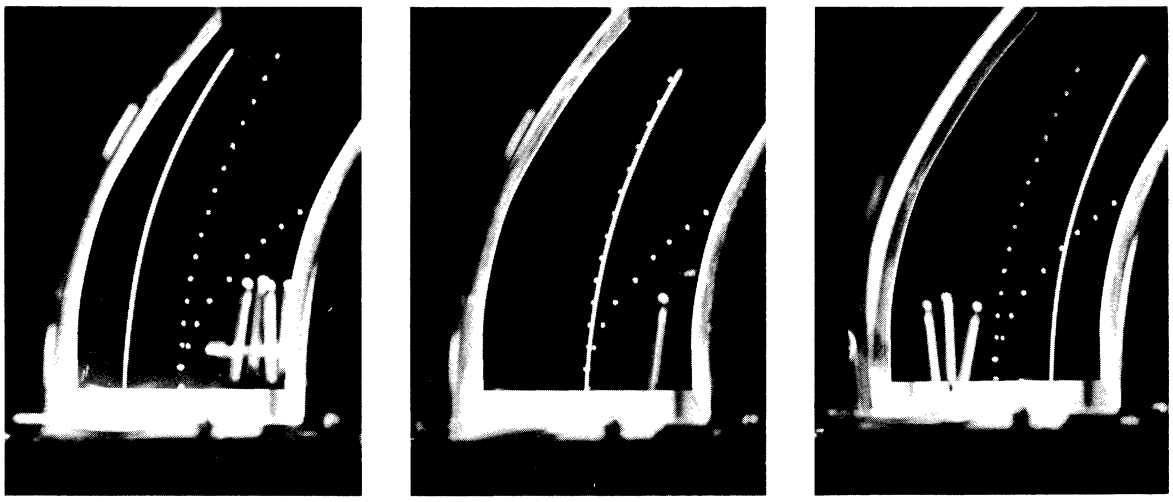

Figure 14a. Smoke Traces of Streamlines $\varpi = 90°$.

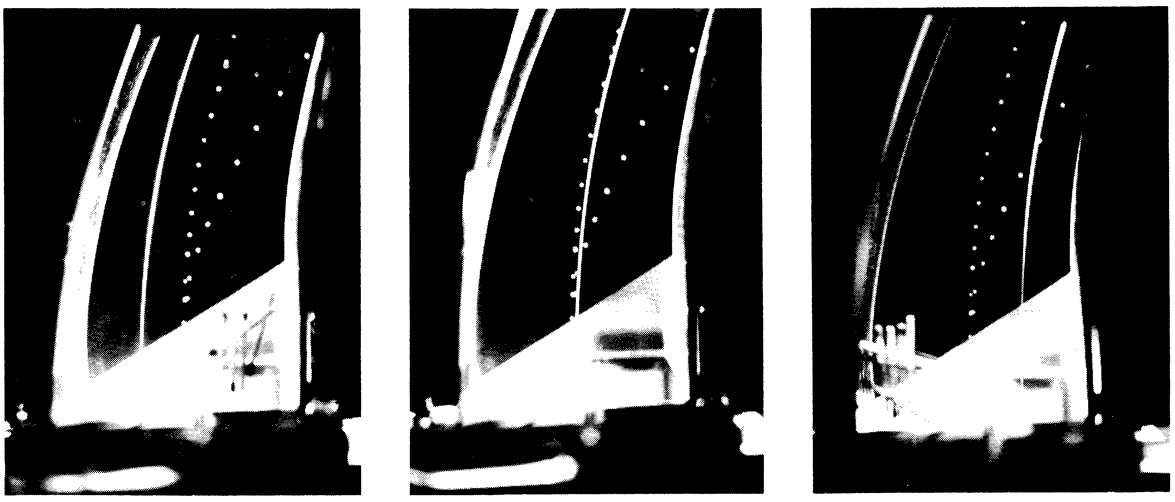

Figure 14b. Smoke Traces of Streamlines $\varpi = 60°$.

The question to be answered by the experimental measurements is: given a physical system for which the mainflow appears to coincide with flow system which, if it is infinite in extent, will yield an exact similarity solution of the boundary layer equations, how well will the similarity solution of the boundary layer equations predict the behavior of the physical system. In particular, how well will the exact solutions predict the boundary layer velocity profiles, the turning of boundary layer flow, the boundary layer thickness, and wall shear stress?

2. Test Procedure

Through the smoke studies, the wall shapes and the regions where the mainstream streamlines best corresponded with the analytical model were determined.

The flow followed the desired pattern very well on the pressure-side-half of the channel a distance somewhat greater than the width of the channel, 5 inches, back from the leading edge. On the suction-side-half the flow did not follow the pattern as well. The deviation increased as the suction-side wall was approached and as the distance from the leading edge increased. From this information four lateral locations were chosen in each channel for making boundary layer traverses.

Figure 15 shows the locations where the measurements were made. Since the systems were to be independent of x^2, two x^2 locations were used for each of two x^1 locations in each channel.

At all four locations in each channel a boundary layer traverse was made for both the flow angle and the velocity magnitude. The stagnation temperature was recorded with each impact pressure measurement.

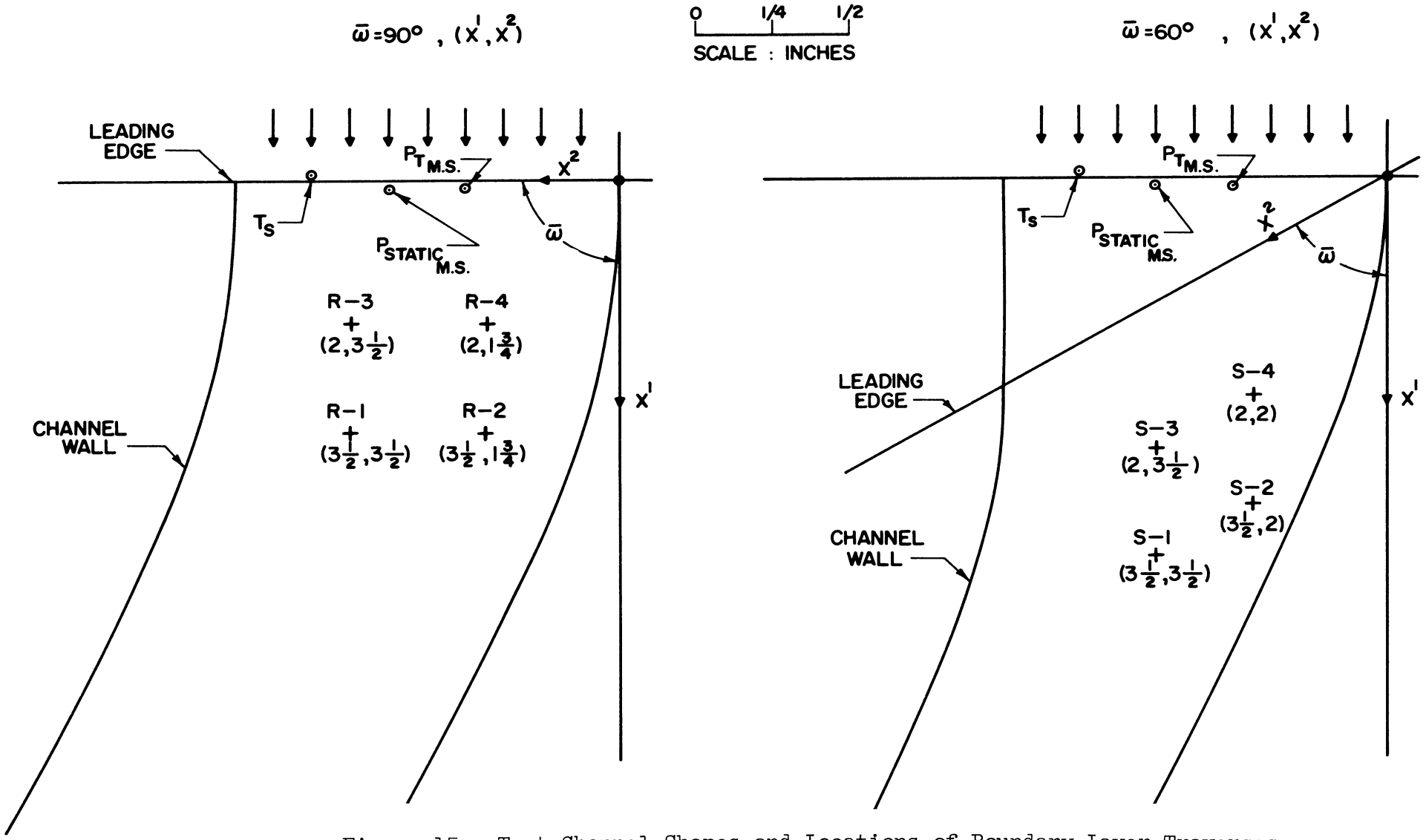

Figure 15. Test Channel Shapes and Locations of Boundary Layer Traverses.

A complete traverse at a given location was made without interruption. The entrance velocity to the channel was approximately 45 fps being constant for any complete traverse.

3. Analysis of Data.

The magnitude of the velocity, $|V|$, for a given location was determined from the relation,

$$P_T - p = \bar{C}_p \frac{1}{2} \rho |V|^2 \tag{145}$$

where P_T - p is the pressure difference measured between boundary layer impact probe and the static pressure at the surface above the probe, $\bar{C}_p$ the probe constant to correct for the viscous effect (see Appendix B), and ρ the fluid density.

The location above the plate at which the velocity existed was determined by the summation of: (1) the distance the probe moved normal to the plate as recorded by the dial indicator, (2) the distance from the bottom of the probe face to its geometric center, (3) a correction due to the "displacement effect".

The "displacement effect" is a phenomena which occurs when total pressure probes are placed in a transverse total pressure gradient and is manifested by the fact that the effective center of the probe is displaced from the geometric center in the direction of increasing total pressure. Investigations into the magnitude of the displacement effect have been conducted by Young and Maas (40) and Livesey (41 and 42). For rectangular faced probes References 40 and 41 suggest a constant

correction of 0.15 - 0.24 times the external dimension of the probe face in the direction of the traverse. A value of 0.18 was used throughout the data reduction.

The fluid properties were obtained from the National Bureau of Standards Circular 564, The Thermal Properties of Gases [43], using the stagnation temperature and the atmospheric pressure for each traverse. The stagnation temperature measured was used because, with the velocities of the experiment, the correction to be applied to obtain the static temperature would be less than 1/10th degree Fahrenheit which is within the accuracy of the measurement itself. The atmospheric pressure was used because the static pressure in the test channel was less than 1 inch of water different from the atmosphere into which the air was discharged.

Because the velocity measurements were expected to be more accurate than the angle measurements it was considered desirable to compare the two measurements individually with the analytical solutions. Therefore from the analytical solutions, which are in terms of velocity components, a reduced velocity magnitude profile and the turning angle of the velocity vector as a function of the similarity parameter η were calculated for each traverse location. Upon vectorially adding the velocity components from the analytical solution, the reduced velocity magnitude becomes

$$\frac{|V(\eta)|}{|V_{m.s.}|} = \left[\frac{(F')^2 + (\chi' G')^2 + 2F'G'\cos\bar{\omega}}{1 + 2\chi'\cos\bar{\omega} + (\chi')^2}\right]^{1/2} \qquad (146)$$

The angle ϕ which the velocity vector makes with the x^1 coordinate line is

$$\phi(\eta) = \arctan\left\{\frac{\bar{F}^2 \chi' \sin\bar{\omega}}{\bar{F}^1 + \bar{F}^2 \chi' \cos\bar{\omega}}\right\} \tag{147}$$

4. Results

The results of the experiment, as shown in Figures 16, 17, 18 and 19, show a substantial agreement with the analytical solutions. The reduced velocities appear to be in best agreement with the analysis. Significant deviations occur only at the locations nearest the suction side in the case of $\bar{\omega} = 90°$ (Figure 16 position R-1 and Figure 17 position R-3).

In Figures 16 and 17, which are for $\bar{\omega} = 90°$, it can be seen that the experimental velocity data agree very well with the analytical solution for positions R-2 and R-4 (see Figure 15 for locations) but some deviation occurs at positions R-1 and R-3. That is, as the point of measurement moves toward the suction side wall the deviation increases. The increase in deviation with movement toward the suction side wall can also be seen in the angular measurements.

It can be seen from Figures 18 and 19, which are for $\bar{\omega} = 60°$, that the experimentally measured reduced velocity profiles agree very well with the analytical solutions for all locations.

In Figures 16 - 19 it is seen that in almost every case the angular measurements show that the boundary layer velocity doesn't turn as much as predicted. This is to be expected because in the physical

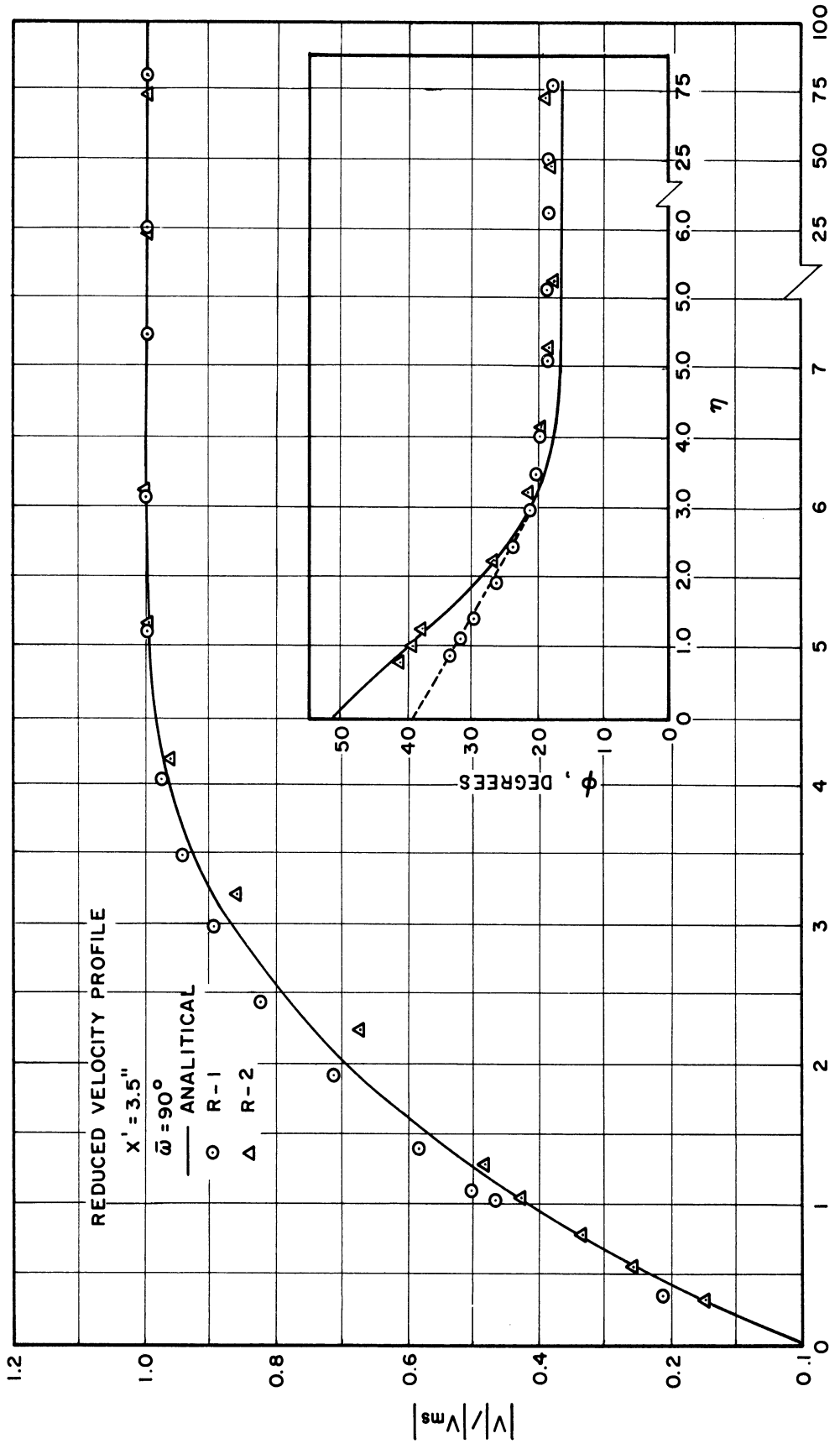

Figure 16. Comparison of Experimental and Analytical Reduced Velocity Profiles Location R-1,2.

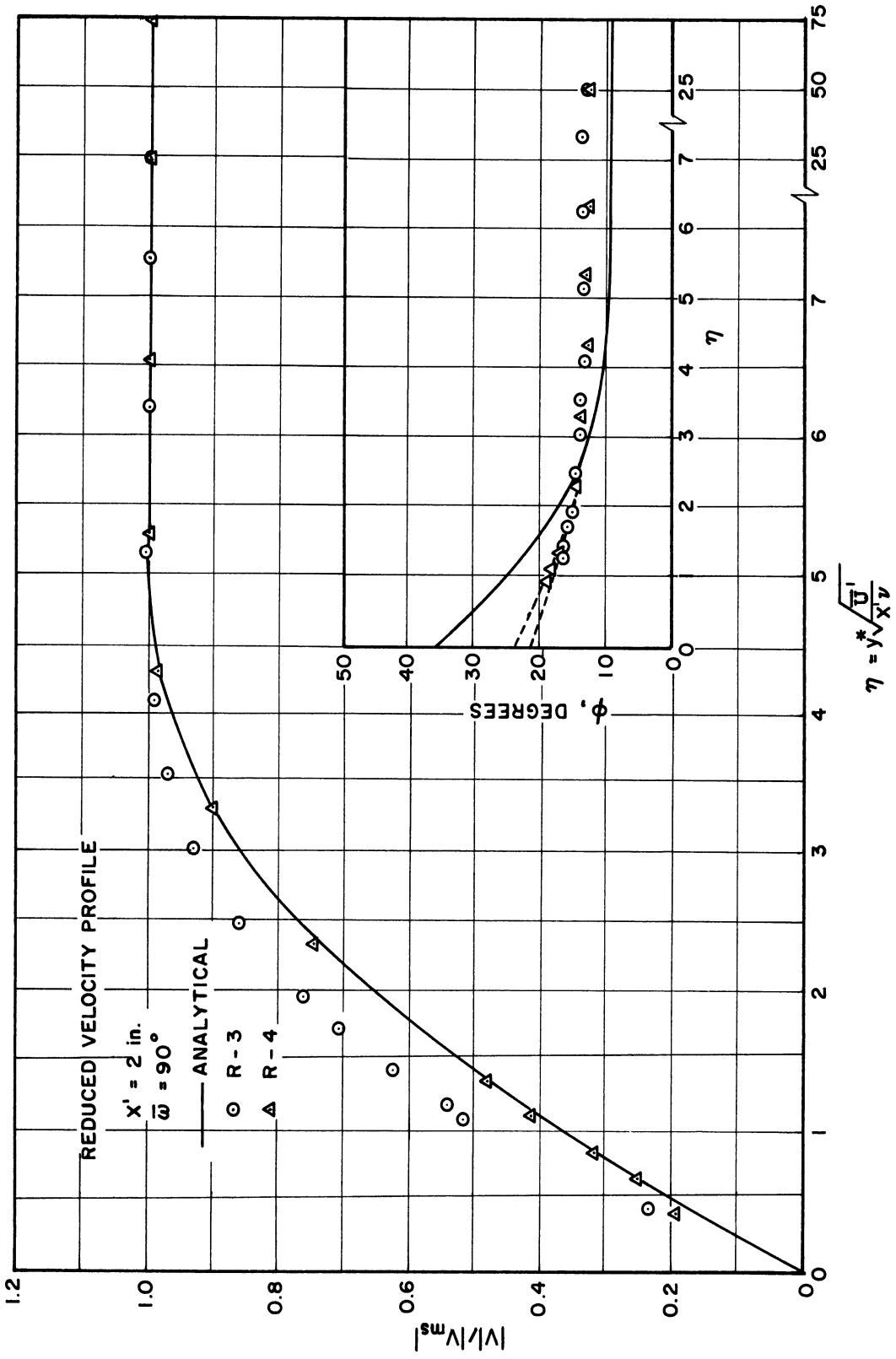

Figure 17. Comparison of Experimental and Analytical Reduced Velocity Profiles Location R-3,4.

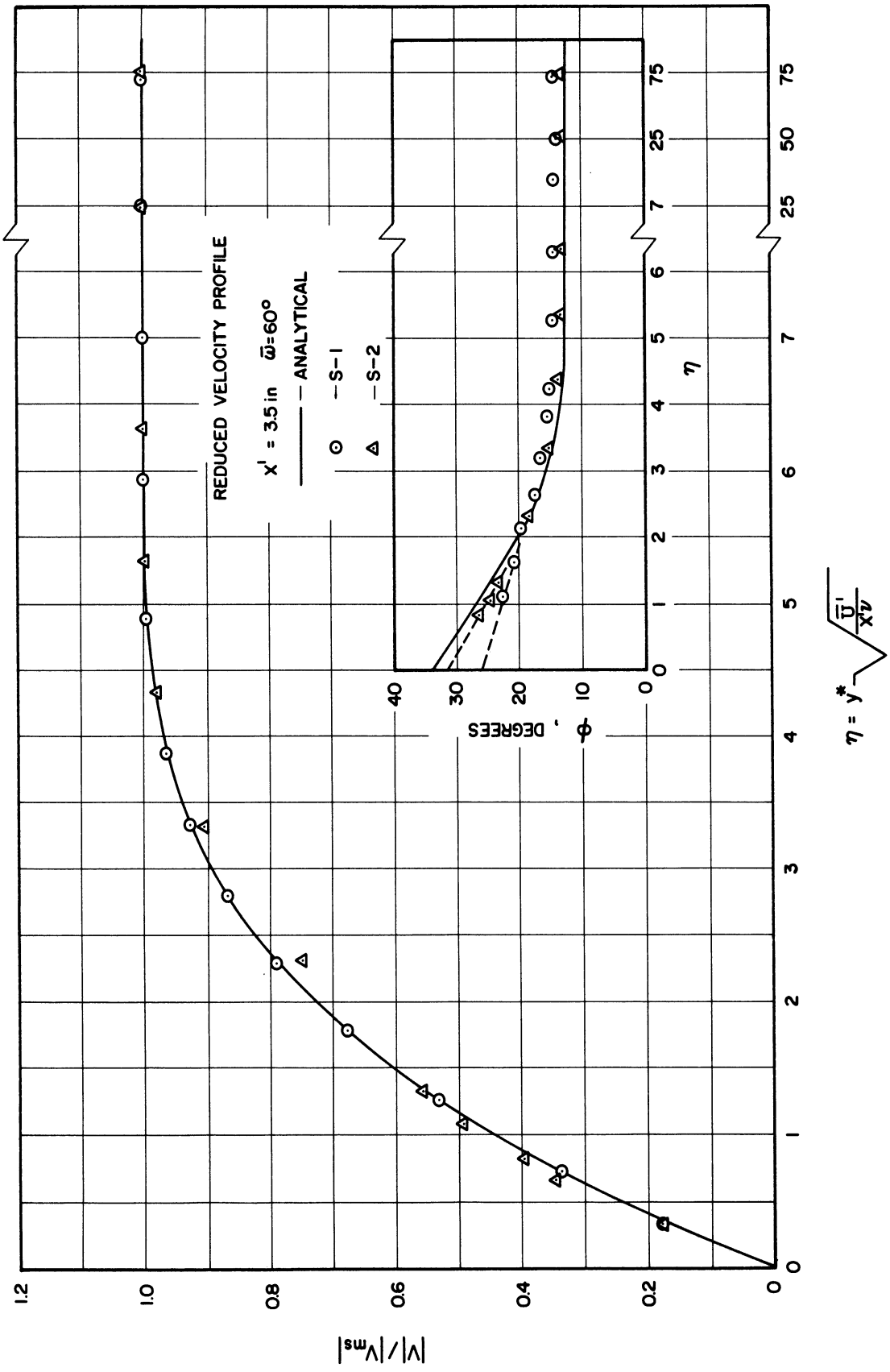

Figure 18. Comparison of Experimental and Analytical Reduced Velocity Profiles Location S-1,2.

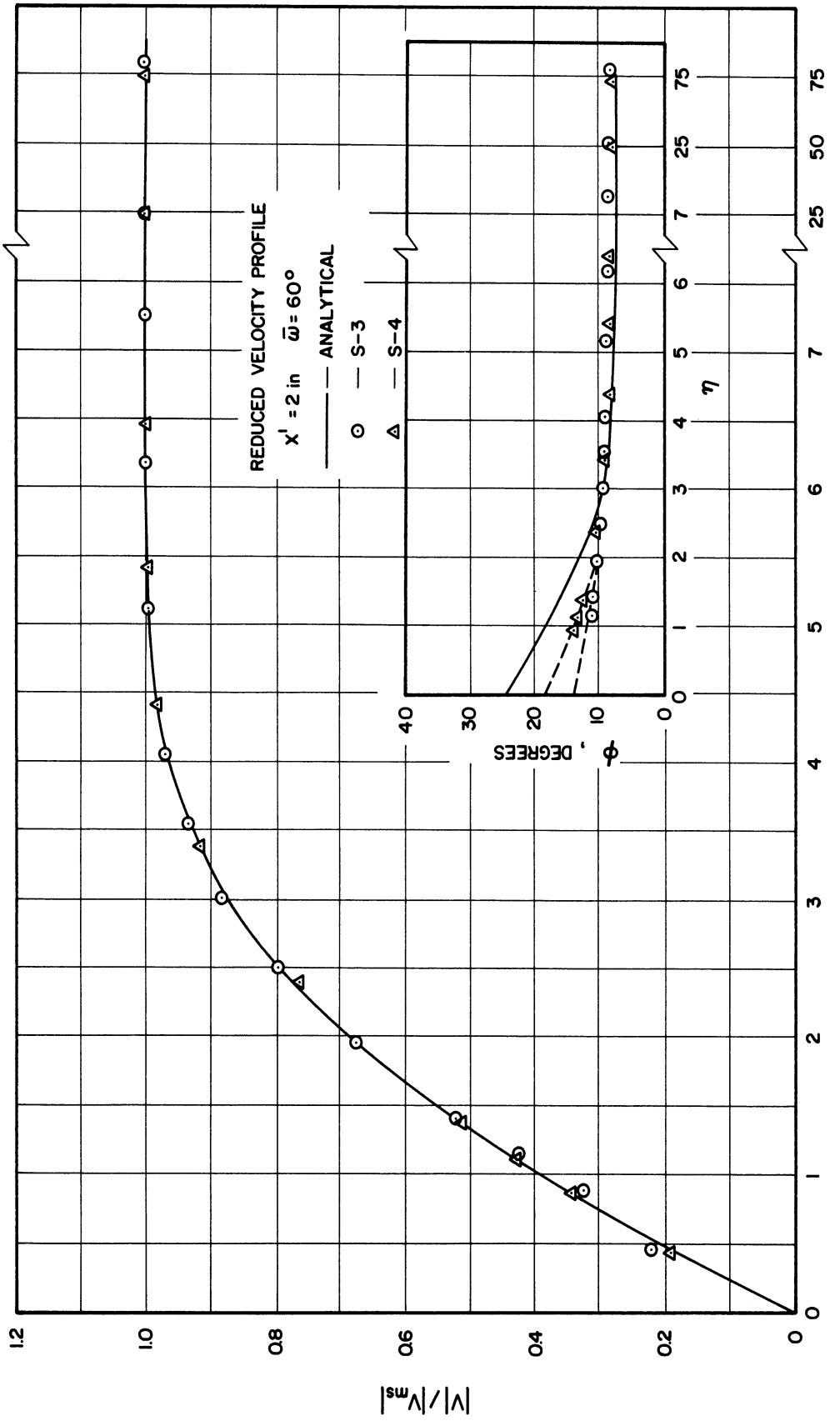

Figure 19. Comparison of Experimental and Analytical Reduced Velocity Profiles Location S-3,4.

system the suction side wall presents an obstruction for the boundary layer flow which undercuts the mainflow. In the analytical model the boundary layer is allowed to continue to turn and undercut the mainflow. In the physical case it is restrained from doing so by the sidewalls. In the vicinity of the suction side wall the boundary layer flow tends to roll up and form a vortex trailing out the channel. The influence of the suction side wall extends into the mainflow in an amount diminishing with distance.

In both the $\bar{\omega} = 90°$ and $\bar{\omega} = 60°$ cases the angular measurements show greater deviation at the positions nearest the leading edge (i.e., Figure 17 as compared with Figure 16 and Figure 19 as compared with Figure 18). This may be due to small differences between the physical systems and analytical models in entrance regions of the channels which could not be detected by the smoke studies.

The velocity profiles in each channel at the locations nearest the pressure side wall (R-2 in Figure 16 and S-2 in Figure 18) show a velocity defect in the approximate region of $1.75 < \eta < 4$. In the analytical model the boundary layer flow, at a location which corresponds to the pressure side wall in the physical system, comes from the region which corresponds to being outside the channel in the physical system. In the physical system there is flow off the pressure side wall into the boundary layer. The fact that the flow off the pressure side wall is insufficient to make up for the lack of flow through the pressure side wall is manifested in the velocity defect.

The slope of the velocity profiles is a measure of the shear stress in the flow. It is noted that in all cases the slope of the experimental data is in good agreement with the analytical solutions at $\eta = 0$, which corresponds to the surface. Hence the surface shear stress as determined from the experimental measurements should be in good agreement with that predicted from the analytical model.

It should be noted that the experimental data with the smallest values of η are for positions at which the probes are resting on the surface of the plate, and for $\eta \cong 75$ the probes are approximately three-quarters of an inch above the surface.

The boundary layer thickness measured is, at each location, in good agreement with that predicted by the analytical model.

From the experimental results it can be said that the similarity solutions will yield meaningful information for finite flow configurations where the mainstream streamlines and mainstream velocities approximate those necessary to admit the boundary layer equations to similarity solutions. The amount of turning of the boundary layer velocity is not predicted as well as the velocity profile, the boundary layer thickness, and wall shear stress. The prediction of the velocity profile, boundary layer thickness, and wall shear stress by the similarity solutions is in particularly good agreement with the experimental measurements.

CHAPTER IV

RESULTS AND CONCLUSIONS

1. The momentum equations for the three dimensional, incompressible, laminar, boundary layer have been analyzed for possible similarity solutions. It was found that by requiring the angle between the coordinate lines to be a constant but unspecified value, that considerable generalization of the classes of mainstream flows which admit to similarity could be made.

2. For each class of mainstream flow systems only particular groups of surface geometries and imbedded coordinate systems are admissible. The admissible surface geometries fall in two groups: (a) surfaces which are applicable to certain surfaces of revolution and (b) surfaces which are developable. For those mainstream flow systems for which the admissible surfaces must be applicable to certain surfaces of revolution, the surfaces of revolution are determined and the necessary and sufficient conditions which other surfaces must satisfy to be applicable to them are found. Admissible coordinate systems imbedded on the surfaces of revolution are found. In every case the coordinate lines are the parallels and loxodromes of the surface of revolution. For those mainstream flow systems for which the admissible surfaces must be developable, the admissible coordinate systems are determined when the surface is the Euclidean plane. The coordinate lines in this case are either a system of circles and logarithmic spirals or two sets of parallel straight lines. In all cases the coordinate lines can be described by a linear relation of some orthogonal coordinate system on the surface.

3. The boundary layer energy equation for the time steady behavior of a constant property system was derived and analyzed for similarity solutions of the temperature profile for each flow system which admits the momentum equations to similarity solutions of the velocity profiles.

4. It was found, in the cases where the surface is developable and the coordinate lines are geodesics, that viscous dissipation must be neglected if similarity solutions of the three-dimensional energy equation are to be obtained, and that the ordinary differential equations for momentum and energy are independent of the coordinate angle. Therefore existing numerical solutions where Cartesian coordinates have been used are also the solutions for flow configurations whose mainstream components vary along any two sets of parallel geodesic lines in the same manner as the mainstream components in the orthogonal case vary along their respective Cartesian coordinate lines.

5. With the experimental measurements it has been found that similarity solutions will reliably predict the boundary layer thickness and boundary layer profiles in those regions of channels where the mainstream flow components approximate those which are necessary to admit the boundary layer equations to similarity solutions. Within the capability of the experiments it appears that the wall shear stress is also reliably predicted by similarity solutions. The prediction of the boundary layer velocity turning angle by similarity solutions is not as good in general.

APPENDICES

Appendix A

DERIVATION OF THE BOUNDARY-LAYER ENERGY EQUATION, EQUATION (14)

The boundary layer energy equation in the general boundary layer coordinates, such as those used by Michal [8] for the momentum equations, to the best of the author's knowledge, does not exist in the usual literature sources.

The form of the boundary layer energy equation in the coordinates used for the momentum equations will be obtained in two ways. The first method uses the three dimensional boundary layer energy equation in Cartesian coordinates. By applying "correspondence principles" to the operation in each term, a form of the equation in the desired coordinates is obtained. Although it is easier to work with the Cartesian form and generalize it, an objection to this method is that there is no guarantee that all the important terms in the more general situation will appear. This is because the boundary layer energy equation is not a complete statement of a fundamental law but is a truncated form having been reduced by applying assumptions for the boundary layer. The second method uses the general energy equation. It is transformed to the coordinate system used for boundary layers and then reduced by applying physical assumptions for the boundary layer.

The second method produces the same form of the equation as the first method. This form is therefore considered to be the correct form of the boundary layer energy equation.

For the first method the three dimensional boundary layer energy equation for time steady flow of an imcompressible fluid with constant

viscosity and thermal conductivity in Cartesian coordinates $(\dot{x}, \dot{y}, \dot{z})$ is obtained from Pai (44 p.142). It is

$$\left(\dot{u}\frac{\partial T}{\partial \dot{x}} + \dot{v}\frac{\partial T}{\partial \dot{y}} + \dot{w}\frac{\partial T}{\partial \dot{z}}\right) = \frac{k}{\rho C_v}\frac{\partial^2 T}{\partial \dot{y}^2} + \frac{\nu}{C_v}\left[\left(\frac{\partial \dot{u}}{\partial \dot{y}}\right)^2 + \left(\frac{\partial \dot{w}}{\partial \dot{y}}\right)^2\right] \qquad \text{(A-1)}$$

where $\dot{u}$, $\dot{v}$, $\dot{w}$, are the fluid velocities in the $\dot{x}$, $\dot{y}$, $\dot{z}$ directions respectively; and the coordinate system is oriented with $\dot{x}$ and $\dot{z}$ on the surface and $\dot{y}$ the normal to the surface.

The left hand side of Equation (A-1) is the intrinsic derivative of the scalar $T(\dot{x}, \dot{y}, \dot{z})$ and from tensor calculus (i.e., Reference 31), it is known that the intrinsic derivative of a scalar has the same form in any coordinate system. Therefore in the general coordinates $\left[x^0, x^1, x^2\right]$ where $\left[x^1, x^2\right]$ are imbedded on the surface and x^0 is normal to the surface, the first term in Equation (A-1) becomes

$$u^1\frac{\partial T}{\partial x^1} + u^0\frac{\partial T}{\partial x^0} + u^2\frac{\partial T}{\partial x^2}$$

or

$$u^\alpha\frac{\partial T}{\partial x^\alpha} + u^0\frac{\partial T}{\partial x^0} \quad , \quad \alpha = 1,2 \qquad \text{(A-2)}$$

The first term on the right hand side of Equation (A-1) can be written as

$$\frac{k}{\rho C_v}\frac{\partial}{\partial y}\left[\frac{\partial T}{\partial y}\right].$$

The covariant derivative, in general coordinates, corresponds to the ordinary partial derivative in Cartesian coordinates. And the covariant derivative of the scalar T is the ordinary partial derivative in any coordinate system. Therefore the above term becomes

$$\frac{k}{\rho C_v} g^{00} \left[\frac{\partial T}{\partial x^0}\right]_{,0} \tag{A-3}$$

By the definition of covariant differentiation the above term becomes

$$\frac{k}{\rho C_v} g^{00} \left[\frac{\partial^2 T}{\partial (x^0)^2} - \left\{ \begin{matrix} m \\ 0\,0 \end{matrix} \right\} \frac{\partial T}{\partial x^m}\right].$$

But for the coordinate system used, the metric components whose indices involve zeros are

$$g^{00} = g_{00} = 1 \;, \quad g^{0\alpha} = g_{\alpha 0} = 0 \,.$$

Therefore, from the definition of the Christoffel symbols, any Christoffel symbol with two or more zero indices is zero. Consequently this term is

$$\frac{k}{\rho C_v} \frac{\partial^2 T}{\partial (x^0)^2} \tag{A-4}$$

In the remaining term of Equation (A-1), the viscous dissapation term, the partial derivative is again replaced by the covariant derivative giving

$$\frac{\nu}{C_v}\left[g^{\alpha\beta} g^{00} u_{\alpha,0} u_{\beta,0}\right].$$

With the definition of covariant differentiation this becomes

$$\frac{\nu}{c_v} g^{\alpha\beta} g^{00} \left[\frac{\partial u_\alpha}{\partial x^0} - \left\{ {\lambda \atop \alpha 0} \right\} u_\lambda\right]\left[\frac{\partial u_\beta}{\partial x^0} - \left\{ {\mu \atop \beta 0} \right\} u_\mu\right] \tag{A-5}$$

Again using the metric components and the definition of the Christoffel symbols, the Christoffel symbols in the above expression are

$$\left\{ {\alpha \atop \beta 0} \right\} = -\frac{1}{2} g^{\alpha\lambda} \frac{\partial g_{\beta\lambda}}{\partial x^0} \tag{A-6}$$

It is well to note that the energy equation has only one independent variable, namely T (x^0, x^1, x^2), because the velocities are known from the solution of the boundary layer momentum equations. Also, that the thermal boundary layer thickness is at most approximately the same as the hydrodynamic boundary layer thickness. This is known from the fact that the Prandtl Number is a measure of the capacity of the fluid to diffuse momentum as compared with its capacity to diffuse heat and that all gases and liquids, with the exception of liquid metals* , have Prandtl numbers which are approximately one or larger. From the above then it can be said that the energy equation need only be valid in the same spatial region as the boundary layer momentum equations. In the boundary layer momentum equations it has been assumed that in the region of validity the space metric components, $g_{\alpha\beta}$ (x^0, x^1, x^2), $\alpha,\beta = 1,2$, can be replaced by

* Equation (A-1) is not valid for liquid metals because of the implicit assumption that the thermal conduction terms in the x^1 and x^2 directions are neglibible as compared with the thermal convection terms in the same directions. This may not be a valid assumption for liquid metals because of their high thermal conductivity.

the first fundamental metric of the surface, which is

$$a_{\alpha\beta}(x^1, x^2) = g_{\alpha\beta}(0, x^1, x^2) \quad , \quad \alpha, \beta = 1, 2 \tag{A-7}$$

Therefore the Christoffel symbol in Equation (A-6) is zero and Equation (A-5) reduces to

$$\frac{\nu}{c_v} a^{\alpha\beta} g^{00} \frac{\partial u_\alpha}{\partial x^0} \frac{\partial u_\beta}{\partial x^0}$$

or

$$\frac{\nu}{c_v} a_{\alpha\beta} \frac{\partial u^\alpha}{\partial x^0} \frac{\partial u^\beta}{\partial x^0} \tag{A-8}$$

Combining Equations (A-2, A-4, A-8), Equation (A-1), in the general coordinates of the boundary layer, becomes

$$u^\alpha \frac{\partial T}{\partial x^\alpha} + u^0 \frac{\partial T}{\partial x^0} = \frac{k}{\rho c_v} \frac{\partial^2 T}{\partial (x^0)^2} + \frac{\nu}{c_v} a_{\alpha\beta} \frac{\partial u^\alpha}{\partial x^0} \frac{\partial u^\beta}{\partial x^0} \tag{A-9}$$

Equation (A-9) may not be complete because it was derived from a truncated, i.e., not complete, form of a fundamental law. A second approach to the boundary layer energy equation will now be presented. In this approach the complete three dimensional energy equation will be reduced for the special case of boundary layer flow.

The time steady energy equation in general coordinates for an imcompressible fluid with constant properties is

$$u^j \frac{\partial T}{\partial x^j} = \frac{k}{\rho c_v} g^{ij} \left[\frac{\partial T}{\partial x^i}\right]_{,j} + 2\frac{\nu}{c_v} g^{ik} g^{jl} \dot{e}_{ij} \dot{e}_{kl} \tag{A-10}$$

where

$$\dot{e}_{ij} \equiv \frac{1}{2}\left(u_{i,j} + u_{j,i}\right) \tag{A-11}$$

and

$i = 0, 1, 2.$

The desired coordinate system has x^1 and x^2 imbedded on the surface and x^0 normal to them. The domain of space in which the equation is to be used, as discussed above, is sufficiently close to the surface defined by $x^0 = 0$ that the space metric can be assumed to be

$$a_{\alpha\beta}(x^1, x^2) \quad , \quad \alpha, \beta = 1, 2 \tag{A-12}$$

$$g^{00} = 1 \quad , \quad g^{0\alpha} = g_{\alpha 0} = 0$$

where $a_{\alpha\beta}$ is the first fundamental metric of the surface.

In this coordinate system Equation (A-10) becomes

$$u^{\alpha}\frac{\partial T}{\partial x^{\alpha}} + u^{0}\frac{\partial T}{\partial x^{0}} = \frac{k}{\rho c_v}\left[a^{\alpha\beta}\left(\frac{\partial T}{\partial x^{\alpha}}\right)_{;\beta} + g^{00}\frac{\partial^2 T}{\partial (x^{0})^2}\right]$$

$$+2\frac{\nu}{c_v}\left[\dot{e}_{\alpha\beta}\dot{e}_{\lambda\mu}a^{\alpha\lambda}a^{\beta\mu} + \dot{e}_{00}\dot{e}_{00}g^{00}g^{00} + 2\dot{e}_{0\alpha}\dot{e}_{0\beta}g^{00}a^{\alpha\beta}\right] \qquad \text{(A-13)}$$

$$\alpha = 1,2$$

The term $a^{\alpha\beta}\left[\frac{\partial T}{\partial x^{\alpha}}\right]_{;\beta}$ represents the thermal conduction parallel to the surface and will be neglected in comparison to the thermal convection parallel to the surface. The fluid therefore may not be a liquid metal.

Because of the nature of the boundary layer, the principal contribution to the viscous dissipation term, the last term in Equation (A-13), comes from the tangential shear in the plane parallel to the surface. Therefore the energy dissipation due to the normal stresses and the remaining shear stresses may be neglected. In the viscous dissipation term of Equation (A-13), only the relation

$$2\dot{e}_{0\alpha}\dot{e}_{0\beta}g^{00}a^{\alpha\beta}$$

contains the terms of the energy dissipation due to the tangential shear parallel to the surface. The above relation also contains terms which are negligible and will therefore be examined more closely. Using the definition of $\dot{e}_{\alpha\beta}$ the above relation becomes

$$\frac{1}{2} g^{oo} a^{\alpha\beta} \left[u_{o;\alpha} + u_{\alpha,o} \right] \left[u_{o;\beta} + u_{\beta,o} \right] \qquad \text{(A-14)}$$

Only the second quantity in each set of parenthesis is associated with the energy dissipation due to the tangential shear in the plane parallel to the surface. The first quantity in each set of parenthesis represents the tangential shears in planes normal to the surface and hence are neglected. The relation now becomes

$$\frac{1}{2} g^{oo} a^{\alpha\beta} u_{\alpha;o} u_{\beta;o} \qquad \text{(A-15)}$$

With the space metric defined in Equation (A-12), the covariant differentiation in the above reduces to the partial derivative of the u_α with respect of x^o. The relationship is then

$$\frac{1}{2} g^{oo} a^{\alpha\beta} \frac{\partial u_\alpha}{\partial x^o} \frac{\partial u_\beta}{\partial x^o} \qquad \text{(A-16)}$$

or

$$\frac{1}{2} a_{\alpha\beta} \frac{\partial u^\alpha}{\partial x^o} \frac{\partial u^\beta}{\partial x^o}$$

With the above assumptions the energy equation, Equation (A-13) takes the following form for the boundary layer:

$$u^\alpha \frac{\partial T}{\partial x^\alpha} + u^o \frac{\partial T}{\partial x^o} = \frac{k}{\rho C_v} \left[\frac{\partial^2 T}{\partial (x^o)^2} \right] + \frac{\nu}{C_v} a_{\alpha\beta} \frac{\partial u^\alpha}{\partial x^o} \frac{\partial u^\beta}{\partial x^o} \qquad \text{(A-17)}$$

Equation (A-17) is identical to Equation (A-9) which was obtained by an independent method.

To obtain the form of the boundary layer energy equation used in the text, Equation (14), two remaining steps must be performed, neither of which have any bearing on the above derivations. The first step is to make the following substitutions;

$$u^\circ = v$$

$$x^\circ = \sqrt{\nu}\, y .$$

The second step is to replace C_v with C_p so the Prandtl number may be introduced. This substitution is valid for an incompressible fluid because thermodynamic relations require them to be identically equal [see for instance VanWylen (45 p.414)]. Therefore Equation (A-17) takes the same form as used in the text, namely,

$$u^\alpha \frac{\partial T}{\partial x^\alpha} + \frac{v}{\sqrt{\nu}} \frac{\partial T}{\partial y} = \frac{1}{P_R} \frac{\partial^2 T}{\partial y^2} + \frac{1}{C_p} a_{\alpha\beta} \frac{\partial u^\alpha}{\partial y} \frac{\partial u^\beta}{\partial y} \qquad (13)$$

$$\alpha, \beta = 1, 2$$

Appendix B

CALIBRATION OF BOUNDARY-LAYER PITOT TUBE FOR VISCOUS EFFECT

As stated in the text, the method of pitot tube calibration was that used by Macmillan [37]. The pitot tube was calibrated over a range of velocities of $1.9 \leq V \leq 49.1$ fps. For the temperatures encountered, this corresponds to a range of Reynolds number of $1.8 \leq R \leq 46.8$. The Reynold's number variation covered the range of conditions encountered in the experimental investigation. The Reynold's number was defined as

$$R \equiv \frac{|V| h}{\nu} \tag{B-1}$$

where h is the internal height of the probe opening, ν the kinematic viscosity of the air, and $|V|$ the magnitude of the velocity of the undisturbed stream at the probe tip.

A probe coefficient, $\bar{C}_p$, is defined as

$$\bar{C}_p \equiv \frac{P_T - p}{\frac{1}{2}\rho |V|^2} \tag{B-2}$$

where P_T is the pressure in the Pitot tube, ρ the density of the air, and p and $|V|$ are the static pressure and the velocity of the undisturbed stream. The density and absolute viscosity, and hence the kinematic viscosity, of the air were obtained from the NBS Circular 564 Table of Thermal Properties of Gases, Reference 43. The pressure and temperature used in this case were the atmospheric pressure and temperature as measured with a mercury barometer and mercury-glass thermometer both in close proximity of the calibrating equipment.

The probe was mounted on the centerline of a vertical pipe just below the entrance section as shown in Figure 20. In the side wall, directly opposite the Pitot tip, a static pressure tap was located. Directly below the pipe was a tank from which the air was continually removed with a variable speed suction fan.

With the experimental configuration used, the total pressure at the probe tip should be atmospheric pressure Pa, (neglecting any viscous losses in the entrance region.) The difference between the pressure in the pitot tube and the atmospheric pressure is then a measure of the viscous effect at the probe.

In Reference 37 a flow meter was placed down-stream of the pipe entrance to obtain the velocity of the undistrubed stream at the probe tip. No difference could be detected between the dynamic head, $\frac{1}{2}\rho|V|^2$, obtained from the use of flow meter and that which is obtained by measuring the difference between the atmospheric pressure and the static pressure in the tube wall opposite the pitot tube. In Reference 37, the atatic tap pressure reading was used to obtain all the dynamic pressures, $\frac{1}{2}\rho|V|^2$, and velocities of the undistrubed stream $|V|$ when calibrating the flat-mouth probes. This was also the method used here. This method is justified here because the pipe entrance and probe body are the same sizes as used in Reference 37, only the shape and dimensions of the probe opening itself are different.

As

$$P_a = p + \frac{1}{2}\rho V^2 \qquad \text{(B-3)}$$

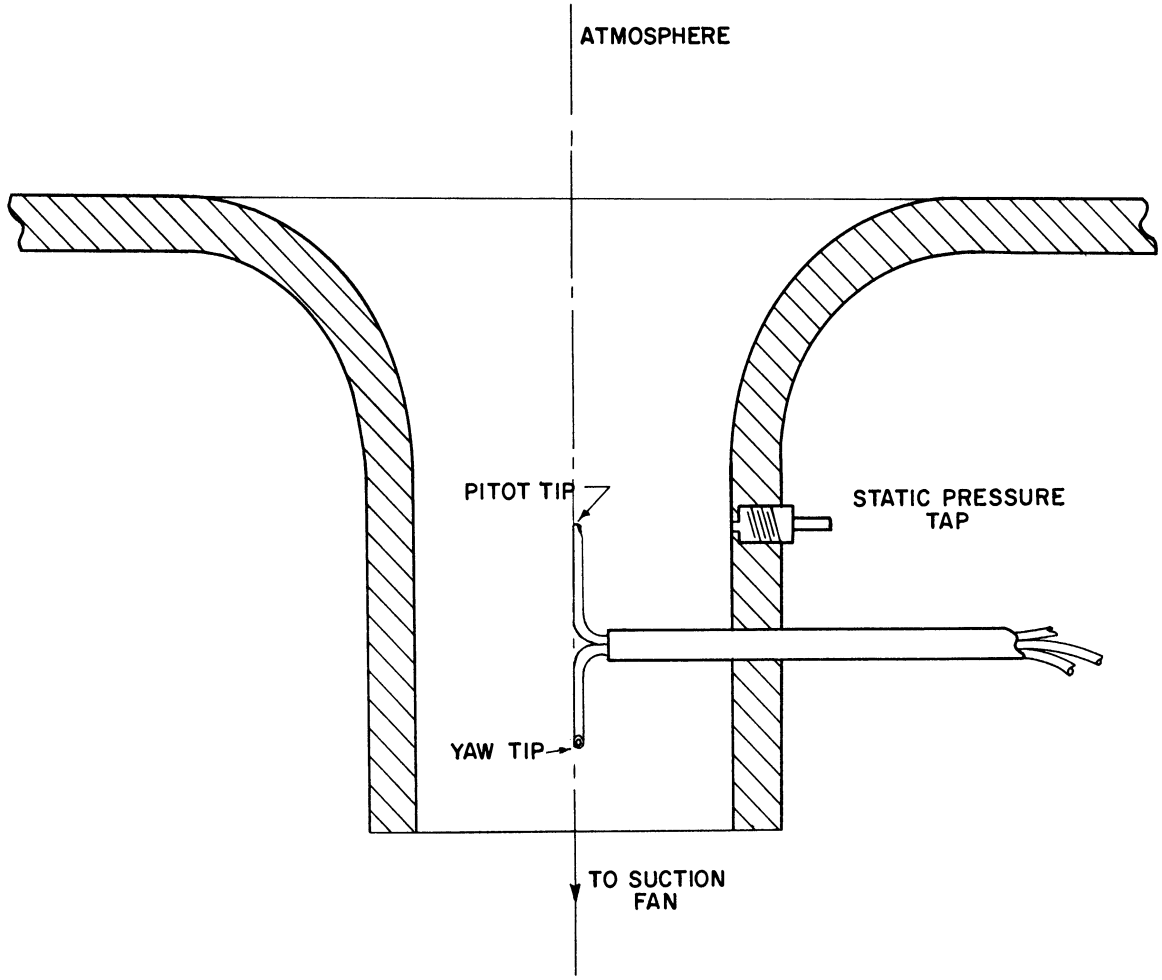

Figure 20. Schematic of System Used for Calibration of Pitot Tube Viscous Effect.

Equation (B-2) can be expressed as

$$\bar{C}_p = 1 + \frac{P_T - P_a}{\frac{1}{2}\rho V^2} \qquad \text{(B-4)}$$

In view of the method described above for obtaining the dynamic head, Equation (B-4) can be written as

$$\bar{C}_p = 1 + \frac{P_T - P_a}{P_a - p} \qquad \text{(B-5)}$$

The second term on the right hand side is simply the ratio of the pressures measured between the pitot tube and the atmosphere, and the static tap and the atmosphere. All these measurements were made on the Chattock-Fry Tilting Manometer.

The results of this calibration are shown in Figure 10, p.92.

Appendix C

NUMERICAL SOLUTIONS FROM YOHNER AND HANSEN [18]

Numerical solutions for Equations (141) and (142), which are

$$\frac{1}{2} F^{1}{}'' F^{1} + F^{1}{}''' = 0 \tag{141}$$

$$-F^{1}{}' F^{2}{}' + \frac{1}{2} F^{2}{}'' F^{1} + F^{2}{}''' + 1 = 0 \tag{142}$$

where

$$F^{1}(0) = F^{1}{}'(0) = F^{2}(0) = F^{2}{}'(0) = 0$$

$$\lim_{\eta \to \infty} F^{1}{}'(\eta) = 1$$

$$\lim_{\eta \to \infty} F^{2}{}'(\eta) = 1 \ ,$$

are found in Yohner and Hansen [18]

They are:

η	$F(\eta)$	$F'(\eta)$	$F''(\eta)$	η	$F(\eta)$	$F'(\eta)$	$F''(\eta)$	η	$F(\eta)$	$F'(\eta)$	$F''(\eta)$
0.000	0.000	0.000	0.332	2.500	0.996	0.751	0.217	5.000	3.283	0.992	0.016
.050	.000	.017	.332	2.550	1.034	.762	.212	5.050	3.333	.992	.015
.100	.002	.033	.332	2.600	1.073	.772	.206	5.100	3.383	.993	.013
.150	.004	.050	.332	2.650	1.111	.783	.201	5.150	3.432	.994	.012
.200	.007	.066	.332	2.700	1.151	.793	.195	5.200	3.482	.994	.011
.250	.010	.083	.332	2.750	1.191	.802	.190	5.250	3.532	.995	.010
.300	.015	.100	.332	2.800	1.231	.812	.184	5.300	3.581	.995	.010
.350	.020	.116	.332	2.850	1.272	.821	.178	5.350	3.631	.996	.009
.400	.027	.133	.331	2.900	1.313	.829	.173	5.400	3.681	.996	.008
.450	.034	.149	.331	2.950	1.355	.838	.167	5.450	3.731	.997	.007
.500	.041	.166	.331	3.000	1.397	.846	.161	5.500	3.781	.997	.007
.550	.050	.182	.331	3.050	1.439	.854	.156	5.550	3.830	.997	.006
.600	.060	.199	.330	3.100	1.482	.862	.150	5.600	3.880	.997	.005
.650	.070	.215	.330	3.150	1.525	.869	.145	5.650	3.930	.998	.005
.700	.081	.232	.329	3.200	1.569	.876	.139	5.700	3.980	.998	.004
.750	.093	.248	.328	3.250	1.613	.883	.134	5.750	4.030	.998	.004
.800	.106	.265	.327	3.300	1.657	.889	.128	5.800	4.080	.998	.004
.850	.120	.281	.326	3.350	1.702	.896	.123	5.850	4.130	.999	.003
.900	.134	.297	.325	3.400	1.747	.902	.118	5.900	4.180	.999	.003
.950	.149	.314	.324	3.450	1.792	.908	.113	5.950	4.230	.999	.003
1.000	.166	.330	.323	3.500	1.838	.913	.108	6.000	4.280	.999	.002
1.050	.182	.346	.322	3.550	1.883	.918	.103	6.050	4.330	.999	.002
1.100	.200	.362	.320	3.600	1.930	.923	.098	6.100	4.380	.999	.002
1.150	.219	.378	.318	3.650	1.976	.928	.093	6.150	4.429	.999	.002
1.200	.238	.394	.317	3.700	2.022	.933	.089	6.200	4.479	.999	.002
1.250	.258	.410	.315	3.750	2.069	.937	.084	6.250	4.529	.999	.001
1.300	.279	.425	.313	3.800	2.116	.941	.080	6.300	4.579	1.000	.001
1.350	.301	.441	.310	3.850	2.163	.945	.076	6.350	4.629	1.000	.001
1.400	.323	.456	.308	3.900	2.211	.949	.072	6.400	4.679	1.000	.001
1.450	.346	.472	.305	3.950	2.258	.952	.068	6.450	4.729	1.000	.001
1.500	.370	.487	.303	4.000	2.306	.956	.064	6.500	4.779	1.000	.001
1.550	.395	.502	.300	4.050	2.354	.959	.061	6.550	4.829	1.000	.001
1.600	.420	.517	.297	4.100	2.402	.962	.057	6.600	4.879	1.000	.001
1.650	.447	.532	.293	4.150	2.450	.964	.054	6.650	4.929	1.000	.001
1.700	.473	.546	.290	4.200	2.498	.967	.051	6.700	4.979	1.000	.000
1.750	.501	.561	.287	4.250	2.546	.969	.047	6.750	5.029	1.000	.000
1.800	.530	.575	.283	4.300	2.595	.972	.044	6.800	5.079	1.000	.000
1.850	.559	.589	.279	4.350	2.644	.974	.042	6.850	5.129	1.000	.000
1.900	.588	.603	.275	4.400	2.692	.976	.039	6.900	5.179	1.000	.000
1.950	.619	.616	.271	4.450	2.741	.978	.036	6.950	5.229	1.000	.000
2.000	.650	.630	.267	4.500	2.790	.980	.034	7.000	5.279	1.000	.000
2.050	.682	.643	.262	4.550	2.839	.981	.032				
2.100	.714	.656	.258	4.600	2.888	.983	.029				
2.150	.747	.669	.253	4.650	2.937	.984	.027				
2.200	.781	.681	.248	4.700	2.987	.985	.025				
2.250	.816	.694	.243	4.750	3.036	.987	.024				
2.300	.851	.706	.238	4.800	3.085	.988	.022				
2.350	.886	.717	.233	4.850	3.135	.989	.020				
2.400	.922	.729	.228	4.900	3.184	.990	.019				
2.450	.959	.740	.223	4.950	3.234	.991	.017				

η	$2F(\eta)$	$2F'(\eta)$	$2F''(\eta)$	η	$2F(\eta)$	$2F'(\eta)$	$2F''(\eta)$	η	$2F(\eta)$	$2F'(\eta)$	$2F''(\eta)$
0.000	0.000	0.000	1.418	2.500	2.229	1.154	-0.070	5.000	4.887	1.008	-0.014
.050	.002	.070	1.368	2.550	2.287	1.151	-.075	5.050	4.937	1.007	-.013
.100	.007	.137	1.318	2.600	2.344	1.147	-.079	5.100	4.987	1.006	-.012
.150	.015	.201	1.268	2.650	2.401	1.143	-.082	5.150	5.038	1.006	-.011
.200	.027	.264	1.219	2.700	2.458	1.139	-.085	5.200	5.088	1.005	-.010
.250	.042	.323	1.170	2.750	2.515	1.134	-.087	5.250	5.138	1.005	-.009
.300	.059	.381	1.121	2.800	2.572	1.130	-.089	5.300	5.188	1.004	-.009
.350	.080	.435	1.073	2.850	2.628	1.126	-.090	5.350	5.239	1.004	-.008
.400	.103	.488	1.025	2.900	2.684	1.121	-.090	5.400	5.289	1.004	-.007
.450	.128	.538	.978	2.950	2.740	1.117	-.091	5.450	5.339	1.003	-.007
.500	.157	.586	.931	3.000	2.796	1.112	-.091	5.500	5.389	1.003	-.006
.550	.187	.631	.886	3.050	2.851	1.107	-.090	5.550	5.439	1.003	-.005
.600	.220	.674	.841	3.100	2.907	1.103	-.090	5.600	5.489	1.002	-.005
.650	.254	.715	.797	3.150	2.962	1.098	-.089	5.650	5.540	1.002	-.004
.700	.291	.754	.753	3.200	3.017	1.094	-.087	5.700	5.590	1.002	-.004
.750	.330	.791	.711	3.250	3.071	1.090	-.086	5.750	5.640	1.002	-.004
.800	.370	.825	.670	3.300	3.126	1.085	-.084	5.800	5.690	1.002	-.003
.850	.412	.858	.629	3.350	3.180	1.081	-.082	5.850	5.740	1.001	-.003
.900	.456	.888	.590	3.400	3.234	1.077	-.080	5.900	5.790	1.001	-.003
.950	.501	.917	.552	3.450	3.287	1.073	-.078	5.950	5.840	1.001	-.002
1.000	.548	.943	.515	3.500	3.341	1.069	-.076	6.000	5.890	1.001	-.002
1.050	.595	.968	.479	3.550	3.394	1.066	-.074	6.050	5.940	1.001	-.002
1.100	.644	.991	.444	3.600	3.448	1.062	-.071	6.100	5.990	1.001	-.002
1.150	.694	1.012	.410	3.650	3.501	1.059	-.069	6.150	6.040	1.001	-.002
1.200	.746	1.032	.378	3.700	3.553	1.055	-.066	6.200	6.090	1.001	-.001
1.250	.798	1.050	.346	3.750	3.606	1.052	-.064	6.250	6.140	1.001	-.001
1.300	.851	1.067	.316	3.800	3.659	1.049	-.061	6.300	6.190	1.000	-.001
1.350	.904	1.082	.287	3.850	3.711	1.046	-.059	6.350	6.240	1.000	-.001
1.400	.959	1.096	.260	3.900	3.763	1.043	-.056	6.400	6.290	1.000	-.001
1.450	1.014	1.108	.233	3.950	3.815	1.040	-.053	6.450	6.340	1.000	-.001
1.500	1.069	1.119	.208	4.000	3.867	1.038	-.051	6.500	6.390	1.000	-.001
1.550	1.126	1.129	.184	4.050	3.919	1.035	-.048	6.550	6.440	1.000	-.001
1.600	1.182	1.137	.161	4.100	3.971	1.033	-.046	6.600	6.490	1.000	-.001
1.650	1.239	1.145	.139	4.150	4.022	1.031	-.044	6.650	6.540	1.000	-.001
1.700	1.297	1.151	.118	4.200	4.074	1.028	-.041	6.700	6.590	1.000	.000
1.750	1.354	1.157	.099	4.250	4.125	1.026	-.039	6.750	6.640	1.000	.000
1.800	1.412	1.161	.081	4.300	4.176	1.025	-.037	6.800	6.690	1.000	.000
1.850	1.471	1.165	.064	4.350	4.228	1.023	-.035	6.850	6.740	1.000	.000
1.900	1.529	1.168	.048	4.400	4.279	1.021	-.033	6.900	6.790	1.000	.000
1.950	1.587	1.170	.033	4.450	4.330	1.019	-.031	6.950	6.840	1.000	.000
2.000	1.646	1.171	.019	4.500	4.381	1.018	-.029	7.000	6.890	1.000	.000
2.050	1.704	1.171	.006	4.550	4.431	1.017	-.027				
2.100	1.763	1.171	-.006	4.600	4.482	1.015	-.025				
2.150	1.822	1.171	-.017	4.650	4.533	1.014	-.023				
2.200	1.880	1.170	-.027	4.700	4.584	1.013	-.022				
2.250	1.938	1.168	-.036	4.750	4.634	1.012	-.020				
2.300	1.997	1.166	-.045	4.800	4.685	1.011	-.019				
2.350	2.055	1.164	-.052	4.850	4.735	1.010	-.018				
2.400	2.113	1.161	-.059	4.900	4.786	1.009	-.016				
2.450	2.171	1.158	-.065	4.950	4.836	1.008	-.015				

LIST OF REFERENCES

1. Prandtl, L. "Über Flussigkeitsbewegung bei sehr kleiner Reibung", Verhandl. III Intern. Math.-Kongr., Heidelberg, 1904; also NACA TM No. 452 (1928)

2. Blausis, H. "Grengschichten in Flüssigkeiten mit kleiner Reibung", Z. Math. Physik, 56 (1908) 4-13; also NACA TM No. 1256.

3. Schlichting, H. Boundary Layer Theory, New York: Pergamon Press, 1955.

4. Goldstein, S. (ed) Modern Developments in Fluid Dynamics, Oxford: Clarendon Press, 1938.

5. Birkoff, G. Hydrodynamics, Princeton, New Jersey, Princeton Univ. Press, 1955.

6. Rouse, H. (ed) Advanced Mechanics of Fluids, Chapter VII, New York: John Wiley and Sons, 1959.

7. Moore, F. K. "Three-Dimensional Boundary Layer Theory", Advances in Applied Mechanics, IV, 1956.

8. Michal, A. D. Matrix and Tensor Calculus, Chapter 18, New York: John Wiley and Sons, 1947.

9. Cooke, J. C. and Hall, M. G. "Boundary Layers in Three Dimensions", Great Britain RAE Report Aero 2635, February 1960.

10. Sedney, R. "Some Aspects of Three-Dimensional Boundary Layer Flows", Quarterly of Applied Mathematics, XV, No. 2, 113.

11. Herzig, H. Z., Hansen, A. G. and Costello, G. R. "A Visualization Study of Secondary Flows in Cascades", NACA Report No. 1163, 1954.

12. Rohlik, H. E., Kofskey, M. G., Allen, H. W. and Herzig, H. Z. "Secondary Flows and Boundary-Layer Accumulations in Turbine Nozzles", NACA Report 1168, 1954.

13. Kofskey, M. G. and Allen, H. W. "Smoke Study of Nozzle Secondary Flows in a Low-Speed Turbine", NACA TN 3260, 1954.

14. Cooke, J. C. "Approximate Calculations of Three-Dimensional Laminar Boundary Layers", Great Britain, RAE Tn Aero 2658, October 1959.

15. Yang, K. T. "An Improved Integral Procedure for Compressible Laminar Boundary-Layer Analysis", ASME paper No. 60-WA-24; also to be published in the Journal of Applied Mechanics.

16. Hansen, A. G. "Possible Similarity Solutions of the Laminar, Incompressible Boundary-Layer Equations", ASME Transactions, 80, October 1958, 1553-1562. Discussion by A. J. A. Morgan.

17. Geis, T. "'Ähnliche' driedimensionale Grenzschichten", Journal of Rational Mechanics and Analysis, 5, No. 4, 1956; also NASA TT F-30, March 1961.

18. Yohner, P. L. and Hansen, A. G. "Some Numerical Solutions of Similarity Equations for Three-Dimensional Laminar Incompressible Boundary Layer Flows", NACA TN 4370.

19. Michal, A. D. "Differential Invariants and Invariant Partial Differential Equations Under Continuous Transformation Groups in Normal Linear Spaces", Proceedings of the National Academy of Sciences, 37, No. 9, September 1952, 623-627.

20. Morgan, A. J. A. "The Reduction by One of the Number of Independent Variables in Some Systems of Partial Differential Equations", Quarterly Journal of Mathematics, Oxford Second Series, 3, No. 12, December 1952, 250-259.

21. Reshotko, E. and Beckwith, I. E. "Compressible Laminar Boundary Layer Over a Yawed Infinite Cylinder with Heat Transfer and Arbitrary Prandtl Number", NACA TN 3986, June 1957.

22. Burgers, J. M. Proc. of the First Internat. Congr. of Applied Mechanics, Delft (1924) 113.

23. van der Hegge Zÿnen, B. G. "Measurements of the Velocity Distribution in the Boundary Layer along a Plane Surface", Thesis from Univ. of Delft, Delft, 1924.

24. Hansen, M. "Die Geschwindigkeitsverteilung in der Grenzschicht an einer eingetauchten Platte", ZAMM, 8, (1928) 185; also NACA Tech. Memo No. 585, 1930.

25. Nikuradse, J. "Laminare Reibungsschichten an der Längsangeströmten Platte", Monograph. Zentrale f. wiss. Berichtswesen, Berlin; R. Oldenbourg, 1942.

26. Gruschwitz, E. "Turbulent Reibungsschichten mit Seckundarstromung", Ingenieur-Archiv., 4, (1935) 355-365.

27. Johnston, J. P. "Three-Dimensional Turbulent Boundary Layer", Sc.D. Thesis, Massachusetts Institute of Technology, 1957; also available as M.I.T. Gas Turbine Laboratory Report No. 39, May 1957.

28. Kuethe, A. M., McKee, P. G. and Curry, W. H. "Measurements in the Boundary Layer of a Yawed Wing", NACA TN 1946, 1949.

29. Senoo, Y. "The Boundary Layer on the End Wall of a Turbine Nozzle Cascade", M.I.T. Gas Turbine Laboratory Report No. 35, October 1956.

30. Hansen, A. G. "On Possible Similarity Solutions for Three-Dimensional Incompressible Laminary Boundary-Layer Flows over Developable Surfaces and with Proportional Mainstream Velocity Components", NACA TM 1437, 1958.

31. McConnell, A. J. Applications of Tensor Analysis, New York: Dover Publications, 1957.

32. Coburn, N. Vector and Tensor Analysis, New York: Macmillan Company, 1955.

33. Eisenhart, L. P. A Treatise on the Differential Geometry of Curves and Surfaces, New York: Dover Publications, 1960.

34. Hansen, A. G. and Herzig, H. Z. "On Possible Similarity Solutions for Three-Dimensional Incompressible Laminar Boundary Layers. I - Similarity with Respect to Stationary Rectangular Coordinates", NACA TN 3768, 1956.

35. Schulze, W. M., Ashby, G. C. Jr. and Erwin, J. R. "Several Combination Probes for Surveying Static and Total Pressure and Flow Direction", NACA TN 2830, 1952.

36. Bradfield, W. S. and Yale, G. E. "Small Pitot Tubes with Fast Pressure Response Time", Journ. of the Aero. Sciences, 18, October 1951, 697.

37. Macmillan F. A. "Viscous Effects on Flattened Pitot Tubes at Low Speeds", Journ. of theRoyal Aeronautical Society, 58, December 1954, 837.

38. Pannell, J. R. "Experiments with a Tilting Manometer for Measurement of Small Pressure Differences", Engineering, September 1913, 343.

39. Falkner, V. M. "A Modified Chattock Gauge of High Sensitivity", Great Britain: ARC R and M No. 1589, January 1934.

40. Young, A. D. and Maas, J. N. "The Behavior of a Pitot Tube in a Transverse Total-Pressure Gradient", Great Britain: ARC R and M No. 1770, 1936.

41. Livesey, J. L. "Design of Total Pressure Probes for Minimum Interference with Measured Flow", Reader's Forum, Journal of the Aeronautical Sciences, 21, (1954) 641.

42. Livesey, J. L. "The Behavior of Transverse Cylindrical and Forward Facing Total Pressure Probes in Transverse Total Pressure Gradients", Journal of the Aeronautical Sciences, 23, October 1956, 949.

43. Table of Thermal Properties of Gases, Chapter 2, National Bureau of Standards Circular 564.

44. Pai, Chih-I, Viscous Flow Theory I-Laminar Flow, New Jersey: Van Nostrand Company, Inc., 1956.

45. VanWylen, G. J. Thermodynamics, New York: John Wiley and Sons, Inc., 1959.